

AMPK controls the speed of microtubule polymerization and directional cell migration through CLIP-170 phosphorylation

Atsushi Nakano^{1,4}, Hisakazu Kato^{3,4}, Takashi Watanabe^{5,6}, Kyung-Duk Min^{1,3}, Satoru Yamazaki¹, Yoshihiro Asano^{3,4}, Osamu Seguchi¹, Shuichiro Higo³, Yasunori Shintani³, Hiroshi Asanuma¹, Masanori Asakura¹, Tetsuo Minamino³, Kozo Kaibuchi⁶, Naoki Mochizuki², Masafumi Kitakaze¹ and Seiji Takashima^{3,4,7}

AMP-activated protein kinase (AMPK) is an energy-sensing Ser/Thr protein kinase originally shown to be regulated by AMP¹. AMPK is activated by various cellular stresses that inhibit ATP production or stimulate ATP consumption². In addition to its role in metabolism, AMPK has recently been reported to reshape cells by regulating cell polarity and division³⁻⁵. However, the downstream targets of AMPK that participate in these functions have not been fully identified. Here, we show that phosphorylation of the microtubule plus end protein CLIP-170 by AMPK is required for microtubule dynamics and the regulation of directional cell migration. Both inhibition of AMPK and expression of a non-phosphorylatable CLIP-170 mutant resulted in prolonged and enhanced accumulation of CLIP-170 at microtubule tips, and slower tubulin polymerization. Furthermore, inhibition of AMPK impaired microtubule stabilization and perturbed directional cell migration. All of these phenotypes were rescued by expression of a phosphomimetic CLIP-170 mutant. Our results demonstrate, therefore, that AMPK controls basic cellular functions by regulating microtubule dynamics through CLIP-170 phosphorylation.

we purified and identified a cytoplasmic linker protein CLIP-170, which has a relative molecular mass of 170,000 (M_r 170K) and is a substrate of AMPK (Supplementary Information, Fig. S1). CLIP-170 is one of the microtubule plus end proteins originally identified as proteins that bind endocytic vesicles to microtubules^{11,12}. CLIP-170 directly binds freshly polymerized distal ends of growing microtubules and rapidly dissociates from the older microtubule lattice¹³. However, a direct link between CLIP-170 and physiological control of cell function has not been fully elucidated. Both recombinant AMPK made by 293T cells and AMPK purified from rat liver efficiently phosphorylated recombinant CLIP-170 (Fig. 1a). Phospho amino acid analysis revealed that AMPK phosphorylates a Ser residue of CLIP-170 (Fig. 1b). A combination of mass spectrometric and multiple mutation analyses of CLIP-170 identified Ser 311 as the only AMPK phosphorylation site. AMPK did not phosphorylate CLIP-115, a close mammalian homologue of CLIP-170, or Ser 737 of CLIP-170, demonstrating an AMPK substrate consensus sequence¹⁴ (Fig. 1c). Recombinant glutathione S-transferase (GST)-fused wild-type CLIP-170 and a Ser 311-to-Ala mutant (S311A) of CLIP-170 were produced in *Escherichia coli*. The wild-type, but not the S311A mutant, was phosphorylated by AMPK and 0.29 mole of phosphate per mole of CLIP-170 was incorporated, indicating that Ser 311 of CLIP-170 is phosphorylated directly by AMPK (Fig. 1d). Next, we generated an antibody against Ser 311-phosphorylated CLIP-170 (p-CLIP-170). The specificity and sensitivity of this antibody were confirmed by the following observations: first the p-CLIP-170 antibody exclusively detected p170 as a single band, even when total cell lysates were assessed; and second, it did not recognize phosphatase-treated p170 (Fig. 1e). Analyses using this antibody also demonstrated the specific phosphorylation of CLIP-170 at Ser 311 by AMPK (Fig. 1f). The amino acid sequence surrounding Ser 311 matches the consensus sequence of a potential AMPK phosphorylation site and is well conserved among various species (Fig. 1g).

Besides the metabolic activity of AMPK, there is growing evidence that AMPK and its upstream kinase liver kinase B1 (LKB1) have pivotal roles in the establishment of cell polarity and cell division^{7,8} in *Drosophila melanogaster*^{6,9} and *Caenorhabditis elegans*¹⁰. In mammalian cells, AMPK is associated with tight junction assembly, and regulates epithelial polarity^{3,4}.

To discover previously unidentified substrates of AMPK, we performed a unique screen using two-step column chromatography combined with an *in vitro* kinase reaction. Using mouse heart homogenates,

¹Division of Cardiovascular Medicine, National Cardiovascular Center and ²Department of Structural Analysis, National Cardiovascular Center, Research Institute Suita, Osaka 565-8565, Japan. ³Department of Cardiovascular Medicine and ⁴Department of Molecular Cardiology, Osaka University Graduate School of Medicine Suita, Osaka 565-0871, Japan. ⁵Institute for Advanced Research, Nagoya University Graduate School of Medicine and ⁶Department of Cell Pharmacology, Nagoya University Graduate School of Medicine, Nagoya, Aichi 466-8550, Japan. ⁷Correspondence should be addressed to S.T. (e-mail: takesima@medone.med.osaka-u.ac.jp)

Received 4 March 2010; accepted 29 April 2010; published online 23 May 2010; DOI: 10.1038/ncb2060

LETTERS

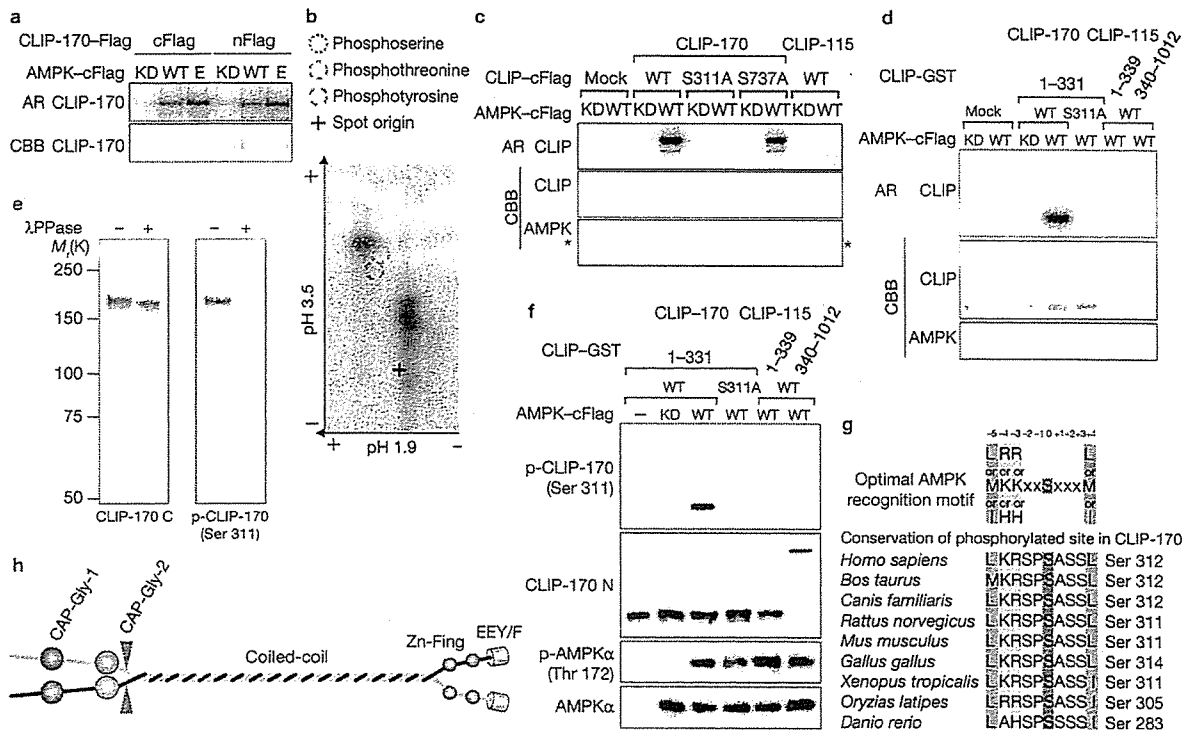


Figure 1 *In vitro* phosphorylation of CLIP-170 Ser311 by AMPK. (a) An autoradiographic (AR) image of mammalian recombinant carboxy-terminally (cFlag) or amino-terminally (nFlag) Flag-tagged CLIP-170 incubated with either recombinant kinase dead (KD), wild-type (WT) or endogenous (E) AMPK. (b) Phospho-amino acid analysis of CLIP-170 phosphorylated by AMPK. Only a Ser residue was phosphorylated (radioactivity indicated by the red circle). (c) An AR of mammalian recombinant cFlag-tagged CLIP-170 (WT, S311A and S737A) and CLIP-115 (WT) incubated with recombinant KD or WT AMPK. AMPK is indicated by an asterisk. (d) An AR image of GST fusion proteins representing amino acids 1–331 of CLIP-170 (WT or S311A), or either the N (1–339) or the C (340–1012) terminus of CLIP-115 incubated with KD or WT AMPK. (e) Lysate of Vero cells treated with or without phosphatase (λ PPase) was subjected to immunoblot analysis with

antibody against the C terminus of CLIP-170 (CLIP-170 C) and a Ser 311 phosphospecific antibody (p-CLIP-170). (f) Immunoblot analysis of the GST-fused CLIP constructs described above with KD or WT AMPK. These samples were blotted using a p-CLIP-170 and a non-phosphospecific antibody against the N terminus of CLIP-170 (CLIP-170 N). CLIP-170 N also recognized CLIP-115. (g) The optimal AMPK recognition motif. The consensus sequence of AMPK is identical to the sequence around Ser 311 of CLIP-170. This residue is highly conserved among various species. (h) Structural model of CLIP-170. Ser 311 is located between the CAP-Gly-2 domain and the coiled-coil region in CLIP-170. Ser 311 is indicated by red arrowheads. CAP-Gly, cytoskeleton-associated protein Gly-rich; Zn-Fing, C-terminal zinc knuckle of CLIP-170; EEY/F, C-terminal amino sequence of CLIP-170; CBB, Coomassie brilliant blue staining. Uncropped images of blots are shown in Supplementary Information, Fig. S5.

Ser 311 is located between a Gly-rich microtubule-binding domain (cytoskeleton-associated protein Gly-rich; CAP-Gly) and a coiled-coil domain (Fig. 1h).

Next, we examined AMPK-induced CLIP-170 phosphorylation in cultured cells. Compound C, an inhibitor of AMPK, reduced the phosphorylation level of CLIP-170 (Fig. 2a), whereas the AMPK activator AICAR (5-aminoimidazole-4-carboxamide ribonucleoside) did not affect CLIP-170 phosphorylation (Supplementary Information, Fig. S2a). The phosphorylation level of acetyl-CoA carboxylase (ACC), which was used as a control, reflected the conventional responses of cells to both Compound C and AICAR. Although Compound C is an inhibitor of AMPK, it can also inhibit several other kinases¹⁵. Therefore, we used short interfering RNAs (siRNAs) to specifically deplete AMPK. Depletion of AMPK with siRNAs specific for either the α_1 or the α_2 catalytic subunit also reduced CLIP-170 phosphorylation (Fig. 2b). These data indicate that phosphorylation of CLIP-170 at Ser 311 is regulated endogenously by AMPK. To explore the significance of AMPK-induced CLIP-170 phosphorylation, we first immunocytochemically investigated the localization

of phosphorylated CLIP-170 in cultured cells. A non-phospho-specific antibody (CLIP-170 C), as well as a Ser 311 phospho-specific antibody (p-CLIP-170), stained the plus ends of microtubules (Fig. 2c, d). To distinguish between the total CLIP-170 population and phosphorylated CLIP-170, Vero cells stably expressing CLIP-170-EGFP were stained with these antibodies. The pattern observed with the CLIP-170 C antibody (red or yellow) completely matched that of CLIP-170-EGFP (Fig. 2e, green), suggesting that CLIP-170-EGFP mimics the localization of endogenous CLIP-170. By contrast, p-CLIP-170 staining mostly overlapped with CLIP-170-EGFP but was located predominantly on the distal side (red or yellow) of CLIP-170-EGFP (Fig. 2f, green). This result suggests that phosphorylated CLIP-170 attaches to microtubules at the more distal end, compared with non-phosphorylated CLIP-170. A marked change in CLIP-170 localization was observed when these cells were treated with Compound C: CLIP-170-EGFP accumulated significantly farther along the length of the microtubules (Fig. 2g, h, green). CLIP-170 C staining again overlapped with CLIP-170-EGFP (Fig. 2g, red or yellow), whereas p-CLIP-170 staining was markedly reduced and localized as only a tiny

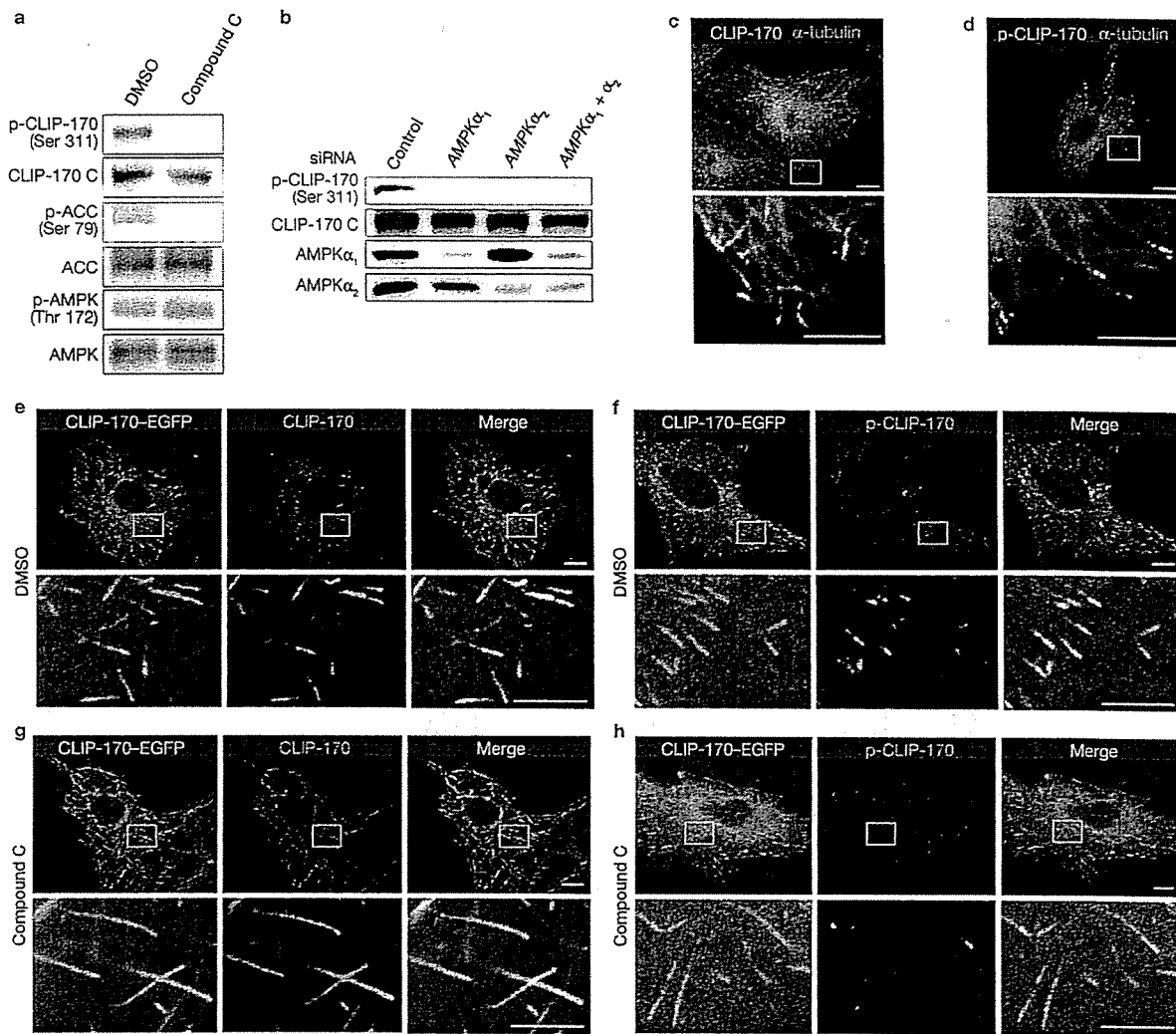


Figure 2 CLIP-170 phosphorylated by AMPK localizes to microtubule tips. (a) Immunoblot analysis of the phosphorylation level of CLIP-170, AMPK, and ACC in cells treated with 0.2% DMSO or Compound C (20 μ M). CLIP-170 C is a non-phosphospecific antibody that recognizes the C terminus of CLIP-170. (b) Immunoblot analysis of the phosphorylation level of CLIP-170 and the expression level of AMPK α_1 and α_2 in cells treated with siRNA targeting AMPK α_1 , α_2 or both subunits of AMPK. (c) Immunostained images of Vero cells stained with anti- α -tubulin and the anti-CLIP-170 C antibodies. (d) Immunostained images of Vero cells stained with α -tubulin and p-CLIP-170 antibodies. (e, f) Immunostained

images of Vero cells stably expressing CLIP-170-EGFP (GFP image, left) and treated with DMSO as a control. These cells were stained with a CLIP-170 C antibody (e, centre) or a p-CLIP-170 antibody (f, centre). (g, h) Immunostained images of Vero cells stably expressing CLIP-170-EGFP (GFP image, left) and treated with Compound C. These cells were stained with a CLIP-170 C antibody (g, centre) or a p-CLIP-170 antibody (h, centre). The merged images of each panel are shown on the right. The white boxed regions in the panels are enlarged below each panel. Scale bars, 10 μ m (c-h, upper rows) and 5 μ m (c-h, bottom rows). Uncropped images of blots are shown in Supplementary Information, Fig. S5.

spot within the CLIP-170-EGFP-positive region (Fig. 2h, red or yellow). Most of the CLIP-170 on microtubules, therefore, was non-phosphorylated, and a small amount of phosphorylated CLIP-170 accumulated at the distal ends. To examine the precise distribution of CLIP-170 on the microtubules under AMPK-inhibited conditions, linescan analysis along the microtubules was performed using double immunocytochemistry with CLIP-170 C and tubulin antibodies. We separately measured total CLIP-170 associated with microtubule plus ends, and CLIP-170 associated with the outermost microtubule tips (within a 0.129- μ m square box at the very end of the microtubules). When compared with the DMSO

control Compound C treatment increased the association of CLIP-170 with microtubules both in the whole tip (6-fold) and at the outer tip (1.7-fold) (Supplementary Information, Fig. S2b-d). Depletion of both AMPK α_1 and α_2 by siRNA also resulted in accumulation of CLIP-170 on microtubule plus ends, similarly to inhibition by Compound C (Supplementary Information, Fig. S2e, f). This characteristic change of CLIP-170 localization prompted us to examine the role of AMPK in the regulation of microtubule dynamics.

To study how AMPK regulates microtubule dynamics, we examined the behaviour of CLIP-170 in living cells. First, we tested whether phosphorylation levels of CLIP-170 affected polymerization of microtubules.

LETTERS

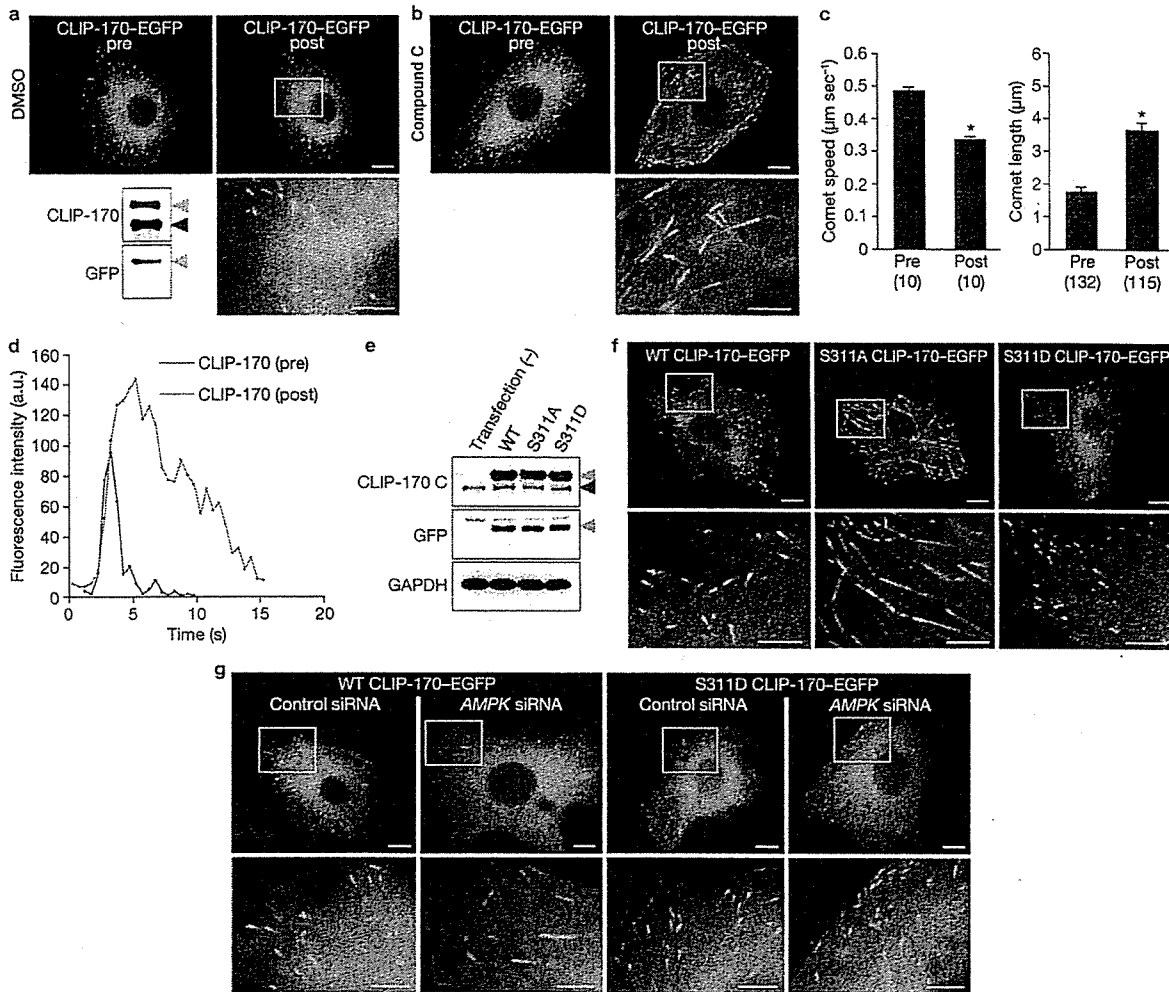


Figure 3 AMPK-phosphorylated CLIP-170 regulates microtubule dynamics. (a, b) GFP images of Vero cells stably expressing CLIP-170-EGFP before (pre) and 10 min after (post) treatment with 0.2% DMSO control (a) or Compound C (20 μ M, b). The immunoblot on the left shows exogenous CLIP-170-EGFP (grey arrowheads) and endogenous CLIP-170 (black arrowhead). (c) Bar graphs showing the speed (left panel) and length (right panel) of a single comet before (pre) and 10 min after (post) Compound C treatment in the same cell. Values are means \pm s.e.m.; *n* shown in parentheses; **P* < 0.01, compared with pre. (d) Fluorescence intensity plots of CLIP-170-EGFP of the same cell before (pre, blue) and 10 min after (post, red) Compound C treatment. (e) Expression levels

of wild-type (WT), S311A and S311D CLIP-170-EGFP in transiently transfected Vero cells were comparable, as determined by immunoblotting using the antibodies indicated on the left. The grey and black arrowheads indicate GFP-tagged exogenous CLIP-170 and endogenous CLIP-170, respectively. (f) GFP images of cells transiently expressing WT (left), S311A (centre) and S311D (right) CLIP-170-EGFP. (g) GFP images of the cells transiently expressing WT and S311D CLIP-170-EGFP treated with control siRNA or siRNA targeting both AMPK α_1 and α_2 . White boxed regions in the panels are enlarged below each panel. Scale bars, 10 μ m (a, b, f, g, upper panels) and 5 μ m (a, b, f, g, enlarged images). Uncropped images of blots are shown in Supplementary Information, Fig. S5.

By live-cell imaging, we observed that stably expressed CLIP-170-EGFP accumulated at the distal ends of microtubules and seemed to move like a comet from the centrosome to the cell periphery (as shown in sequential images converted to video, Supplementary Information, Movie 1). The speed of the CLIP-170 comets coincided with that of microtubule polymerization^{16,17}. Consistent with our results in fixed cells (Fig. 2), 10-min inhibition of AMPK by Compound C in living cells also resulted in elongated CLIP-170 comets, compared with control DMSO-treated cells (Fig. 3a-c). Moreover, the speed of the comets was reduced by Compound C (Fig. 3c; Supplementary Information, Movie 2). To analyse the CLIP-170 behaviour more precisely, we measured the fluorescence intensity values

along the CLIP-170-EGFP tracks over time in the same living cells before and 10 min after Compound C treatment. This fluorescence intensity analysis of CLIP-170-EGFP demonstrated that Compound C markedly increased the peak fluorescence intensity and slowed the dissociation of CLIP-170 from the older part of the microtubules (Fig. 3d). Using the same cell line stably expressing CLIP-170-EGFP, depletion of AMPK by siRNA also reduced the speed of the comets and increased the length of CLIP-170 comets (Supplementary Information, Fig. S2g-i, Movie 3). To elucidate the specific role of CLIP-170 Ser 311 phosphorylation by AMPK, we compared the phenotypes of cells transiently transfected with wild-type and two Ser 311 mutants of CLIP-170. S311A CLIP-170-EGFP

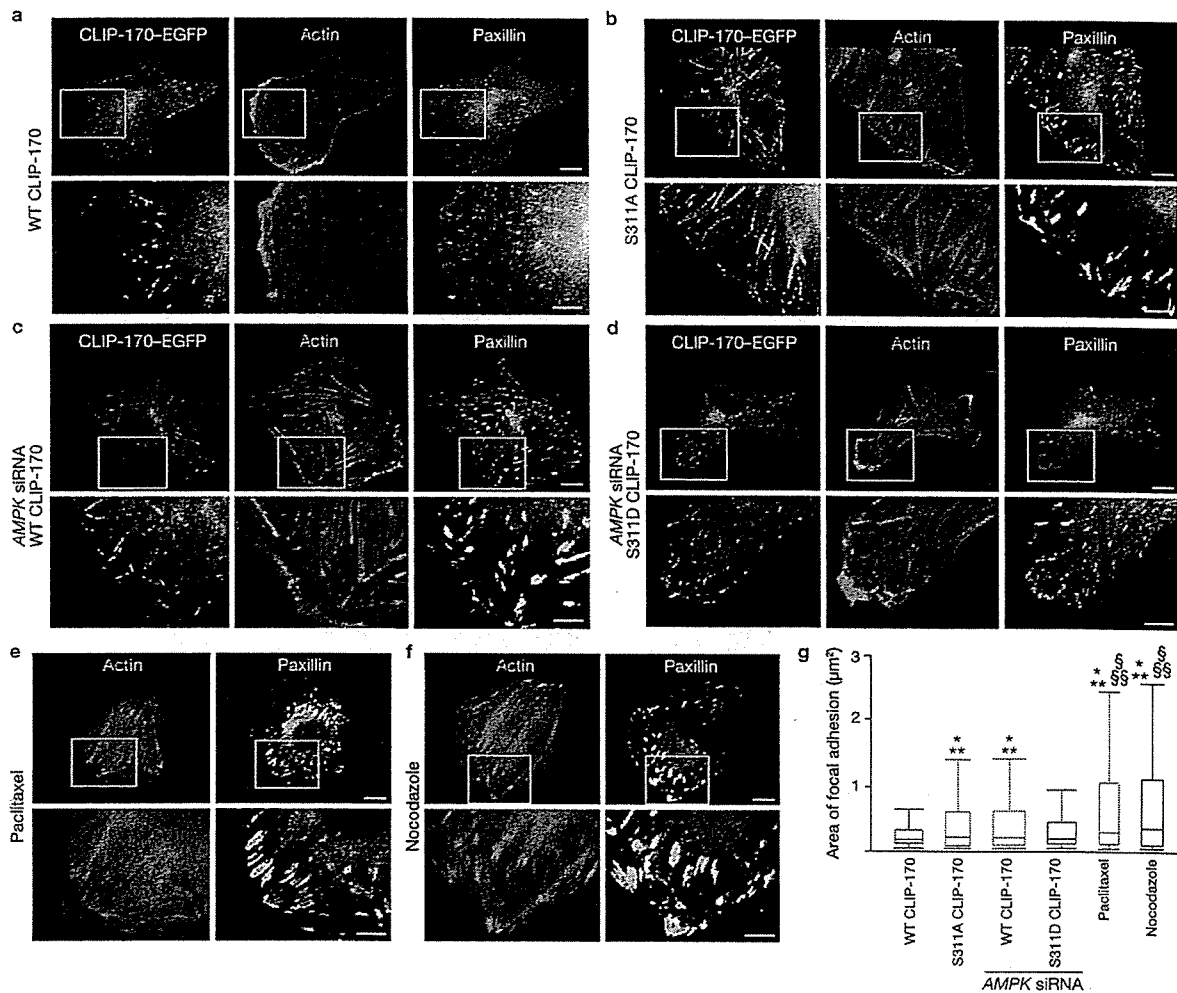


Figure 4 Loss of CLIP-170 phosphorylation increases the size of focal adhesions. (a, b) Immunostained images of Vero cells transiently expressing wild-type (WT; a) and S311A (b) CLIP-170-EGFP (GFP image, left). These cells were stained with fluorescein-conjugated phalloidin (centre) and a paxillin antibody (right) to visualize actin microfilaments and focal adhesions, respectively. (c, d) Immunostained images of Vero cells transiently expressing WT (c) and S311D (d) CLIP-170-EGFP (GFP image, left) treated with siRNA targeting both *AMPK* α_1 and α_2 . These cells were stained with fluorescein-conjugated phalloidin (centre) and a paxillin antibody (right). (e, f) Immunostained images of Vero cells treated with 5 μ M paclitaxel (e) or 10 μ M nocodazole (f). These

cells were stained with fluorescein-conjugated phalloidin (left) and a paxillin antibody (right). The white boxed regions in the panels are enlarged below each panel. Scale bars, 10 μ m (a–f, upper row) and 5 μ m (a–f, bottom row). (g) Box and whisker plots of the area stained with a paxillin antibody showing the 25th percentile (bottom line of each box), median (middle line of each box), 75th percentile (top line of each box), and the 5th and 95th percentiles (each whisker); $n = 10$ for each group; * $P < 0.01$, compared with WT CLIP-170; ** $P < 0.01$, compared with S311D CLIP-170 treated with *AMPK* siRNA; † $P < 0.01$, compared with S311A CLIP-170; ‡ $P < 0.01$, compared with WT CLIP-170 treated with *AMPK* siRNA.

is a non-phosphorylatable mutant, and a Ser 311-to-Asp mutant (S311D CLIP-170-EGFP) is a phosphomimetic mutant. These EGFP fusion proteins were equally expressed in Vero cells (Fig. 3e). S311A CLIP-170-EGFP accumulated as comets with longer tails and moved more slowly than wild-type CLIP-170-EGFP (Fig. 3f centre; Supplementary Information, Table S1, Movie 4). By contrast, S311D CLIP-170-EGFP had the same comet length and moved with the same speed as wild-type CLIP-170-EGFP (Fig. 3f, right; Supplementary Information, Table S1, Movie 5). These findings are consistent with the observation that most of the endogenous CLIP-170 was phosphorylated by AMPK. Furthermore, S311D CLIP-170-EGFP rescued the phenotypes caused by siRNA depletion of AMPK (Fig. 3g; Supplementary Information, Table S1,

Movie 6). Also, in the cells treated with Compound C, transfection of S311D CLIP-170-EGFP restored comet speed and length. Quantitative data of comet speed and length in various conditions are summarized in Supplementary Information, Table S1.

CLIP-170 binds only to the growing phase of microtubules. To further examine microtubule dynamics during the shortening phase, Vero cells stably expressing α -tubulin-EGFP were observed before and 10 min after Compound C treatment. Compound C markedly decreased the microtubule shortening distance (Supplementary Information, Fig. S2j, Movie 7). This change in microtubule behaviour may stabilize microtubules. We then observed microtubule stability by staining them with an antibody against detyrosinated tubulin (Glu tubulin,

LETTERS

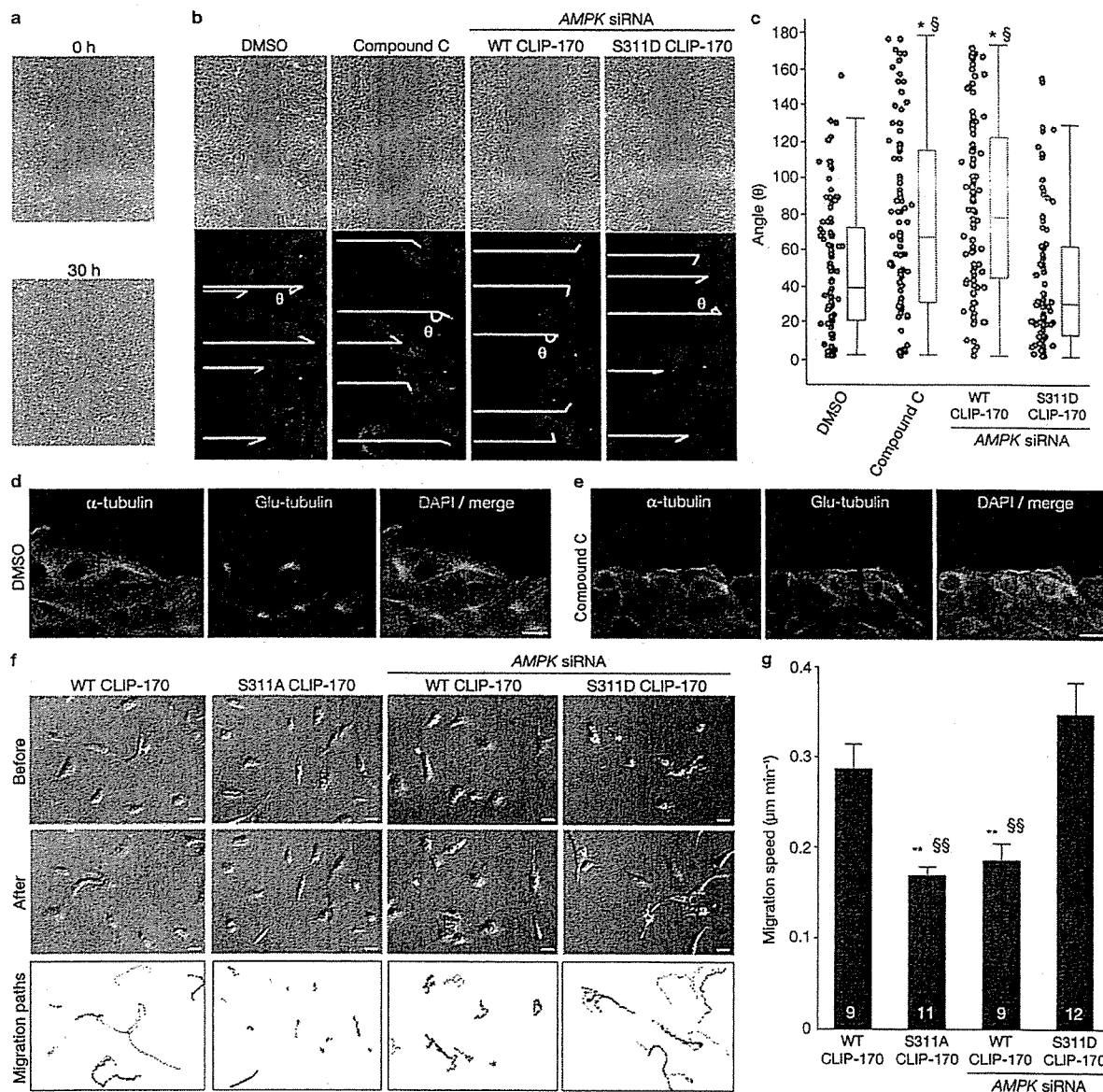


Figure 5 Phosphorylation of CLIP-170 at Ser 311 is essential for cell polarity and directional cell migration. (a) Phase contrast microscopy images of Vero cells before (upper panel) and 30 h after (lower panel) scratch. (b) Phase contrast microscopy images (upper panels) and immunostained images of Vero cells stained with a γ -tubulin antibody (lower panels) after being subjected to a scratch assay. Images were captured 12 h after incubation. The cells were treated by either repeated administration of DMSO control or Compound C, or transiently transfected with wild-type (WT) or S311D CLIP-170 and siRNA targeting both *AMPK α_1* and *α_2* . To assess cell polarity, the angles (θ) between the lines of γ -tubulin and the scratched line at the centre of each nucleus were measured as a marker for MTOC reorientation (lower panels). (c) Box and whisker plots of angles (θ) with actual data points shown on the left; $n=100$ per group; * $P < 0.01$, compared with DMSO; † $P < 0.01$, compared with S311D CLIP-170 treated

with *AMPK* siRNA. (d, e) Images of Vero cells immunostained with an α -tubulin (left, green) and a detyrosinated (Glu) tubulin antibody (centre, red) after being subjected to a scratch assay following repeated treatment with control DMSO (d) or Compound C (e) for 6 h. DAPI stained nucleus (blue). The merged images of each panel are shown on the right. Scale bars, 20 μ m. (f) Time lapse images acquired by differential interference contrast of cells transiently expressing WT, S311A, and WT or S311D CLIP-170 treated with siRNA targeting both *AMPK α_1* and *α_2* . Images acquired before (upper line of each panel) and after 12 h (middle line of each panel) are shown. The bottom-row of each panel shows the individual paths of migrating cells over 12 h. Scale bars, 30 μ m. (g) Bar graphs showing the migration speed of the cells from (f); Numbers in the bars indicate n . Values represent means \pm s.e.m.; ** $P < 0.01$, compared with WT CLIP-170. † $P < 0.01$, compared with S311D CLIP-170 treated with *AMPK* siRNA.

named for the newly exposed C-terminal glutamate residue). The amount of stable microtubules was greater in cells transiently expressing S311A CLIP-170-EGFP (Supplementary Information, Fig. S3b)

than in cells transiently expressing wild-type CLIP-170 (Supplementary Information, Fig. S3a). Cell depleted of *AMPK* by siRNA (Supplementary Information, Fig. S3g), or treated with Compound C (Supplementary

LETTERS

Information, Fig. S3d) also showed the same phenotype as cells expressing S311A CLIP-170. These phenotypes were rescued by S311D CLIP-170 (Supplementary Information, Fig. S3f, i). Collectively, these data suggest that phosphorylation of CLIP-170 at Ser 311 by AMPK is necessary for proper CLIP-170 dissociation from microtubules, and that this modification of CLIP-170 is essential for efficient polymerization and depolymerization of microtubules. Dynamic modulation of microtubule polymerization and stability by AMPK-phosphorylated CLIP-170 might represent a previously unknown mechanism through which AMPK establishes cell polarity. Therefore, we further examined the role of CLIP-170 phosphorylation by AMPK during cell polarization and subsequent cell migration.

During cell migration, microtubules target focal adhesions and regulate cell-extracellular matrix (ECM) adhesion¹⁶⁻²⁰. Thus, we first examined whether phosphorylation of CLIP-170 at Ser 311 affects the size of focal adhesions. Isolated Vero cells transiently expressing wild-type CLIP-170-EGFP formed an actin meshwork in protruding lamellipodium. Furthermore, staining focal adhesions with a paxillin antibody revealed small, scattered spots located predominantly at the protruding lamellipodium (Fig. 4a). By contrast, expression of S311A CLIP-170-EGFP caused loss of lamellipodium formation and adhesion maturation, which resulted in significantly enlarged spots (Fig. 4b). Similar phenotypes were observed when AMPK was depleted by siRNA (Fig. 4c) or inhibited by Compound C (Supplementary Information, Fig. S4b). These AMPK depletion phenotypes were almost completely rescued by the expression of S311D CLIP-170-EGFP (Fig. 4d, g; Supplementary Information, Fig. S4d). Treatment with paclitaxel and nocodazole (Fig. 4e, f), both of which disturb microtubule dynamics, resulted in similar phenotypes of abnormal size of focal adhesion as cells expressing S311A CLIP-170-EGFP and cells depleted of AMPK. These data indicate that AMPK-dependent phosphorylation of CLIP-170 regulates the size of focal adhesions by regulating microtubule dynamics. The fact that inhibiting AMPK-induced phosphorylation of CLIP-170 altered the size of focal adhesions and lamellipodium formation suggests an important role of the AMPK-CLIP-170 signalling axis in cell polarity and migration. We examined the effect of AMPK inhibition on cell polarity using the scratch assay. The leading cells started to polarize and migrated towards a scratched line, closing the gap in about 30 h (Fig. 5a). However, repeated treatment with Compound C and depletion of AMPK by siRNA both inhibited closure of the gap and interfered with microtubule-organizing centre (MTOC) reorientation in leading cells. Expression of S311D CLIP-170 rescued AMPK depletion (Fig. 5b, c; Supplementary Information, Fig. S4g, h). The first two layers of the leading cells showed that the stabilized microtubules stained with a detyrosinated (anti-Glu) tubulin antibody were clearly polarized towards the leading edge (Fig. 5d). By contrast, AMPK inhibition by Compound C increased the amount of stable microtubules, which lost their orientation towards the leading edge (Fig. 5e). Finally, we tested the effect of CLIP-170 phosphorylation on free cell migration. Wild-type CLIP-170-expressing cells migrated with active lamellipodium formation. By contrast, S311A CLIP-170-expressing cells and wild-type CLIP-170-expressing cells treated with AMPK siRNA showed diminished migration and fewer membrane extensions (Fig. 5f). Again, expression of S311D CLIP-170 rescued the effect of siRNA AMPK knockdown of (Fig. 5g; Supplementary Information, Movie 8). These data suggest that AMPK-induced phosphorylation of CLIP-170 is required to establish

front-rear polarity and proper cell migration, presumably through the regulation of microtubule tip dynamics.

We have shown here that CLIP-170 is a strong candidate AMPK substrate that regulates cell polarity through alteration of its dynamics on the plus ends of microtubules. Recently, abnormal mitotic phenotypes were observed for both AMPK- and LKB1-null *Drosophila*. They demonstrated that AMPK phosphorylates myosin regulatory light chain (MRLC) directly, and a phosphomimetic MRLC transgene rescued the polarity phenotypes induced by loss of the AMPK pathway⁶. However, the transgene did not rescue all phenotypes, suggesting that AMPK signalling is mediated by additional downstream targets.

The dynamics of CLIP-170 on microtubules were recently and precisely investigated both *in vitro* and *in vivo*^{13,17}. In these reports, CLIP-170 turnover on microtubules was rapid, and the diffusion of CLIP-170 was rate-limiting for its binding to microtubule plus ends. They also showed that the ends of growing microtubules contain a surplus of sites to which CLIP-170 can bind, and the older lattice has a lower affinity for CLIP-170 than the newer, growing ends of the microtubules. These changes in the affinity of plus end proteins for microtubules may be essential for their effects on microtubule dynamics.

We could not demonstrate an altered affinity of phosphorylated CLIP-170 for the microtubule plus end *in vitro* because of the difficulty associated with reconstituting the plus end as *in vivo*. However, we speculate, for the following reasons, that non-phosphorylated CLIP-170 increased its affinity to microtubules. First, linescan analysis showed that depletion of AMPK activity increased the association not only of total CLIP-170 with the microtubule but also of CLIP-170 at the outer tip. Second, the fluorescence intensity analysis measured in living cells indicated that non-phosphorylated CLIP-170 increased the peak fluorescence intensity and slowed its dissociation from the plus end of microtubules. Third, phosphorylated CLIP-170 localized within the more distal portion of the total CLIP-170 population. These results support the hypothesis that the phosphorylation status of CLIP-170 at Ser 311 determines its affinity for microtubules. Because CLIP-170 turnover on microtubules is rapid, phosphorylation may be a suitable modification to regulate its affinity for microtubules. We conclude that phosphorylation of CLIP-170 alters its affinity for microtubule plus ends and that this phenomenon might contribute to the rapid turnover of CLIP-170, which is necessary for efficient microtubule polymerization.

The observation that the phosphorylation status of CLIP-170 regulates the growth rate of microtubules has not been reported. The precise mechanisms remain unclear; however we speculate that Ser 311 phosphorylation is necessary to reduce the affinity of CLIP-170 for the microtubule lattice and promote the efficient turnover of CLIP-170 at the plus end, similarly to a microtubule polymerase.

Another intriguing phenotype of AMPK depletion is the marked enhancement of microtubule stabilization in migrating cells. Moreover, AMPK depletion impaired the polarized stabilization of microtubules towards the leading edge. AMPK depletion not only reduced the speed of polymerization but also decreased the shortening distance of microtubules. Because both phenomena prolong the lifetime of microtubules, these two changes might cause the ubiquitous enhancement of microtubule stabilization.

Expression of the non-phosphorylatable CLIP-170 S311A mutant and depletion of AMPK disrupted front-rear polarity and reduced cell migration. The precise mechanisms of this phenotype are unclear, but decreased

LETTERS

microtubule polymerization and unpolarized microtubule stabilization might affect the function of microtubules, which are required to establish cell polarity. We have shown that inhibiting CLIP-170 phosphorylation resulted in significant enlargement of focal adhesions, as detected with a paxillin antibody. Enlarged focal adhesions are similar to the phenotype observed in cells treated with paclitaxel or nocodazole, both of which disrupt microtubule dynamics. Microtubules bind to paxillin and help the cell adhesion system to destabilize focal adhesions and promote cell motility^{21,22}. These functions suggest that microtubules play a key part in cell polarity and migration through interactions with focal adhesion molecules. Taken together, the results suggest that AMPK promotes the appropriate formation of focal adhesions, the subsequent establishment of cell polarity, and directional cell migration through efficient polymerization of microtubules, by phosphorylating CLIP-170 at Ser 311.

Under normal cell culture conditions, neither enhanced activation of AMPK by AICAR nor S311D CLIP-170-EGFP altered microtubule dynamics, indicating a high basal phosphorylation of CLIP-170. This might be caused by a high affinity of AMPK for CLIP-170, or colocalization of AMPK and CLIP-170.

The results of our broad substrate screening method suggest that CLIP-170 is one of the most important substrates of AMPK in various organs. We believe that observing microtubule dynamics is necessary to evaluate multiple functions of AMPK. Also, similarly to paclitaxel or nocodazole treatment, strong inhibition of microtubule dynamics by the CLIP-170 S311A mutant may have clinical implications. The interaction between AMPK and CLIP-170 might be a therapeutic target for treatment of conditions such as cancer, tumour angiogenesis and neointimal hyperplasia. □

METHODS

Methods and any associated references are available in the online version of the paper at <http://www.nature.com/naturecellbiology/>

Note: Supplementary Information is available on the Nature Cell Biology website.

ACKNOWLEDGEMENTS

We thank M. Amano and S. Fukuhara for helpful discussions, and M. Koyama (Olympus Corporation) for technical advice regarding microscopy. This research was supported by: a Grants-in-Aid from the Ministry of Health, Labour and Welfare of Japan; Grants-in-Aid from the Ministry of Education, Culture, Sports, Science and Technology of Japan; grants from the Japan Heart Foundation; grants from the Japan Cardiovascular Research Foundation; a grant from the Japan Society for the Promotion of Science; a grant from the Mochida Memorial Foundation for Medical and Pharmaceutical Research; and a Grant-in-Aid from the Japan Medical Association.

AUTHOR CONTRIBUTIONS

A.N. designed and conducted the study, performed most of the experiments, and wrote the manuscript; S.T. designed and conducted the study, performed the biochemical experiments and wrote the manuscript; H.K. carried out

immunoblot analysis; K.M. independently counted the number of cells; S.Y. helped to generate the plasmids; Y.A., O.S., S.H., Y.S., H.A., M.A. and T.M. discussed the results and reviewed the manuscript; T.W. and K.K. generated and provided antibodies and Vero cells and reviewed the manuscript; N.M. conducted and supported the biological experiments and wrote the manuscript; M.K. supervised all work.

COMPETING FINANCIAL INTERESTS

The authors declare no competing financial interests.

Published online at <http://www.nature.com/naturecellbiology/>

Reprints and permissions information is available online at <http://npg.nature.com/reprintsandpermissions/>

1. Yeh, L. A., Lee, K. H. & Kim, K. H. Regulation of rat liver acetyl-CoA carboxylase. Regulation of phosphorylation and inactivation of acetyl-CoA carboxylase by the adenylate energy charge. *J. Biol. Chem.* **255**, 2308–2314 (1980).
2. Hardie, D. G. AMP-activated/SNF1 protein kinases: conserved guardians of cellular energy. *Nature Rev. Mol. Cell Biol.* **8**, 774–785 (2007).
3. Zhang, L., Li, J., Young, L. H. & Caplan, M. J. AMP-activated protein kinase regulates the assembly of epithelial tight junctions. *Proc. Natl Acad. Sci. USA* **103**, 17272–17277 (2006).
4. Zheng, B. & Cantley, L. C. Regulation of epithelial tight junction assembly and disassembly by AMP-activated protein kinase. *Proc. Natl Acad. Sci. USA* **104**, 819–822 (2007).
5. Mirouse, V., Swick, L. L., Kazgan, N., St. Johnston, D. & Brenman, J. E. LKB1 and AMPK maintain epithelial cell polarity under energetic stress. *J. Cell Biol.* **177**, 387–392 (2007).
6. Lee, J. H. *et al.* Energy-dependent regulation of cell structure by AMP-activated protein kinase. *Nature* **447**, 1017–1020 (2007).
7. Williams, T. & Brenman, J. E. LKB1 and AMPK in cell polarity and division. *Trends Cell Biol.* **18**, 193–198 (2008).
8. Jansen, M., Ten Klooster, J. P., Offerhaus, G. J. & Clevers, H. LKB1 and AMPK family signaling: the intimate link between cell polarity and energy metabolism. *Physiol. Rev.* **89**, 777–798 (2009).
9. Martin, S. G. & St. Johnston, D. A role for *Drosophila* LKB1 in anterior–posterior axis formation and epithelial polarity. *Nature* **421**, 379–384 (2003).
10. Watts, J. L., Morton, D. G., Bestman, J. & Kempthorne, K. J. The *C. elegans par-4* gene encodes a putative serine-threonine kinase required for establishing embryonic asymmetry. *Development* **127**, 1467–1475 (2000).
11. Rickard, J. E. & Kreis, T. E. Identification of a novel nucleotide-sensitive microtubule-binding protein in HeLa cells. *J. Cell Biol.* **110**, 1623–1633 (1990).
12. Pierre, P., Scheel, J., Rickard, J. E. & Kreis, T. E. CLIP-170 links endocytic vesicles to microtubules. *Cell* **70**, 887–900 (1992).
13. Dragestein, K. A. *et al.* Dynamic behavior of GFP-CLIP-170 reveals fast protein turnover on microtubule plus ends. *J. Cell Biol.* **180**, 729–737 (2008).
14. Hardie, D. G., Carling, D. & Carlson, M. The AMP-activated/SNF1 protein kinase subfamily: metabolic sensors of the eukaryotic cell? *Annu. Rev. Biochem.* **67**, 821–855 (1998).
15. Bain, J. *et al.* The selectivity of protein kinase inhibitors: a further update. *Biochem. J.* **408**, 297–315 (2007).
16. Perez, F., Diamantopoulos, G. S., Stalder, R. & Kreis, T. E. CLIP-170 highlights growing microtubule ends *in vivo*. *Cell* **96**, 517–527 (1999).
17. Bieling, P. *et al.* CLIP-170 tracks growing microtubule ends by dynamically recognizing composite EB1/tubulin-binding sites. *J. Cell Biol.* **183**, 1223–1233 (2008).
18. Wu, X., Kodama, A. & Fuchs, E. ACF7 regulates cytoskeletal-focal adhesion dynamics and migration and has ATPase activity. *Cell* **135**, 137–148 (2008).
19. Rodriguez, O. C. *et al.* Conserved microtubule-actin interactions in cell movement and morphogenesis. *Nat. Cell Biol.* **5**, 599–609 (2003).
20. Small, J. V., Geiger, B., Kaverina, I. & Bershadsky, A. How do microtubules guide migrating cells? *Nature Rev. Mol. Cell Biol.* **3**, 957–964 (2002).
21. Turner, C. E. Paxillin and focal adhesion signalling. *Nat. Cell Biol.* **2**, E231–E236 (2000).
22. Broussard, J. A., Webb, D. J. & Kaverina, I. Asymmetric focal adhesion disassembly in motile cells. *Curr. Opin. Cell Biol.* **20**, 85–90 (2008).

METHODS

Reagents and antibodies. The following reagents were purchased: Compound C (Calbiochem); AMPK (Upstate); DAPI (Molecular Probes); AICAR (5-aminoimidazole-4-carboxamide ribonucleoside; Cell Signaling) and Geneticin (Invitrogen). Generation of a CLIP-170 C (1:2,000 dilution for immunoblot; 1:200 dilution for immunostain) and a CLIP-170 N (1:4,000 dilution) antibody was described previously²³. The deetyrosinated (Glu) tubulin antibody (1:400 dilution) was a gift from G. G. Gundersen²⁴. The remaining antibodies purchased were: anti-AMPK α , AMPK α_1 , AMPK α_2 , phospho-Thr 172 AMPK α , ACC and phospho-Ser 79 ACC antibodies (each 1:200 dilution; Cell Signaling); anti-paxillin antibody (1:200 dilution, Zymed Laboratories); anti- α -tubulin (1:400) and γ -tubulin antibodies (1:500 dilution; Sigma-Aldrich); anti-GFP antibody (1:2,500 dilution; Chemicon); anti-GAPDH (glyceraldehyde-3-phosphate dehydrogenase) antibody (1:5,000 dilution; Chemicon); horseradish peroxidase-coupled sheep anti-rabbit and anti-mouse IgG (Cappel); and Alexa Fluor 350-, Alexa Fluor 488- and Alexa Fluor 568-labelled secondary antibodies and Alexa Fluor 555-conjugated phalloidin (each 1:500 dilution; Molecular Probes).

Generation of polyclonal antibodies specific for the pS311 of CLIP-170. A phospho-specific polyclonal antibody to CLIP170 (Ser 311) was generated as follows. Ser-phosphorylated and non-phosphorylated peptides corresponding to CLIP170 amino acid sequences S311 (amino acids 305–316, SLKRSP(pS) ASSLS) were synthesised. Rabbits were immunized 5 times with the keyhole limpet hemocyanin-phosphopeptide conjugates mixed with Freund's complete adjuvant, and bled 7 days after the last immunisation. Phosphopeptide-reactive antibody was captured by a column containing phosphopeptide-conjugated sepharose. The antibody was then eluted, and those reactive to sequences other than phosphoserine were removed using a column containing non-phosphorylated peptides. Specific reactivity with the targeted phosphoserine sequence was confirmed by an ELISA in which phosphorylated and non-phosphorylated peptides were coated.

Plasmids. A set of cDNA fragments encoding rat AMPK α (NM_019142), full-length mouse CLIP-170 and amino acids 1–331 of mouse CLIP-170 (BC007191), as well as full-length mouse CLIP-115 and amino acids 1–339 and 340–1012 of CLIP-115 (NM_009990) were PCR amplified from rat and mouse heart cDNA libraries and inserted into pENTR/D-TOPO vectors (pENTR-WT AMPK α , pENTR-WT CLIP-170, pENTR-WT CLIP-170 1–331, pENTR-WT CLIP-115, pENTR-WT CLIP-115 1–339, and pENTR-WT CLIP-115 340–1012) using Gateway Technology (Invitrogen). The kinase-dead (KD) AMPK α (a Thr 172 Ala mutant) was generated by PCR using pENTR-WT AMPK α 1 as a template and the following primers: 5'-TTTTTAAGAGCTAGCTGTGGCTCGCC-3' and 5'-GCCACAGCTAGCTCTTAAAAATTAC-3'. S311A and S737A CLIP-170 were also generated by PCR using pENTR-WT CLIP-170 as a template and the following primer pairs: forward 5'-CGAAGCCC-TGCTGCCTCCTCCTCAGCTCCATGAGC-3' and reverse 5'-GGAGGAG-GCAGCAGGGCTTCGCTTCAGGCTGGCGGGCG-3' and forward 5'-AAAGCCAATGCGAAGGTAAGTAACTGGAGCTCGAGACTTA-3' and reverse 5'-TTTACCTTCGGCATTTGGCTTTCCGAAGCGCATCAAGATCC-3', respectively (underlined nucleotides indicate mutated sites). To prepare Flag-tagged protein, pENTR-WT AMPK α , pENTR-KD AMPK α , pENTR-WT CLIP-170, pENTR-S311A CLIP-170, pENTR-S737A CLIP-170, and pENTR-WT CLIP-115 were subcloned into pEF-DEST51/cFlag vectors (yielding pEF-DEST51-WT AMPK α , pEF-DEST51-KD AMPK α , pEF-DEST51-WT CLIP-170, pEF-DEST51-S311A CLIP-170, pEF-DEST51-S737A CLIP-170, and pEF-DEST51-WT CLIP-115, respectively) or a pcDNA3.1/nFlag-DEST vector (pcDNA3.1-WT CLIP-170) using the Gateway system. To prepare the GST fusion protein, pENTR-WT CLIP-170 1–331, pENTR-WT CLIP-115 1–339, and pENTR-WT CLIP-115 340–1012 were subcloned into pDEST15 vectors (pDEST15-WT CLIP-170 1–331, pDEST15-WT CLIP-115 1–339, and pDEST15-WT CLIP-115 340–1012, respectively) using the Gateway system. The pEGFP-CLIP-170 construct was produced as described by Fukata *et al.*²³. Mutant CLIP-170 constructs in which Ser 311 was replaced with Ala or Asp were generated by PCR using pEGFP-CLIP-170 as the template and the following primers: Ala forward 5'-CGCAGCCCTGCTGCCTCTCCCTCAGTCCATGAGC-3' and reverse 5'-GGAAGAGGCAGCAGGGCTGCGCTTCAGGCTGGCGGACG-3' and Asp forward 5'-CGCAGCCCTGATGCCTCTCCCTCAGTCCATGAGC-3' and

reverse 5'-GGAAGAGGCATCAGGGCTGCGCTTCAGGCTGGCGGACG-3' (underlined nucleotides indicate mutated sites).

Cell culture, plasmid transfection, and siRNAs. The 293T cells were obtained from the American Type Culture Collection. Preparation of Vero cells and generation of Vero cells stably expressing CLIP-170-EGFP or tubulin-EGFP were performed as described by Fukata *et al.*²³. All cells were maintained in Dulbecco's modified Eagle's medium (Sigma-Aldrich) supplemented with 10% foetal calf serum (Equitech-Bio) at 37°C in a 5% CO₂ atmosphere at constant humidity. Vero cells stably expressing CLIP-170-EGFP were selected in the presence of geneticin (1.5 mg ml⁻¹). Vero and 293T cells were transfected with plasmids using Lipofectamine 2000 reagent (Invitrogen), according to the manufacturer's protocol. To knock down AMPK, Vero cells were transfected with siRNAs (50 nmol l⁻¹) targeting AMPK α (sense: gaggagagcuauugauuTT; antisense: uaucaaaauagcucucucTT) and AMPK α (sense: gcuguuugguagguuuuTT; antisense: uuuuaccuacacaaacagcTT) (B-Bridge International) using Lipofectamine 2000, according to the manufacturer's protocol. As a negative control, siControl (B-Bridge International) was used. After incubation with siRNAs for 40 h, the cells were analysed. When we used cells transiently transfected CLIP-170-EGFP mutant, we screened the cells by the expression level of each CLIP-170-EGFP protein by measuring the total fluorescence intensity of EGFP throughout the whole cell with background subtraction. Then we selected the cells expressing similar amount of CLIP-170-EGFP proteins for assay when we compared the dynamics of each CLIP-170 transfectant.

Animals. Female C57BL/6J mice (Japan animals, Osaka, Japan) were used in the study. All procedures conformed to the *Guide for the Care and Use of Laboratory Animals* (NIH publication no. 85-23, revised 1996) and were approved by the Osaka University Committee for Laboratory Animal Use.

Protein purification. Recombinant Flag-tagged AMPK, CLIP-170, and CLIP-115 proteins were purified as follows: 293T cells transfected with pEF-DEST51/cFlag plasmid encoding WT or KD AMPK α , WT, S311A and S737A CLIP-170 and WT CLIP-115 were lysed in lysis buffer A (20 mM MOPS, pH 7.4, 10% glycerol, 0.15 M NaCl, 1% CHAPS, 1 mM EDTA, protease inhibitor cocktail (Nacalai Tesque), 50 mM β -glycerophosphate, 25 mM NaF, and 1 mM Na₃VO₄) and immunoprecipitated with anti-Flag M2 agarose (Sigma) at 4°C for 1 h. The beads were washed three times with lysis buffer A and eluted with elution buffer (20 mM Tris-HCl, pH 7.4, 10% glycerol, 0.3 mM NaCl, 0.1% CHAPS, 0.5 mg ml⁻¹ Flag peptide (Sigma), and 1 mM dithiothreitol (DTT)) at 4°C for 1 h. After centrifugation, the supernatants were used as recombinant Flag-tagged proteins. Recombinant CLIP-170-GST and CLIP-115-GST proteins were purified as follows: BL21-AI chemically competent *E. coli* (Invitrogen) were transformed with a DEST15 plasmid encoding WT CLIP-170 1–331, WT CLIP-115 1–339, or WT CLIP-115 340–1012, and induced with 0.02% L-arabinose (Sigma) at 20°C for 12 h. The cells were collected by centrifugation and lysed by sonication in phosphate-buffered saline (PBS) containing 5 mM EDTA and protease inhibitor cocktail. After addition of 1% Triton X-100, the cell lysates were agitated at 4°C for 30 min and pulled down with glutathione sepharose 4 Fast Flow (GE Healthcare) at 4°C for 1.5 h. After being washed three times, the proteins were eluted with 10 mM reduced glutathione and ultrafiltrated in elution buffer using a Nanosep 10K Device (Pall Life Science).

Screening for AMPK substrates. Organs obtained from C57BL/6J animals were homogenised in lysis buffer B (20 mM MOPS, pH 7.4, 10% glycerol, 0.1% CHAPS, 2 mM EDTA, 1 mM DTT, and a protease inhibitor cocktail) using a Polytron homogeniser (Kinematica). After homogenization, CHAPS was added to a final concentration of 1%, and the homogenates were incubated at 4°C with agitation for 15 min, followed by centrifugation at 10,000g for 30 min. The supernatant was filtered and loaded onto a TSK-GEL SuperQ-5PW (7.5x75 mm, TOSOH) anion-exchange column pre-equilibrated with Column Buffer A, which consists of 20 mM MOPS (pH 7.4), 10% glycerol, and 2 mM EDTA. After being washed with column buffer A, the proteins were eluted with a linear gradient of NaCl (0–1 M over 60 min) at a flow rate of 0.5 ml min⁻¹. The fractions (0.5 ml each) were collected, and a 50- μ l aliquot of each fraction was analysed using an *in vitro* kinase assay, as described below. These hot samples were prepared in the presence of 0.3% TEA (trifluoroacetic acid), 0.1% OG (*n*-octyl- β -D-thioglucoopyranoside), and 20% acetonitrile and loaded onto a 5Ph-AR-300 (4.6x250 mm, Nacalai Tesque)

reverse-phase HPLC column pre-equilibrated with column buffer B, which consists of 0.1% TFA and 0.1% OG. After being washed with column buffer B, the proteins were eluted with a linear gradient of acetonitrile (30–50% over 60 min) at a flow rate of 0.5 ml min⁻¹. Each fraction was analysed by SDS-PAGE and visualized by silver staining and autoradiography. After the purification was scaled up, the procedures described above were again performed using cold ATP instead of γ -³²P ATP. Target cold bands matching the hot bands were excised from the gel and analysed using MALDI-Qq-TOF MS/MS.

In vitro kinase assay. Fraction samples were preheated at 65°C for 20 min and incubated with KD or WT AMPK-cFlag in the presence of 0.2 mM AMP, 0.8 mM MgCl₂, and 5 μ Ci of γ -³²P ATP (GE Healthcare Bio-Science) at 30°C for 60 min and ultrafiltrated in PBS containing 0.1% SDS using a Nanosep 10K Device (Pall Life Science). Each fraction sample was analysed by SDS-PAGE and visualised by AR. Recombinant Flag-tagged or GST-fused CLIP proteins were also incubated with KD or WT AMPK-cFlag, as described above. Each protein was analysed by SDS-PAGE and either visualized by Coomassie brilliant blue or autoradiography, or examined by immunoblotting. For the CLIP-170 phosphorylation assay, purified GST-CLIP-170 was incubated with PKA or PKC or AMPK purified from rat liver in the presence of 0.2 mM AMP (AMPK), 10 mM MgCl₂, and 5 μ Ci of γ -³²P ATP at 30°C for 60 min, analysed by SDS-PAGE and visualised by autoradiography.

Phosphorylation assay. Phosphorylation assays were carried out at 30°C in a reaction volume of 10 μ l containing Tris-HCl (20 mM, pH 7.4), glycerol (10%), NaCl (0.3 mM), AMP (0.2 mM), MgCl₂ (0.8 mM), γ -³²P ATP (10 μ Ci, 1.7 pmol), AMPK purified from rat liver (0.2 units), and GST-fused CLIP-170 protein. After 60 min, reactions were terminated by the addition of SDS-stop solution, and the CLIP-170 protein and a known concentration of BSA as a volume control were analysed by SDS-PAGE followed by Coomassie brilliant blue staining. From the intensity of each BSA band, the amount of CLIP-170 protein was estimated. With the autoradiogram as a guide, the ³²P-labelled CLIP-170 protein was excised from the gel. Its radioactivity and several known concentrations of γ -³²P ATP were measured using a Cerenkov counter. The moles of CLIP-170 protein used in this assay and mole of ³²P incorporated into the CLIP-170 protein were estimated based on a standard curve.

Phospho-amino acid analysis. CLIP-170-cFlag was incubated with AMPK-cFlag in the presence of γ -³²P ATP, as described above. The reaction samples were separated by SDS-PAGE, stained with Coomassie brilliant blue, and visualised by AR. The radiolabelled band was excised from the gel and digested with trypsin. The hydrolysate was dried and resuspended in 5% TFA and 50% acetonitrile containing phospho-amino acid standards and then spotted onto thin-layer cellulose plates. Electrophoresis was performed using pH 1.9 buffer (0.22% formic acid and 7.8% acetic acid) for the first dimension and pH 3.5 buffer (5% acetic acid, 0.5% pyridine, and 0.5 mM EDTA) for the second dimension. The standards were then labelled with ninhydrin, and the plates were analysed by autoradiography.

Biochemical analysis. Protein expression levels in Vero cells were investigated as follows. To inhibit AMPK, cells were serum-starved for 5 h; incubated with 0.2% DMSO, Compound C (20 μ M) or AICAR (2 mM) for 10 min; lysed in lysis buffer A; and agitated at 4°C for 15 min. After centrifugation, the supernatants were analysed by SDS-PAGE and examined by immunoblotting. For the phosphatase treatment, cells were lysed in lysis buffer C (50 mM Tris-HCl, pH 7.5, 0.01% Brij 35, 0.1 M NaCl, 0.1 mM EGTA, 2 mM DTT, 2 mM MnCl₂, protease inhibitor cocktail, 50 mM β -glycerophosphate, 25 mM NaF and 1 mM Na₂VO₄) and agitated at 4°C for 15 min. After centrifugation, the supernatants were incubated at 30°C for 30 min in the presence of either 20 units μ l⁻¹ λ protein phosphatase (New England Biolabs) or 0.5 mM EDTA.

Immunocytochemistry and fluorescence imaging. Vero cells and Vero cells stably or transiently expressing CLIP-170-EGFP were seeded on a collagen-coated 35-mm glass dishes (Asahi Techno Glass Corporation). When we stained cells with a detyrosinated tubulin antibody, Vero cells were seeded on a polylysine coated glass dishes to avoid integrin-dependent cell contact. Cells were washed once with warm PBS and fixed with 100% methanol for 10 min at -20°C, followed by 1% paraformaldehyde for 5 min at room temperature. Next, the cells were permeabilized with 0.01% Triton X-100 in PBS for 5 min at room temperature

and then immunostained with anti-CLIP-170 C, anti-p-CLIP-170, anti-paxillin, anti- α -tubulin and anti-detyrosinated tubulin antibodies and DAPI for 1 h. For the staining with Alexa Fluor 555-conjugated phalloidin, cells were fixed with 3% paraformaldehyde at room temperature for 5 min. For secondary reactions, each species-matched Alexa 350-, 488- or 568-labelled secondary antibody was used. Fluorescence images of EGFP, Alexa 350, Alexa 488, Alexa 555, and Alexa 568 were recorded with an Olympus IX-81 inverted fluorescence microscope (Olympus) equipped with a cooled CCD CoolSNAP-HQ camera (Roper Scientific) using a PLAPO 60X or 100X (Olympus) oil immersion objective lens. All intensity profiles were analysed in MetaMorph 7.1.3.0 software (MDS Analytical Technologies). Line intensity analysis was performed as described by Komarova *et al.*²⁵. Briefly, for the linescan analysis, the intensity profiles along 1 pixel depth line at the microtubule tips were analysed. To estimate the amount of CLIP-170 bound either to the outermost microtubule tips within a box of four pixels (within a 0.129- μ m square box) on a side (outer tip) or to the entire microtubule tips within a rectangle covering the entire positively stained tip (total bound), integrated fluorescence intensity at each area was measured for each channel after external background of the same area was subtracted. To quantify the amount of stabilized and total tubulin, the integrated fluorescence intensity stained with a detyrosinated tubulin antibody or an α -tubulin antibody was measured throughout whole cell with background subtraction and divided by the cell area. To measure the paxillin-positive area, lines at every fluorescent border were detected automatically, and each area enclosed by these lines was calculated using WinROOF Ver.6.0 (MITANI Corporation).

Time-lapse imaging and tracking. Vero cells and Vero cells stably or transiently expressing CLIP-170-EGFP were seeded on a collagen-coated 35-mm glass dish at a density of 4×10^4 cm⁻², starved for 5 h, and stimulated as indicated in the figures. The fluorescence images were recorded with an Olympus IX-81 inverted fluorescence microscope (Olympus) equipped with a cooled CCD CoolSNAP-HQ camera (Roper Scientific) using a PLAPO $\times 60$ or $\times 100$ (Olympus) oil immersion objective lens controlled by MetaMorph version 7.1.3.0. An EGFP image was obtained every second through a U-MNIBA2 filter (Olympus), which had a 470–495 excitation filter and a 510–550 emission filter. For fluorescence intensity plots of CLIP-170-EGFP, fluorescent images were acquired as described by Komarova *et al.*²⁵. Briefly, time-lapse series of 30 images were acquired with a 500-msec interval using stream acquisition mode. CLIP-170 kinetics were analysed on 16-bit depth images after subtraction of the external background. We measured the fluorescence intensity values within the line of 1 pixel in width along the CLIP-170-EGFP tracks over time. We determined the beginning of a comet as the point at which fluorescence intensity showed a rapid rise and the end of a comet as the point at which fluorescence intensity reached baseline. Differential interference contrast (DIC) images were obtained every 10 min. MetaMorph was used to convert a series of time lapse images to video format and obtain tracking images.

Scratch assay. Vero cells were plated on a collagen-coated dish at a density of 2×10^4 cm⁻² and transiently transfected with WT, S311A, or S311D CLIP-170-EGFP using Lipofectamine 2000. One hour later, siRNA was administered using the same procedure. After 40 h, cells were plated on a collagen-coated 35-mm glass dish at a density of 8×10^4 cm⁻². When we stained cells with a detyrosinated tubulin antibody, Vero cells were seeded on a polylysine coated glass dishes. After 8 h, a scratch line was made with a p200 pipette tip, and the dishes were washed once with fresh medium. Repeated observations of the edge of the same scratched lesion were performed. Either 0.2% DMSO (control) or Compound C (20 μ M) was administered every 2 h, and the medium was replaced every 4 h. After 12 h, the cells were fixed and immunostained with a γ -tubulin antibody, as described above. For the cell polarity analysis, the angles (θ) of each cell to the scratched line were measured. First, we drew line A from the point stained with a γ -tubulin antibody to the centre of the nucleus. Next, we drew line B from the centre of the nucleus to the scratched line. The angles (θ) between lines A and B were determined. The distance of gap closure was calculated as the total distance of the gap closed over 12 h. Also, the numbers of cells in the first two layers from the edge that were perpendicular with respect to their migration direction were calculated.

Cell migration assay. Vero cells were prepared as described for the scratch assay. Cells were plated on a collagen-coated 35-mm glass dish at a density of 5×10^3 cm⁻². After 3 h, DIC images were recorded every 10 min for 12 h with an Olympus IX-81 inverted fluorescence microscope equipped with an ONICS stage top incubator sys-

DOI: 10.1038/ncb2060

METHODS

tem and an INUG2 temperature and CO₂ control unit (Tokai Hit). RFP images were also recorded at the same time to assess whether the siRNA duplex was effectively delivered into each cell by the co-transfection of control siRNA labelled with Alexa Fluor 546 (Qiagen) and siRNA targeting for AMPK. To determine cell trajectories, the centrioles of the cell nuclei were tracked throughout time-lapse movies, and we made migration tracking images using MetaMorph 7.1.3.0 software. Migration speed was expressed as the average of each migration speed obtained every 10 min.

Statistical analyses. Box and whisker plots show the entire population. Other data are expressed as means \pm s.e.m. The two-tailed Student's *t*-test was used to

analyse differences between two groups. Differences among multiple groups were compared by one-way ANOVA, followed by a post hoc comparison using the Dunnett method with JMP 8.0.1 software (SAS Institute). *P* < 0.01 was considered statistically significant.

23. Fukata, M. *et al.* Rac1 and Cdc42 capture microtubules through IQGAP1 and CLIP-170. *Cell* 109, 873–885 (2002).
24. Palazzo, A. F. *et al.* Cdc42, dynein, and dynactin regulate MTOC reorientation independent of Rho-regulated microtubule stabilization. *Curr. Biol.* 11, 1536–1541 (2001).
25. Komarova, Y. *et al.* EB1 and EB3 control CLIP dissociation from the ends of growing microtubules. *Mol. Biol. Cell* 16, 5334–5345 (2005).

DOI: 10.1038/ncb2060

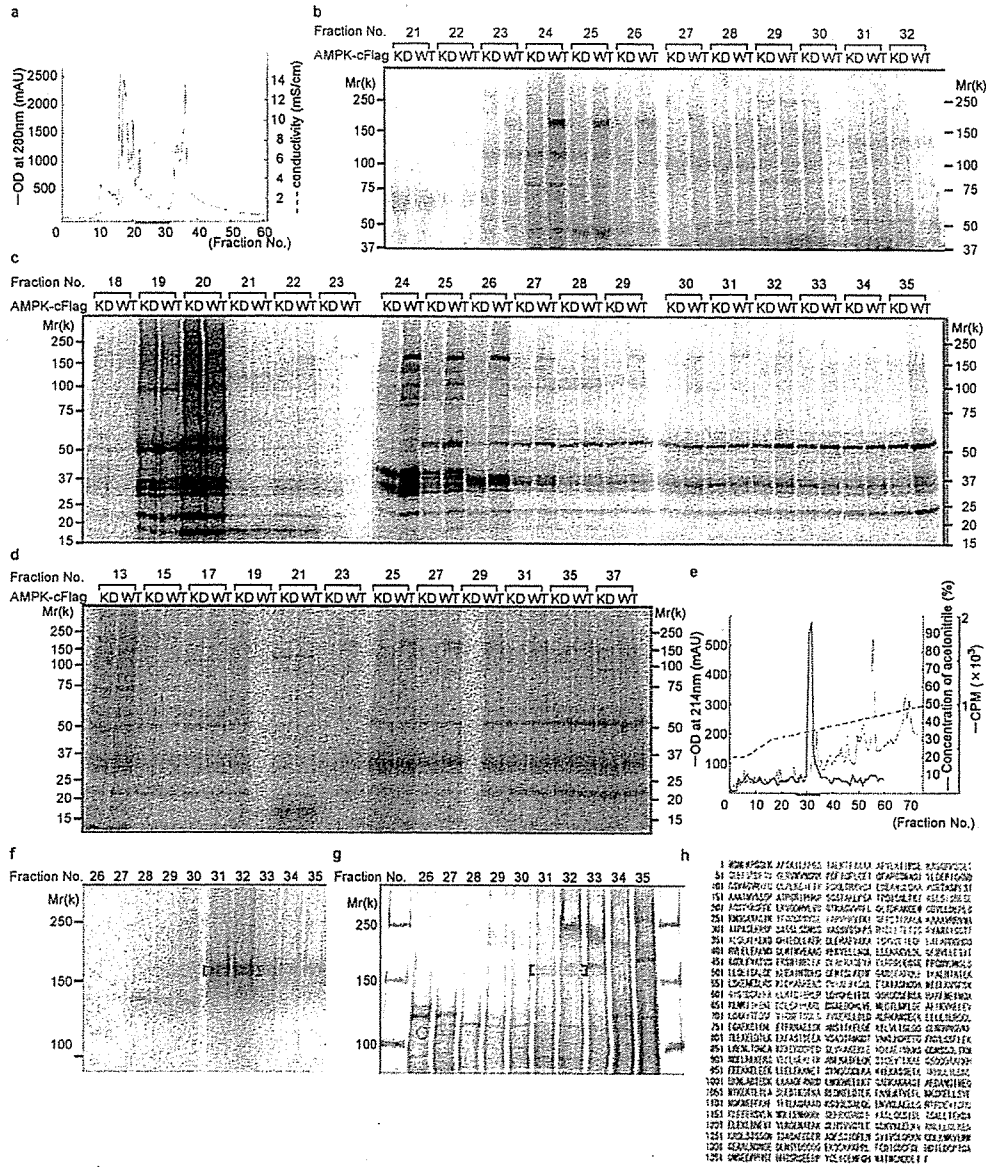


Figure S1 Screening of AMPK substrate in various organs. (a) A graphic chart of the fractions acquired from homogenised mouse heart using an anion exchange column with an NaCl concentration gradient (dotted line). The solid line represents the optical density (OD) of each sample. Further analysis was performed using fractionated samples, indicated by the red line. (b-d) In vitro kinase reaction. A wide range of fractionated samples from mouse heart (b), placenta (c), and liver (d) were incubated with recombinant kinase-dead (KD) or wild-type (WT) AMPK in the presence of [γ - 32 P] ATP, separated by SDS-PAGE, and visualised by autoradiography. A 32 P-incorporated ~170 kDa polypeptide (p170) was detected in fractions treated with WT AMPK but not in fractions treated with KD AMPK (fractions 23 to 27 in b). (e) A graphic chart

of the fractions containing AMPK-induced 32 P-incorporated proteins from mouse heart using a reverse-phase high-performance liquid chromatography (HPLC) column with an acetonitrile concentration gradient (dotted line). The solid black line represents the optical density (OD) of each sample. The radioactivity of each refractionated sample was measured using a Cerenkov counter (blue line). Further analysis was performed using refractionated samples, indicated by the red line. (f, g) Images obtained by autoradiography (f) and silver staining (g) of samples that were refractionated by reverse-phase HPLC. Red brackets denote p170 incorporated 32 P by AMPK. (h) Amino acid sequence of CLIP-170. Sequence analysis by MALDI-Qq-TOF MS/MS revealed p170 to be CLIP-170. Matching amino acids are shown in red letters.

SUPPLEMENTARY INFORMATION

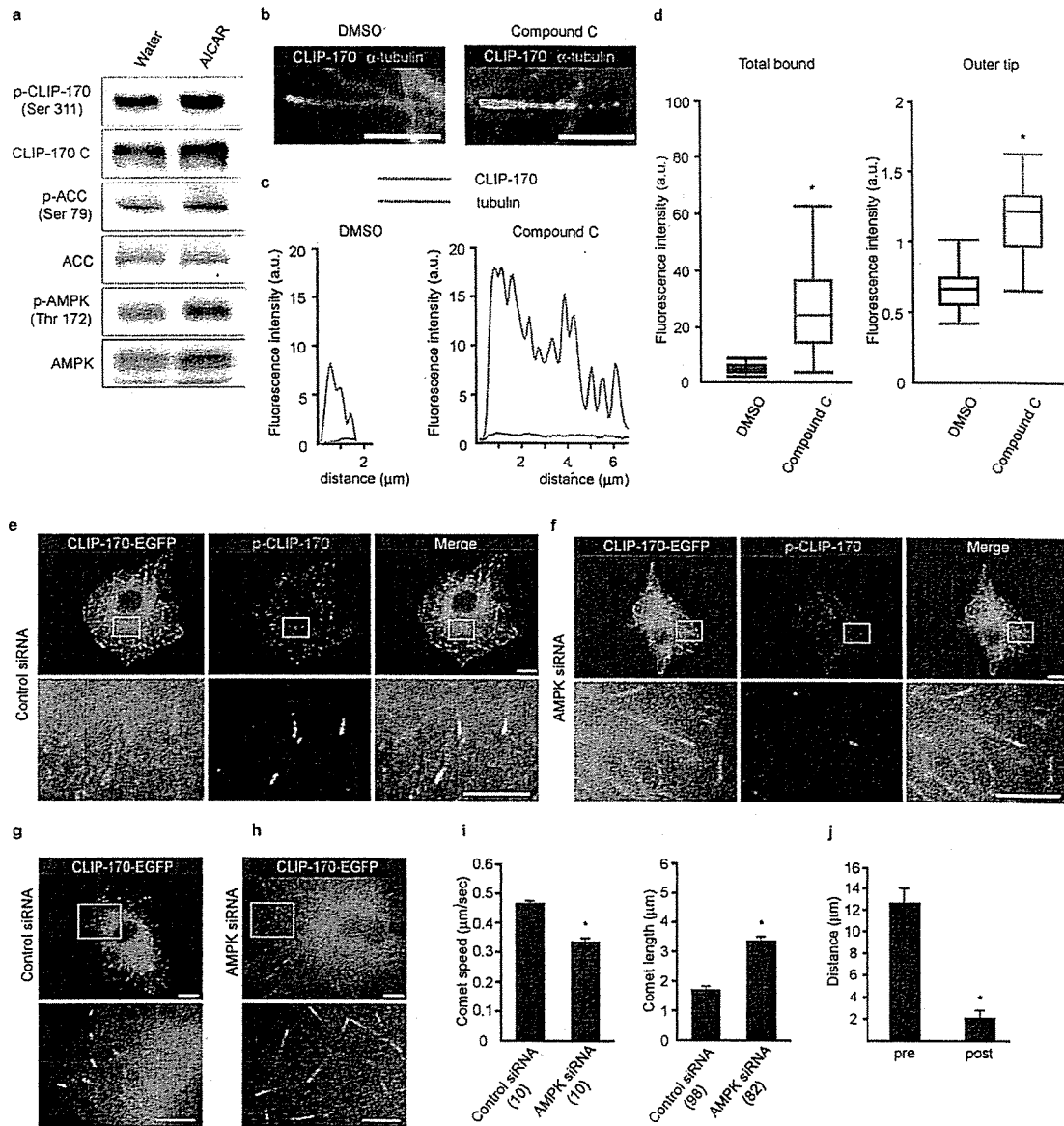


Figure S2 (a) Lysates from Vero cells treated with 2 mM of AICAR were analysed for the phosphorylation of CLIP-170, ACC, and AMPK. (b) Images of Vero cells that were immunostained with both a CLIP-170 C antibody and an α -tubulin antibody after DMSO (left) or Compound C (right) treatment. The scale bars represent 3 μ m. (c) Linescan analysis along the staining area by a CLIP-170 C (green) and an α -tubulin (red) antibody corresponding to figure (b), which shows the distribution of CLIP-170 treated with DMSO (left) or Compound C (right). (d) Box and whisker plots of the intensity of CLIP-170 bound to the whole tip (left) or to its outer part (right) after treatment with DMSO (blue) or Compound C (red). $n=30$, $*p<0.01$ versus DMSO. (e, f) Immunostained images of Vero cells stably expressing WT CLIP-170-EGFP (GFP image, each shown in the left) and treated with control siRNA (e) and siRNA targeting both AMPK α 1 and α 2 (f). These cells

were stained with a p-CLIP-170 antibody (centre). The merged images are shown on the right. The boxed regions in the panels are enlarged below each panel. The scale bars represent 10 μ m (upper row) and 5 μ m (lower row). (g, h) GFP images of Vero cells stably expressing CLIP-170-EGFP treated with control siRNA (g) or siRNA targeting both AMPK α 1 and α 2 (h). The white boxed regions in the panels are enlarged below each panel. The scale bars represent 10 μ m (g, h upper row) and 5 μ m (enlarged images of g, h). (i) Bar graphs showing the speed (left) and length (right) of a single comet of cells treated with control siRNA or siRNA targeting both AMPK α 1 and α 2. Values are means \pm s.e.m. n are given in parentheses. $*p<0.01$ versus control siRNA. (j) Bar graphs showing the shortening distance measured for 30 microtubules before and after Compound C treatment. Values represent means \pm s.e.m. $*p<0.01$ versus pre.

SUPPLEMENTARY INFORMATION

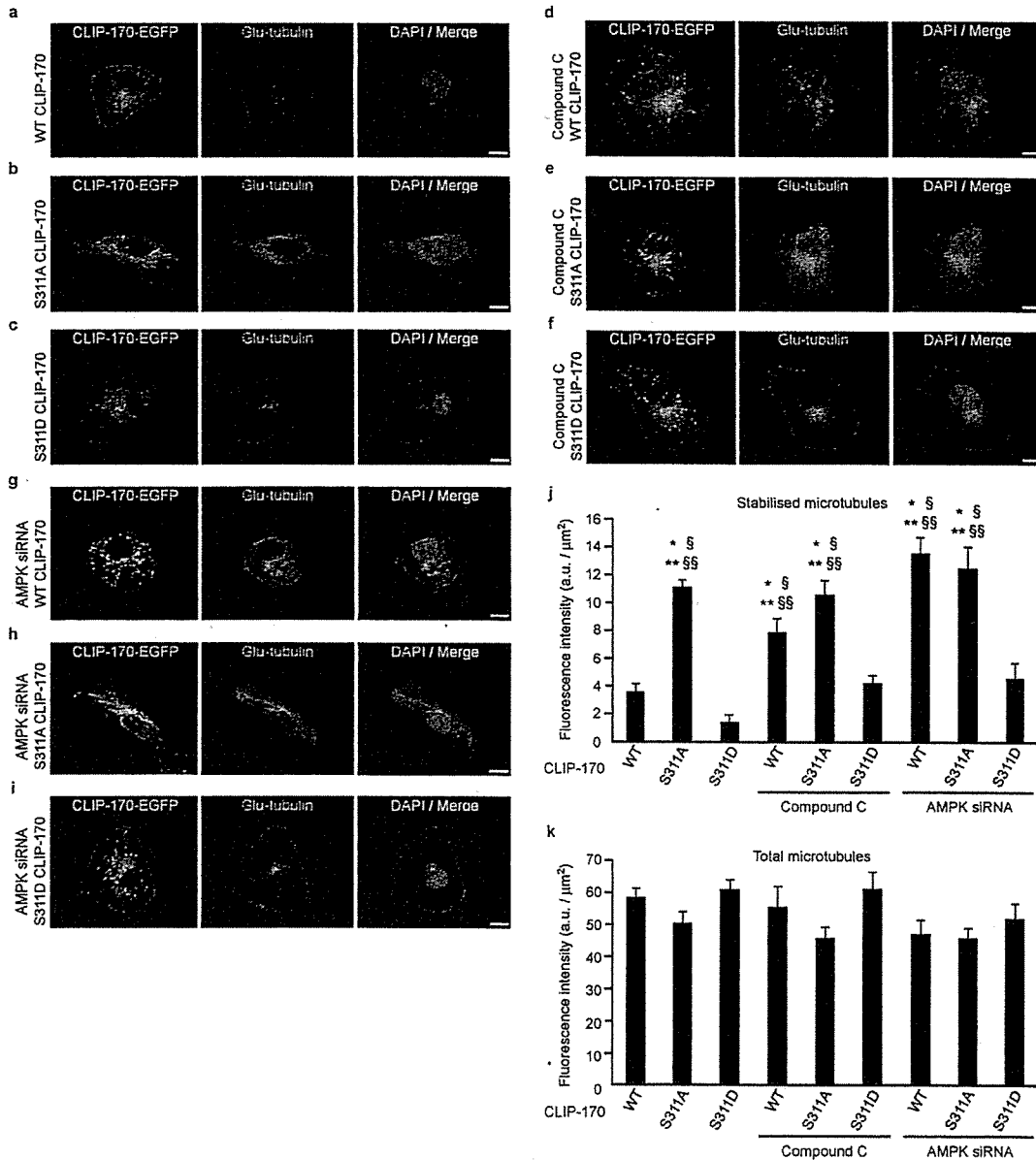


Figure S3 Loss of CLIP-170 phosphorylation increases stabilised microtubules. (a-c) Immunostained images of Vero cells transiently expressing WT (a), S311A (b) and S311D (c) CLIP-170-EGFP (GFP image, each left, green). These cells were stained with a detyrosinated (Glu) tubulin antibody (each centre, red) to visualise stable microtubules. (d-f) Immunostained images of Vero cells transiently expressing WT (d), S311A (e) and S311D (f) CLIP-170-EGFP (GFP image, each left, green) treated with Compound C. These cells were also stained with a detyrosinated (Glu) tubulin antibody (each centre, red). (g-i) Immunostained images of Vero cells expressing WT (g), S311A (h) and S311D (i) CLIP-170-EGFP (GFP image, each left, green) treated with siRNA targeting

both AMPK α 1 and α 2. These cells were also stained with a detyrosinated (Glu) tubulin antibody (each centre, red). DAPI stained nucleus (blue). Yellow dotted line indicates border zone of cells and fluorescence intensity in this area was measured. The scale bars represent 10 μm . (j, k) Bar graphs showing the amount of stabilised microtubules (j, detyrosinated tubulin antibody positive) and total microtubules (k, α -tubulin antibody positive) in various conditions. Y axis indicates fluorescence intensity divided by the area size of cells. Values are means \pm s.e.m. $n=10$ for each group. * $p<0.01$ versus WT CLIP-170. ** $p<0.01$ versus S311D CLIP-170. $\$p<0.01$ versus S311D CLIP-170 with Compound C. $\$\$p<0.01$ versus S311D CLIP-170 with AMPK siRNA.

SUPPLEMENTARY INFORMATION

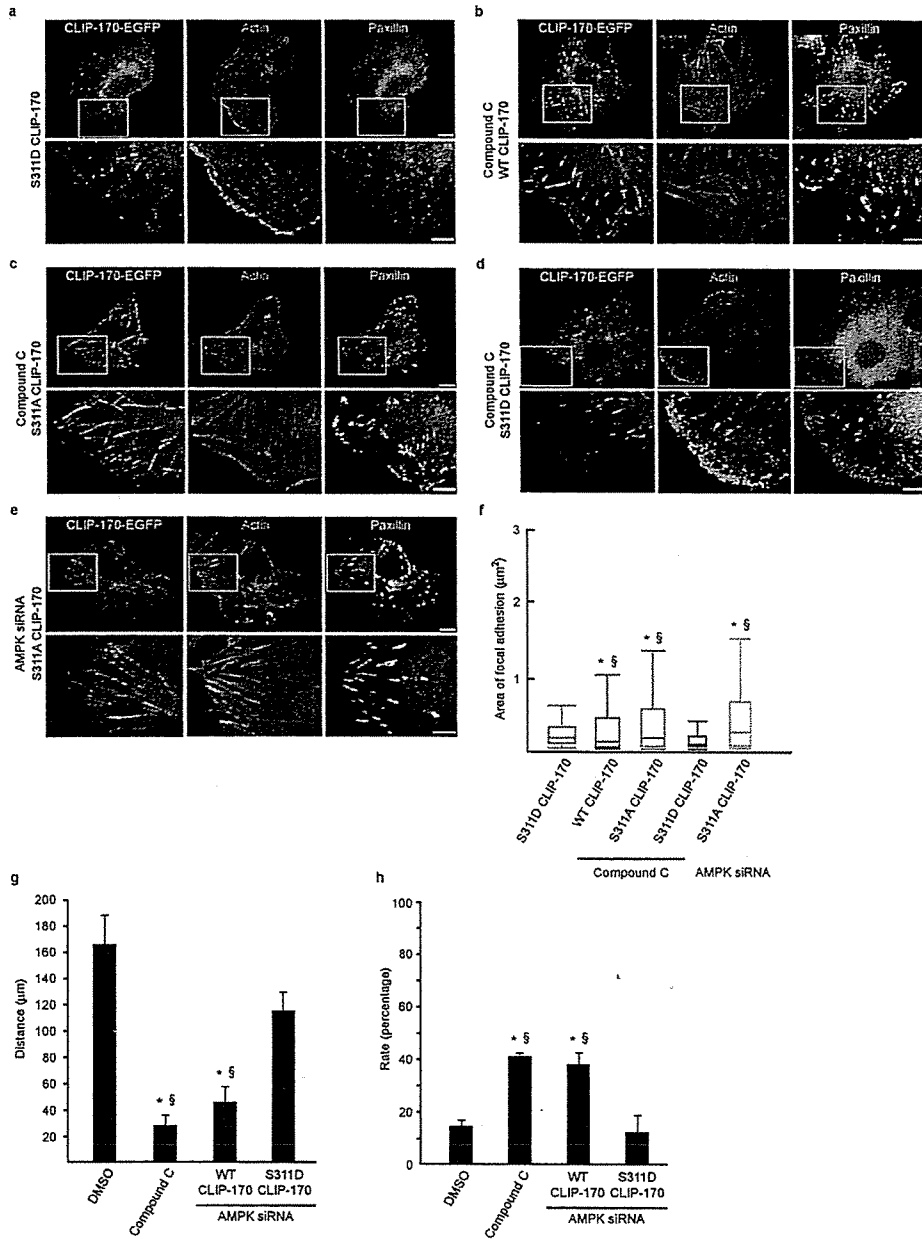


Figure S4 Loss of CLIP-170 phosphorylation increases the size of focal adhesion. (a) Immunostained images of Vero cells transiently expressing S311D CLIP-170-EGFP (GFP image, left). These cells were stained with fluorescein-conjugated phalloidin (centre) and a paxillin antibody (right) to visualise actin microfilaments and focal adhesions, respectively. (b-d) Immunostained images of Vero cells transiently expressing WT (b), S311A (c) and S311D (d) CLIP-170-EGFP (GFP image, left) treated with Compound C. These cells were also stained with fluorescein-conjugated phalloidin (centre) and a paxillin antibody (right). (e) Immunostained images of Vero cells transiently expressing S311A CLIP-170-EGFP (GFP image, left) treated with siRNA targeting both AMPK α 1 and α 2. These cells were also stained with fluorescein-conjugated phalloidin (centre) and a paxillin antibody (right). The white boxed regions in the panels are enlarged below each panel.

The scale bars represent 10 μ m (a-e, upper row) and 5 μ m (a-e, bottom row). (f) Box and whisker plots of the area stained with a paxillin antibody showing the 25th percentile (bottom line of each box), median (middle line of each box), 75th percentile (top line of each box), and the 5th and 95th percentiles (each whisker). $n=10$ for each group. * $p<0.01$ versus S311D CLIP-170. $\$p<0.01$ versus S311D CLIP-170 with Compound C. (g) Bar graph showing the distance of the gap closed 12 h after scratch. The cells were treated by either repeated administration of DMSO or Compound C, or transfected with WT or S311D CLIP-170 and siRNA targeting both AMPK α 1 and α 2. (h) Bar graphs showing the rate of cells that are perpendicular with respect to their migration direction in the first two layers of the leading cells. Values are means \pm s.e.m. of triplicates. * $p<0.01$ versus DMSO. $\$p<0.01$ versus S311D CLIP-170 with siRNA for AMPK.

SUPPLEMENTARY INFORMATION

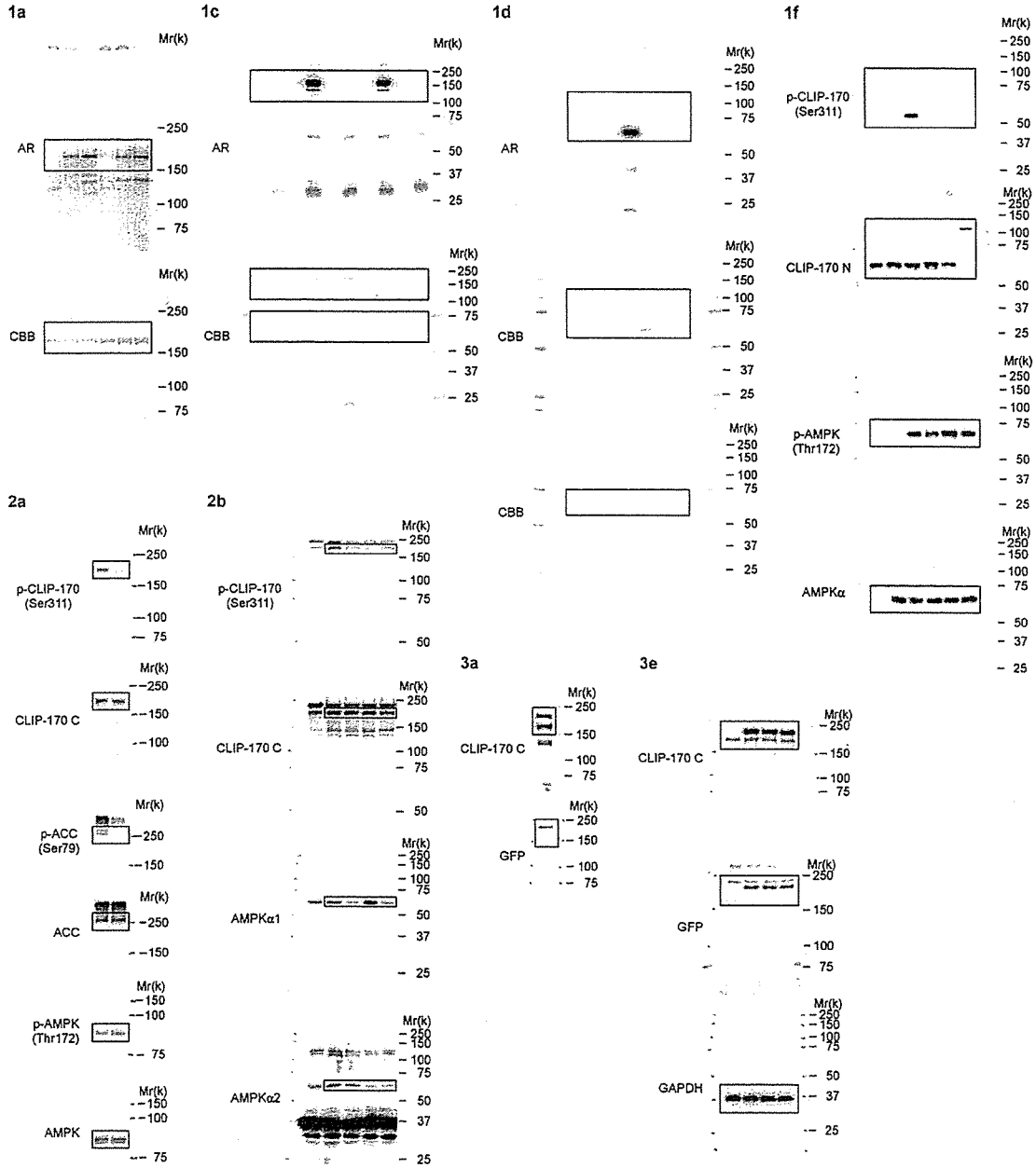


Figure S5 Uncropped versions of the immunoblots shown in the main figures.

SUPPLEMENTARY INFORMATION

Table S1 Properties of comet dynamics on microtubules in Vero cells transiently expressing different CLIP-170-EGFP constructs treated with various conditions. Cells were treated with compound C for 10 min or transfected with siRNA targeting both AMPK α 1 and α 2. Values are means \pm s.e.m. * p <0.01 versus WT CLIP-170 before Compound C. ** p <0.01 versus S311D CLIP-170 before Compound C. *** p <0.01 versus S311D CLIP-170 after Compound C. § p <0.01 versus WT CLIP-170 with siRNA for AMPK. §§ p <0.01 versus S311D CLIP-170 with siRNA for AMPK. WT, wild type.

treatment	CLIP-170	comet speed (μ m/sec)	comet length (μ m)
Before Compound C	WT	0.48 \pm 0.01 (n=10)	1.80 \pm 0.05 (n=132)
	S311A	0.26 \pm 0.02 (n=10) * **	3.20 \pm 0.11 (n=109) * **
	S311D	0.54 \pm 0.01 (n=10)	1.56 \pm 0.04 (n=99)
After Compound C	WT	0.34 \pm 0.01 (n=10) * ***	3.68 \pm 0.09 (n=115) * ***
	S311A	0.24 \pm 0.03 (n=10) * ***	3.42 \pm 0.11 (n=108) * ***
	S311D	0.48 \pm 0.02 (n=10)	1.62 \pm 0.05 (n=91)
AMPK siRNA	WT	0.34 \pm 0.02 (n=10)	3.29 \pm 0.15 (n=92)
	S311A	0.22 \pm 0.02 (n=10) § §§	3.32 \pm 0.12 (n=87) § §§
	S311D	0.50 \pm 0.01 (n=10)	1.49 \pm 0.03 (n=127)

SUPPLEMENTARY INFORMATION

Supplementary Movie Legends

Movie S1 Time lapse imaging of a cell stably expressing WT CLIP-170-EGFP and treated with DMSO (control). An EGFP image was obtained every second for 1 min at baseline and then 2 min, 10 min, and 20 min after administration of DMSO. The scale bar represents 10 μm .

Movie S2 Time lapse imaging of a cell stably expressing WT CLIP-170-EGFP and treated with Compound C. An EGFP image was obtained every second for 1 min at baseline and then 2 min, 10 min, and 20 min after administration of Compound C. The scale bar represents 10 μm .

Movie S3 Time lapse imaging of a cell stably expressing WT CLIP-170-EGFP and treated with siRNA targeting both AMPK α 1 and α 2. An EGFP image was obtained every second for 1 min. The scale bar represents 10 μm .

Movie S4 Time lapse imaging of a cell transiently expressing S311A CLIP-170-EGFP. An EGFP image was obtained every second for 1 min. The scale bar represents 10 μm .

Movie S5 Time lapse imaging of a cell transiently expressing S311D CLIP-170-EGFP. An EGFP image was obtained every second for 1 min. The scale bar represents 10 μm .


Movie S6 Time lapse imaging of a cell transiently expressing WT (upper half) or S311D (lower half) CLIP-170-EGFP treated with control siRNA (left) or siRNA targeting both AMPK α 1 and α 2 (right). An EGFP image was obtained every second for 1 min. The scale bar represents 10 μm .

Movie S7 Time lapse imaging of a cell stably expressing tubulin-EGFP before (left) and 10 minutes after (right) Compound C treatment. An EGFP image was obtained every second for 2 min. The scale bar represents 10 μm .

Movie S8 Cell migration assay. Time lapse imaging of cells transiently expressing WT CLIP-170 (upper left panel), S311A CLIP-170 (upper right panel), WT CLIP-170 treated with siRNA targeting both AMPK α 1 and α 2 (lower left panel) and S311D CLIP-170 treated with siRNA targeting both AMPK α 1 and α 2 (lower right panel). A DIC image (upper half), and a merged image of DIC and RFP (lower half) were obtained every 10 min for 12 h. An RFP image indicates effective delivery of siRNA for AMPK into each cell.

Circulation

JOURNAL OF THE AMERICAN HEART ASSOCIATION

American Heart Association 
Learn and Live...

Sirolimus-Eluting Stent Versus Balloon Angioplasty for Sirolimus-Eluting Stent Restenosis: Insights From the j-Cypher Registry

Mitsuru Abe, Takeshi Kimura, Takeshi Morimoto, Takuya Taniguchi, Futoshi Yamanaka, Kazuhiro Nakao, Nobuhito Yagi, Nobuaki Kokubu, Yoichiro Kasahara, Yu Kataoka, Yoritaka Otsuka, Atsushi Kawamura, Shunichi Miyazaki, Koichi Nakao, Kenji Horiuchi, Akira Ito, Hiroshi Hoshizaki, Ren Kawaguchi, Manabu Setoguchi, Tsukasa Inada, Koichi Kishi, Hiroki Sakamoto, Nobuyuki Morioka, Masao Imai, Hiroki Shiomi, Hiroshi Nonogi, Kazuaki Mitsudo and for the j-Cypher Registry Investigators

Circulation 2010;122:42-51; originally published online Jun 21, 2010;

DOI: 10.1161/CIRCULATIONAHA.109.905802

Circulation is published by the American Heart Association, 7272 Greenville Avenue, Dallas, TX 75214

Copyright © 2010 American Heart Association. All rights reserved. Print ISSN: 0009-7322. Online ISSN: 1524-4539

The online version of this article, along with updated information and services, is located on the World Wide Web at:

<http://circ.ahajournals.org/cgi/content/full/122/1/42>

Data Supplement (unedited) at:

<http://circ.ahajournals.org/cgi/content/full/CIRCULATIONAHA.109.905802/DC1>

Subscriptions: Information about subscribing to *Circulation* is online at <http://circ.ahajournals.org/subscriptions/>

Permissions: Permissions & Rights Desk, Lippincott Williams & Wilkins, a division of Wolters Kluwer Health, 351 West Camden Street, Baltimore, MD 21202-2436. Phone: 410-528-4050. Fax: 410-528-8550. E-mail: journalpermissions@lww.com

Reprints: Information about reprints can be found online at <http://www.lww.com/reprints>

Interventional Cardiology

Sirolimus-Eluting Stent Versus Balloon Angioplasty for Sirolimus-Eluting Stent Restenosis: Insights From the j-Cypher Registry

Mitsuru Abe, MD; Takeshi Kimura, MD; Takeshi Morimoto, MD, MPH; Takuya Taniguchi, MD; Futoshi Yamanaka, MD; Kazuhiro Nakao, MD; Nobuhito Yagi, MD; Nobuaki Kokubu, MD; Yoichiro Kasahara, MD; Yu Kataoka, MD; Yoritaka Otsuka, MD; Atsushi Kawamura, MD; Shunichi Miyazaki, MD; Koichi Nakao, MD; Kenji Horiuchi, MD; Akira Ito, MD; Hiroshi Hoshizaki, MD; Ren Kawaguchi, MD; Manabu Setoguchi, MD; Tsukasa Inada, MD; Koichi Kishi, MD; Hiroki Sakamoto, MD; Nobuyuki Morioka, MD; Masao Imai, MD; Hiroki Shiomi, MD; Hiroshi Nonogi, MD; Kazuaki Mitsudo, MD; for the j-Cypher Registry Investigators

Background—Optimal treatment strategies for restenosis of sirolimus-eluting stents (SES) have not been adequately addressed yet.

Methods and Results—During the 3-year follow-up of 12 824 patients enrolled in the j-Cypher registry, 1456 lesions in 1298 patients underwent target-lesion revascularization (TLR). Excluding 362 lesions undergoing TLR for stent thrombosis or TLR using treatment modalities other than SES or balloon angioplasty (BA), 1094 lesions with SES-associated restenosis in 990 patients treated with either SES (537 lesions) or BA (557 lesions) constituted the study population for the analysis of recurrent TLR and stent thrombosis after the first TLR. Excluding 24 patients with both SES- and BA-treated lesions, 966 patients constituted the analysis set for the mortality outcome. Cumulative incidence of recurrent TLR in the SES-treated restenosis lesions was significantly lower than that in the BA-treated restenosis lesions (23.8% versus 37.7% at 2 years after the first TLR; $P < 0.0001$). Among 33 baseline variables evaluated, only hemodialysis was identified to be the independent risk factor for recurrent TLR by a multivariable logistic regression analysis. After adjusting for confounders, repeated SES implantation was associated with a strong treatment effect in preventing recurrent TLR over BA (odds ratio, 0.44; 95% confidence interval, 0.32 to 0.61; $P < 0.0001$). The 2-year mortality and stent thrombosis rates between the SES- and the BA-treated groups were 10.4% versus 10.8% ($P = 0.4$) and 0.6% versus 0.6%, respectively.

Conclusions—Repeated implantation of SES for SES-associated restenosis is more effective in preventing recurrent TLR than treatment with BA, without evidence of safety concerns. (*Circulation*. 2010;122:42-51.)

Key Words: restenosis ■ angioplasty ■ stents ■ balloon

Although sirolimus-eluting stents (SES) significantly reduce the rates of angiographic restenosis and target-lesion revascularization (TLR),¹ the widespread use of SES in complex lesions was reported to be associated with higher TLR rates in real-world clinical practice.^{2,3}

In patients with bare-metal stent restenosis, several prospective multicenter randomized trials demonstrated that the implantation of SES was superior to balloon angioplasty (BA),^{4,5} implantation of bare-metal stent,⁶ or vascular brachytherapy.⁷ Although a few previous small observational studies compared the use of SES for restenosis of SES with the use of BA in preventing recurrent TLR,⁸⁻¹⁰ there is no report from either randomized trials or large-scale observational

Editorial see p 5
Clinical Perspective on p 51

Received September 2, 2009; accepted April 22, 2010.

From the Division of Cardiology (M.A., T.T., F.Y., Kazuhiro Nakao, N.Y., N.K., Y. Kasahara, Y. Kataoka, Y.O., H.N.), National Cardiovascular Center, Suita; Department of Cardiovascular Medicine (T.K., H. Shiomi), and Center for Medical Education (T.M.), Graduate School of Medicine, Kyoto University, Kyoto; Division of Internal Medicine (A.K.), Central Hospital, Fukuyama; Division of Cardiology (S.M.), Department of Internal Medicine, Kinki University School of Medicine; Division of Cardiology (A.I.), Osaka City General Hospital; Division of Cardiology (T.I.), Osaka Red Cross Hospital; Division of Cardiology (N.M.), Kishiwada Tokushukai Hospital, Osaka; Division of Cardiology (Koichi Nakao, K.H.), Saiseikai Kumamoto Hospital Cardiovascular Center, Kumamoto; Division of Cardiology (H.H., R.K.), Gunma Prefectural Cardiovascular Center, Gunma; Division of Cardiology (M.S.), National Hospital Organization Kagoshima Medical Center, Kagoshima; Division of Cardiology (K.K.), Tokushima Red Cross Hospital, Tokushima; Division of Cardiology (H. Sakamoto), Japanese Red Cross Society Wakayama Medical Center, Wakayama; Division of Cardiology (M.I., K.M.), Kurashiki Central Hospital, Kurashiki, Japan.

The online-only Data Supplement is available with this article at <http://circ.ahajournals.org/cgi/content/full/CIRCULATIONAHA.109.905802/DC1>.

Correspondence to Dr Takeshi Kimura, Department of Cardiovascular Medicine, Graduate School of Medicine, Kyoto University, 54 Shogoin, Kawahara-cho, Sakyo-ku, Kyoto, 606-8507, Japan. E-mail taketaka@kuhp.kyoto-u.ac.jp

© 2010 American Heart Association, Inc.

Circulation is available at <http://circ.ahajournals.org>

DOI: 10.1161/CIRCULATIONAHA.109.905802

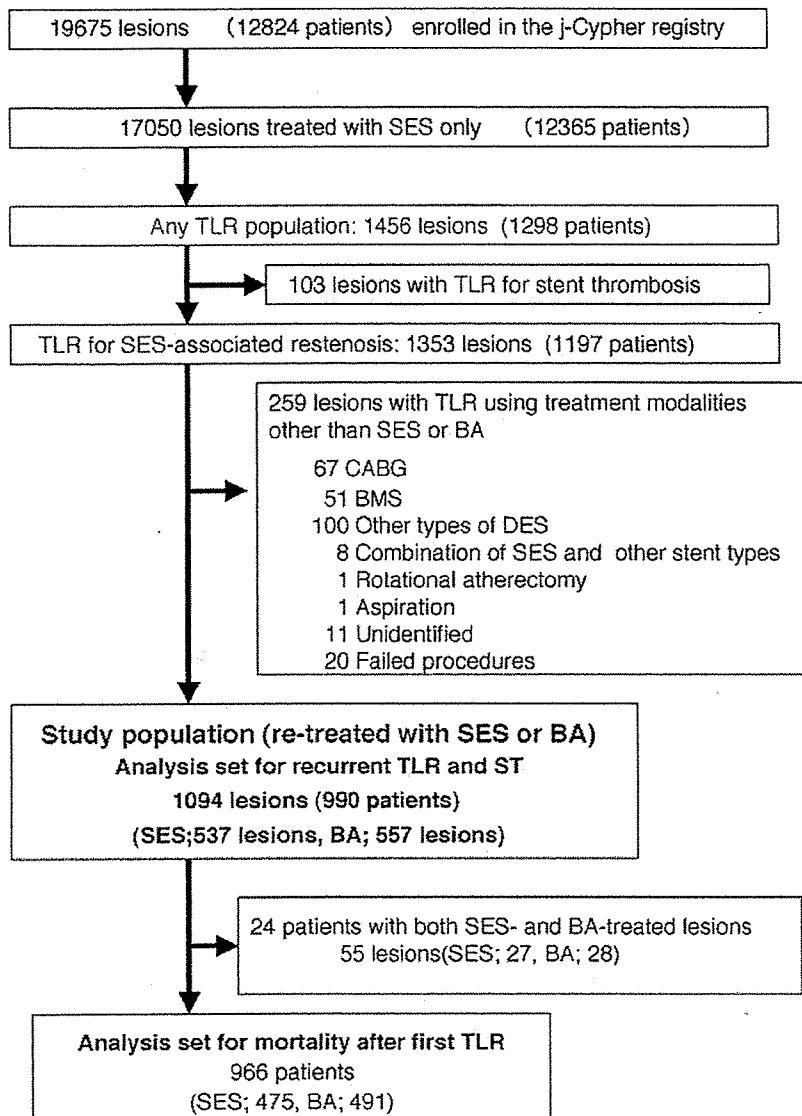


Figure 1. Patient and lesion flowchart for the current analysis. BMS indicates bare-metal stent; CABG, coronary artery bypass grafting; and DES, drug-eluting stent.

studies investigating the efficacy of SES for restenosis associated with SES use.

Although there are potential concerns for increased risk of death or stent thrombosis (ST) associated with repeated SES implantation for the treatment of SES restenosis, safety issues of this treatment strategy have not been adequately addressed yet.

In this report, we compared the incidences of recurrent TLR, ST, and mortality between the 2 groups of lesions with SES-associated restenosis treated with either SES or BA by analyzing the 3-year follow-up data from the large-scale cohort of the j-Cypher registry.³

Methods

Study Population

The j-Cypher registry is a physician-initiated prospective multicenter observational study in Japan enrolling consecutive patients undergoing SES implantation, and the study protocol and main results were reported previously.³ The relevant review boards in all 37 partici-

pating centers (see online-only Data Supplement) approved the study protocol. Written informed consent was obtained from all patients.

Follow-up data were obtained until October 2008 from hospital charts or by contacting patients and/or referring physicians at 30 days, 6 months, 1 year, and yearly thereafter. Data on TLR and the treatment modalities for TLR were prospectively collected. Clinical follow-up was continued after the TLR events.

Among 12 824 patients with 19 675 lesions enrolled in the registry, 17 050 lesions in 12 365 patients were treated exclusively with SES. During the 3-year follow-up (median, 829 days; interquartile range (IQR), 498 to 1108 days), 1456 lesions (8.5%) in 1298 patients underwent TLR. Multiple lesions within the same patient were considered to be independent observations for lesion-specific analyses. Cumulative incidences of TLR based on lesion estimated by the Kaplan-Meier method were 5.7% at 1 year, 8.1% at 2 years, and 10.0% at 3 years. Excluding 103 lesions with TLR for ST, 1353 lesions underwent TLR for SES-associated restenosis. Excluding 259 lesions with TLR using treatment modalities other than SES or BA, 1094 lesions with SES-associated restenosis in 990 patients (1 lesion in 899 patients, 2 lesions in 79 patients, 3 lesions in 11 patients, and 4 lesions in 1 patient) treated either with SES (537 lesions) or BA (557 lesions) constituted the study population for the

Table 1. Baseline Characteristics of Patients Undergoing TLR by SES or BA for SES-Associated Restenosis

Characteristics	SES (n=475)	BA (n=491)	P
Age, y	67.4±10.2	67.7±10.0	0.6
Age ≥80 y	48 (10)	52 (11)	0.8
Male sex	366 (77)	382 (78)	0.8
Body mass index	23.7±3.5	23.9±3.3	0.4
Body mass index ≥25.0	163 (34)	171 (35)	0.9
Hypertension	361 (76)	373 (76)	1.0
Diabetes mellitus	225 (47)	286 (58)	0.0007
Insulin therapy	62 (13)	101 (21)	0.002
Current smoking	89 (19)	86 (18)	0.6
eGFR <30, without hemodialysis	23 (6)	26 (6)	0.7
Hemodialysis	61 (13)	76 (15)	0.2
Acute coronary syndrome	110 (23)	95 (19)	0.1
STEMI	44 (9)	30 (6)	0.06
Non-STEMI	10 (2)	8 (2)	0.6
Unstable angina pectoris	56 (12)	57 (12)	0.9
Prior myocardial infarction	135 (28)	149 (30)	0.5
Prior stroke	51 (11)	49 (10)	0.7
Peripheral vascular disease	82 (17)	65 (13)	0.08
Prior heart failure	60 (13)	57 (12)	0.6
Diseased vessels			0.1
Single-vessel disease	163 (34)	183 (37)	
Double-vessel disease	135 (28)	136 (28)	
Triple-vessel disease	82 (17)	76 (15)	
Unprotected LMCA	36 (8)	53 (11)	
Prior CABG	59 (12)	43 (9)	
Ejection fraction (%)	57.4±13.7	55.5±13.6	0.051
Ejection fraction ≤40%	55 (12)	57 (12)	1.0
Emergent procedure	43 (9)	39 (8)	0.5

Ejection fraction in 138 patients (59 in SES and 79 in BA) was missing. Ejection fraction >40% was imputed in patients with missing values for ejection fraction. CABG indicates coronary artery bypass grafting; eGFR, estimated glomerular filtration rate; LMCA, left main coronary artery; and STEMI, ST-segment elevation myocardial infarction. Values are mean±SD or n (%).

current analysis (Figure 1). The duration of follow-up after the first TLR was not statistically different between SES-treated (median, 627 days; IQR, 343 to 877 days) and BA-treated lesions (median, 580 days; IQR, 292 to 844 days; $P=0.1$). Incidences of recurrent TLR and ST on lesion basis after the first TLR were compared between the SES-treated lesions and the BA-treated lesions. Excluding 24 patients with both SES- and BA-treated lesions, 966 patients constituted the analysis set for the mortality outcome after first TLR.

Choice of the treatment strategy at the time of TLR was left to the discretion of the individual operators. Among 557 lesions treated with BA, "plain old" balloon angioplasty was performed in 471 lesions, and cutting balloon was used in 86 lesions.

Recommended antiplatelet regimen after SES implantation was aspirin (≥81 mg daily) indefinitely and thienopyridine (200 mg of ticlopidine or 75 mg of clopidogrel daily) for at least 3 months. Antiplatelet regimen after BA for SES-associated restenosis and duration of antiplatelet therapy were left to the discretion of each attending physician.

Outcomes and Definitions

The primary outcome for the current analysis is recurrent TLR after the first TLR for SES-associated restenosis. TLR was defined as

Table 2. Baseline Lesion and Procedural Characteristics of Lesions Undergoing TLR by SES or BA for SES-Associated Restenosis

	SES (n=537)	BA (n=557)	P
Lesion location			0.003
LAD	223 (42)	200 (36)	
LCx	66 (12)	101 (18)	
RCA	205 (38)	210 (38)	
LMCA	22 (4)	37 (7)	
Saphenous vein graft	19 (4)	7 (1)	
De novo lesion	388 (72)	359 (64)	0.006
In-stent restenosis	80 (15)	145 (26)	<0.0001
STEMI culprit lesion	22 (4)	15 (3)	0.2
Ostial location	64 (12)	83 (15)	0.1
Chronic total occlusion	57 (11)	81 (15)	0.050
Severe calcification	84 (16)	89 (16)	0.9
Bifurcation lesion	121 (23)	143 (26)	0.2
Side branch stenting	34 (6)	58 (10)	0.01
Complex lesion (B2&C)	423 (79)	458 (82)	0.1
Lesion length ≥30 mm	125 (23)	169 (30)	0.01
Reference diameter <2.5 mm	166 (31)	170 (31)	0.9
Use of intravascular ultrasound	258 (48)	210 (38)	0.0005
Direct stenting	100 (19)	55 (10)	<0.0001
Additional dilatation	267 (50)	281 (50)	0.8
Maximum inflation pressure, atm	18.2±3.4	18.5±3.5	0.2
No. of stents used, median (IQR)	1 (1–2)	1 (1–2)	0.0003
Length of stents used, median (IQR), mm	28 (18–46)	33 (23–51)	0.0003
Minimal stent size, median (IQR), mm	3.0 (2.5–3.0)	2.5 (2.5–3.0)	0.001

Values are mean±SD or n (%) unless otherwise indicated. Maximum inflation pressure in 4 lesions (2 in SES and 2 in BA) and minimal stent size in 1 lesion (1 in BA) were missing. LAD indicates left anterior descending coronary artery; LCx, left circumflex coronary artery; and RCA, right coronary artery. Other abbreviations as in Table 1.

either percutaneous coronary intervention or coronary artery bypass grafting surgery due to restenosis or ST of the target lesion that included the proximal and distal edge segments and the ostium of the side branches. Retreatment for restenosis in the side branch of a bifurcation lesion was also included in TLR. There was no distinction of whether TLR was clinically or angiographically driven.

The secondary outcomes included mortality and ST after the first TLR. ST was defined as definite ST according to the Academic Research Consortium definition.¹¹ In comparing the incidences of recurrent TLR and ST between SES and BA treatment, analyses were done on a lesion basis. Lesion was defined as the area covered by single or multiple overlapping stents. When 2 stents were placed without overlap, these 2 areas were regarded as 2 separate lesions. When multiple overlapping stents were placed from left main coronary artery to left anterior descending coronary artery, these areas were regarded as 2 separate lesions despite placement of overlapping stents. Lesions located within 3 mm from the ostium were regarded as ostial lesions.

Coronary angiographic parameters such as reference vessel diameter, percent diameter stenosis, and lesion length were assessed in each participating center either by visual assessment or quantitative angiographic measurement. A bifurcation lesion was defined as that involving a side-branch of ≥2.2 mm in diameter. Lesion complexity

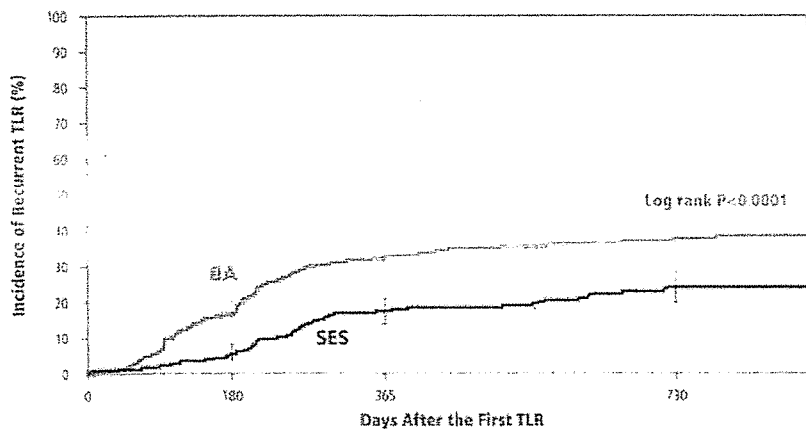


Figure 2. Cumulative incidences of recurrent TLR in SES-associated restenosis lesions treated with SES as compared with those treated with BA. Abbreviations as in Figure 1.

Days after the first TLR	0	180	365	730
BA				
Cumulative incidence		16.8%	32.4%	37.7%
Number of events		85	154	171
Number of lesions at risk	557	387	270	123
SES				
Cumulative incidence		5.7%	17.0%	23.8%
Number of events		28	77	97
Number of lesions at risk	537	440	327	156

and angiographic patterns of restenosis were determined by the site investigators according to the American Heart Association/American College of Cardiology lesion type classification¹² and the scheme of Mehran et al,¹³ respectively. Angiographic data at first TLR were collected in 1045 lesions (96%) of 1094 lesions with first TLR. Outcome according to angiographic patterns of restenosis was evaluated in 1022 lesions treated either with SES (508 lesions) or BA (514 lesions), excluding 23 lesions with retreatment for restenosis in the side branch of a bifurcation lesion.

Statistical Analysis

Continuous variables are presented with mean±SD or median and IQR, and categorical variables are expressed as number and percentages. Categorical variables were compared with the χ^2 test. Continuous variables were compared with the *t* test or Wilcoxon rank-sum test based on the distribution. Incidences of the primary and secondary outcomes were estimated by the Kaplan-Meier method, and differences were assessed with the log-rank test.

In an attempt to adjust for the differences in baseline clinical, angiographic, and procedural characteristics between the SES- and BA-treated lesions, a multivariable logistic regression model was constructed using recurrent TLR within 1 year after the first TLR as dependent variable and 33 baseline factors as well as the treatment strategy of SES-associated restenosis (SES or BA treatment) as independent variables. Baseline factors used for analysis were those present at the time of initial entry into the j-Cypher registry, but not those present at the time of the first TLR. A multivariable logistic regression model instead of Cox proportional hazard model was used, because restenosis has been well known to be a time-related phenomenon, and also the timing of TLR could be highly influenced by physicians' and patients' decision. Actually, proportional hazard assumption for the variables was not verified. By using a logistic regression model, we could minimize the influence of the timing of TLR on the analysis of risk factors for recurrent TLR. Eligible lesions for logistic regression analysis included those lesions with recurrent TLR events within the first year after the first TLR relative to those lesions with complete follow-up and without recurrent TLR events at 1 year after the first TLR. Continuous variables were dichotomized by clinically meaningful reference values as shown in Table 1 and 2. We selected variables with $P < 0.05$ in the univariate analyses together with the treatment strategy of SES-associated restenosis

(SES or BA) and included them simultaneously in a multivariable model. Independent risk factors for recurrent TLR were expressed as odds ratios (ORs) and their 95% confidence intervals.

All analyses were conducted by physicians (M.A. and T.K.) and a statistician (T.M.) using JMP 8 (SAS Institute Inc, Cary, NC), and reported *P* values were 2-sided. The study sponsor was not involved in the study design; in the collection, analysis, and interpretation of data; writing of the report; or decision to submit the manuscript for publication.

Results

Baseline Characteristics

Baseline patient, lesion, and procedural characteristics were significantly different between SES- and BA-treated lesions. Patients treated with BA were more likely to have diabetes mellitus, especially diabetes on insulin therapy (Table 1).

Lesions treated with SES were more frequently saphenous vein graft lesions, de novo lesions, and those treated with use of intravascular ultrasound and direct stenting. Lesions treated with BA were more likely to be left circumflex coronary artery lesions, in-stent restenosis, side branch stenting, and long lesion length (≥ 30 mm), and they were treated with a greater number and longer stents (Table 2).

Incidence and Risk Factors of Recurrent TLR

Cumulative incidence of recurrent TLR in SES-treated lesions was significantly lower than that in BA-treated lesions (17.0% and 23.8% versus 32.4% and 37.7% at 1 year and 2 years after the first TLR, respectively; $P < 0.0001$) (Figure 2). Late catch-up phenomenon was observed in both groups comparing year 1 and 2 at follow-up, and there does not appear to be a significant difference between both treatment strategies.

Risk factors of recurrent TLR were evaluated by univariate (Table 3) and multivariate analysis (Table 4). Lesions included in the analysis for risk factors of recurrent TLR were 231 lesions

Table 3. Univariate Correlates of Recurrent TLR Within 1 Year After Treatment of SES-Associated Restenosis

Variable	Recurrent TLR		P
	Yes (n=231)	No (n=593)	
SES implantation	77 (33)	325 (55)	<0.0001
Age ≥80 y	25 (11)	47 (8)	0.2
Male sex	179 (77)	455 (77)	0.8
Body mass index ≥25.0	68 (29)	214 (36)	0.07
Hypertension	175 (76)	449 (76)	1.0
Diabetes mellitus	132 (57)	323 (54)	0.5
Insulin therapy	48 (21)	105 (18)	0.3
Current smoking	35 (15)	111 (19)	0.2
Treatment for hypercholesterolemia	115 (50)	272 (46)	0.3
eGFR <30, without hemodialysis	15 (6)	24 (4)	0.1
Hemodialysis	46 (20)	67 (11)	0.002
Acute coronary syndrome	53 (23)	124 (21)	0.5
Prior myocardial infarction	56 (24)	160 (27)	0.4
Prior stroke	27 (12)	60 (10)	0.5
Peripheral vascular disease	34 (15)	85 (14)	0.9
Prior heart failure	39 (17)	66 (11)	0.03
Diseased vessels			0.2
Single vessel disease	75 (32)	192 (32)	
Double vessel disease	55 (24)	182 (31)	
Triple vessel disease	50 (22)	103 (17)	
Unprotected LMCA	28 (12)	56 (9)	
Prior CABG	23 (10)	60 (10)	
Ejection fraction ≤40	29 (13)	64 (11)	0.5
Emergent procedure	24 (10)	49 (8)	0.3
Lesion location			0.7
LAD	79 (34)	234 (39)	
LCx	39 (17)	82 (14)	
RCA	93 (40)	228 (38)	
LMCA	12 (5)	34 (6)	
Saphenous vein graft	7 (3)	13 (2)	
De novo lesion	142 (61)	412 (69)	0.03
In-stent restenosis	62 (27)	113 (19)	0.02
STEMI culprit lesion	4 (2)	25 (4)	0.06
Ostial location	33 (14)	79 (13)	0.7
Chronic total occlusion	28 (12)	72 (12)	1.0
Severe calcification	52 (23)	85 (14)	0.006
Bifurcation lesion	58 (25)	140 (24)	0.7
Side branch stenting	21 (9)	48 (8)	0.6
Complex lesion (B2&C)	190 (82)	481 (81)	0.7
Lesion length ≥30 mm	71 (31)	156 (26)	0.2
Reference diameter <2.5 mm	65 (28)	182 (31)	0.5
Use of intravascular ultrasound	86 (37)	275 (46)	0.02
Direct stenting	17 (7)	83 (14)	0.006
Additional dilatation	111 (48)	308 (52)	0.3

Values are mean±SD or n (%) unless otherwise indicated. Abbreviations as in Tables 1 and 2.

Table 4. Univariate and Multivariable Analysis for the Risk Factors for Recurrent TLR Within 1 Year After Treatment of SES-Associated Restenosis

Variable	Univariate Odds Ratio (95% CI)	Multivariate	
		Odds Ratio (95% CI)	P
SES implantation (vs BA)	0.41 (0.30–0.56)	0.44 (0.32–0.61)	<0.0001
Hemodialysis	1.95 (1.29–2.94)	1.61 (1.02–2.53)	0.04
Prior heart failure	1.62 (1.05–2.48)	1.44 (0.91–2.26)	0.1
De novo lesion	0.70 (0.51–0.96)	0.90 (0.55–1.51)	0.7
In-stent restenosis	1.56 (1.09–2.22)	1.21 (0.69–2.16)	0.5
Severe calcification	1.74 (1.18–2.54)	1.53 (0.99–2.33)	0.054
Use of IVUS	0.69 (0.50–0.94)	0.78 (0.56–1.08)	0.1
Direct stenting	0.49 (0.27–0.82)	0.70 (0.39–1.22)	0.2

CI indicates confidence interval; IVUS, intravascular ultrasound.

with recurrent TLR events within the first year after the first TLR and 593 lesions that completed 1-year follow-up without recurrent TLR after the first TLR, excluding 270 lesions followed up less than 1 year without TLR. Univariate correlates of recurrent TLR included hemodialysis, prior heart failure, de novo lesion, in-stent restenosis, severe calcification, use of intravascular ultrasound, and direct stenting (Table 3).

Among 33 baseline variables evaluated, only hemodialysis was identified to be the independent risk factor for recurrent TLR by a multivariable logistic regression analysis (Table 4). After adjustment for the differences in baseline characteristics, repeated SES implantation to treat SES-associated restenosis as compared with treatment with BA was significantly associated with less recurrent TLR (OR, 0.44; 95% confidence interval, 0.32 to 0.61; $P<0.0001$).

Angiographic Results

Reference vessel diameter in SES-treated lesions was larger than that in BA-treated lesions. However, percent diameter stenosis and minimal luminal diameter were similar between the 2 groups (Table 5).

Relative to angiographic patterns of SES-associated restenosis, focal pattern was more prevalent than nonfocal pattern (Figure 3). Angiographic patterns of SES-associated restenosis were similarly distributed in the SES-treated lesions and

Table 5. Angiographic Findings at the First TLR

	SES (n=508)	BA (n=514)	P
Reference diameter, mm	2.95±0.48	2.88±0.45	0.02
Minimal lumen diameter, mm	0.70±0.46	0.67±0.47	0.3
Percent diameter stenosis	76.4±14.7	76.8±15.6	0.6
Angiographic patterns of restenosis			0.3
Monofocal	376 (74)	384 (75)	
Multifocal	32 (6)	38 (7)	
Diffuse	46 (9)	54 (11)	
Proliferative	20 (4)	10 (2)	
Occlusive	34 (7)	28 (5)	

Values are mean±SD or n (%).

Angiographic Patterns of SES-associated Restenosis

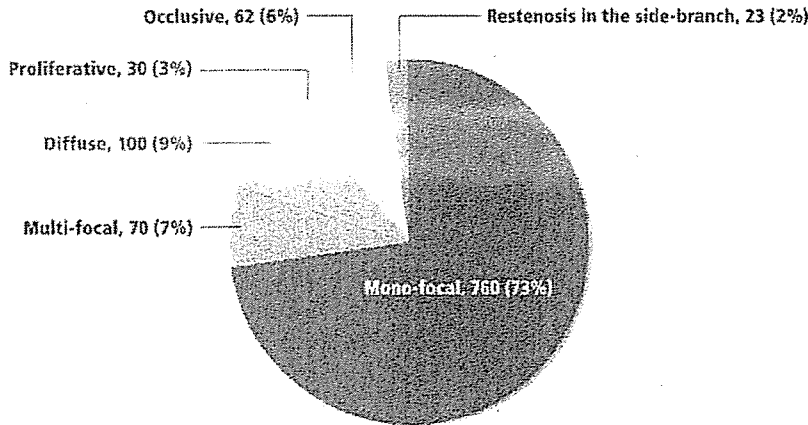


Figure 3. Distribution of angiographic patterns of SES-associated restenosis.

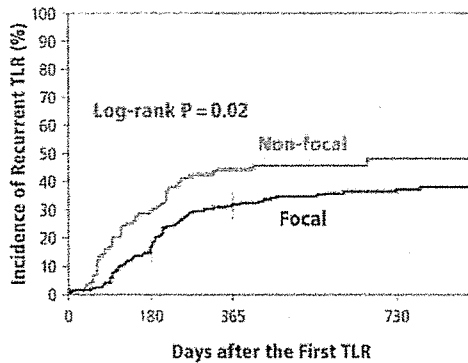
the BA-treated lesions. Cumulative incidence of recurrent TLR events for nonfocal restenosis was significantly higher than that for focal restenosis in the BA-treated lesions, but not in the SES-treated lesions (Figure 4). Cumulative incidence of recurrent TLR events for the SES-treated lesions was significantly lower than that for the BA-treated lesions in both focal and nonfocal restenosis (Figure 5).

Mortality and Stent Thrombosis

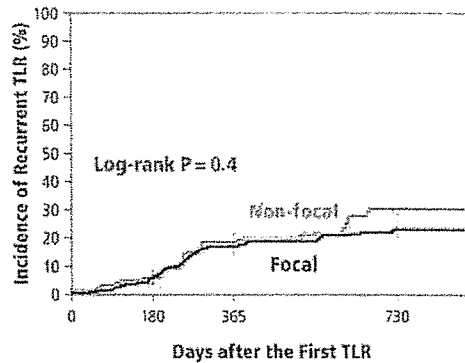
Incidence of death after first TLR were evaluated among 475 patients treated with only SES and 491 patients treated with only BA for SES-associated restenosis. The overall mortality rates were not significantly different between SES- and BA-treated patients (4.5% and 10.4% versus 6.6% and 10.8% at 1 year and 2 years after the first TLR, respectively; $P=0.4$) (Figure 6).

Cumulative Incidence of Recurrent TLR

A BA-treated Lesions



B SES-treated Lesions



Days after the First TLR	0	180	365	730		0	180	365	730	
Non-focal						Non-focal				
Cumulative incidence		29.8%	43.8%	47.7%			5.4%	19.5%	30.1%	
Number of events		25	35	37			5	16	21	
Number of lesions at risk	92	54	38	22		100	80	59	23	
Focal						Focal				
Cumulative incidence		14.7%	31.5%	36.8%			5.6%	16.8%	23.0%	
Number of events		56	112	125			21	58	72	
Number of lesions at risk	422	301	206	90		403	337	249	120	

Figure 4. Cumulative incidences of recurrent TLR according to the patterns of SES-associated restenosis (focal versus nonfocal) in (A) the BA-treated lesions and (B) the SES-treated lesions.

Cumulative Incidence of Recurrent TLR

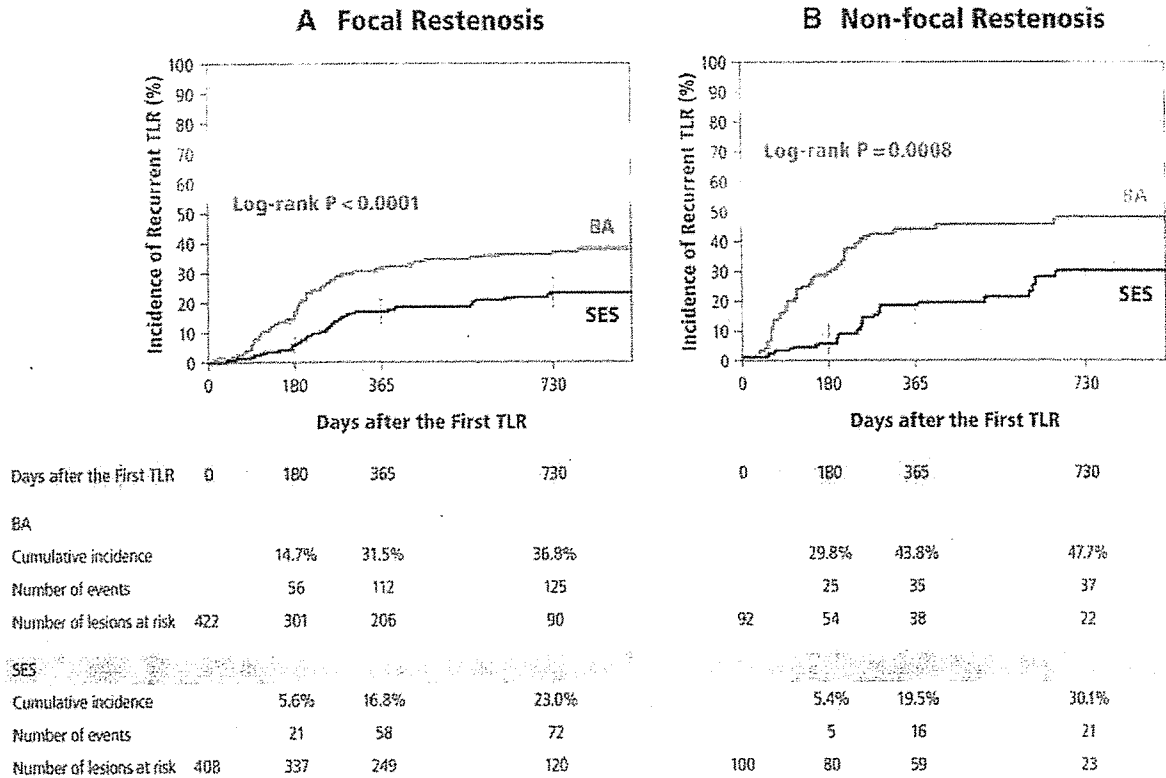


Figure 5. Cumulative incidences of recurrent TLR according to the modalities of TLR (BA versus SES) in (A) the focal restenosis lesions and (B) the nonfocal restenosis lesions.

Cumulative incidences of definite ST between SES- and BA-treated lesions were 0.2% and 0.6% versus 0.6% and 0.6% at 1 year and 2 years after the first TLR, respectively (Figure 7).

Discussion

The main findings of the present study are that use of repeated SES implantation to treat SES-associated restenosis as compared with treatment with BA had a very strong treatment effect in preventing recurrent TLR and that repeated SES implantation was not associated with higher mortality nor increased incidence of ST as compared with treatment with BA.

Optimal treatment strategy of SES-associated restenosis has not been adequately defined yet. Because of the profound antirestenotic efficacy of SES, the studies investigating the outcome of various treatment strategies for SES-associated restenosis are often hampered by the small number of the study patients. However, with expanding indication of SES to more complex lesions, management of restenosis of SES has emerged as a clinically relevant issue. The very large sample size and inclusion of many complex patients in the j-Cypher registry provides an opportunity to evaluate the clinical outcome of patients after the first TLR for SES-associated restenosis.

To date, there is no report from either randomized trials or large-scale observational studies investigating the efficacy of SES over BA treatment for restenosis of SES. The results

from a few previous small observational studies were not consistent in terms of efficacy of repeated SES implantation to prevent recurrent TLR as compared with use of BA.⁸⁻¹⁰ Cosgrave et al⁸ identified 250 drug-eluting stent-associated restenosis in 203 patients and divided these lesions into 2 groups: focal and nonfocal. For focal restenotic lesions, the incidence of TLR after drug-eluting stent implantation and BA treatment was 8.6% and 11.4%, respectively, whereas for nonfocal restenotic lesions, incidence was 22.6% and 24%, respectively. Kitahara et al⁹ reported that in 101 patients with 102 lesions undergoing TLR for SES-associated restenosis, recurrent TLR tended to be lower with SES implantation than with treatment with BA, both in the focal type (12.5% versus 35.5%) and in the nonfocal type (35.3% versus 50.0%), respectively, during the mean follow-up of 13.0±8.9 months. Angiographic analysis in the present study demonstrated consistent reduction in the rate of recurrent TLR by use of repeated SES implantation in both the focal-type and the nonfocal type SES-associated restenosis.

Our current analysis revealed a very strong treatment effect of repeated SES implantation over BA in preventing recurrent TLR in a large number of patients with adjustment for differences in baseline characteristics. Until otherwise proven by adequately sized randomized trials, our current observation supports the choice of repeated SES implantation for SES-associated restenosis.

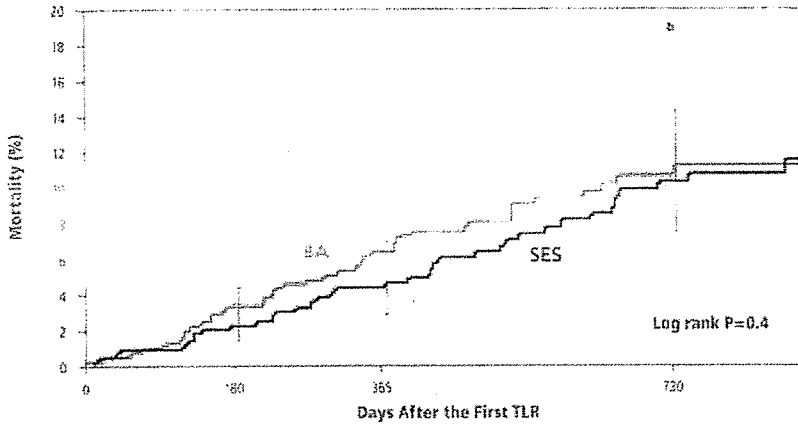


Figure 6. Cumulative incidences of death after the first TLR in patients treated with SES as compared with those treated with BA for SES-associated restenosis.

Days after the first TLR	0	180	365	730
BA				
Overall mortality		3.5%	6.6%	10.8%
Number of events		16	38	41
Number of patients at risk	491	414	354	174
SES				
Overall mortality		2.5%	4.5%	10.4%
Number of events		11	19	36
Number of patients at risk	475	414	350	186

It is interesting to note that Kim et al¹⁰ reported that the recurrent TLR rate at 1 year was 3.3% for the SES group and 8.3% for the BA group. The reported incidences of both groups were extremely low compared with other studies, including ours. The discrepancy in the rate of recurrent TLR might be related to some differences in lesion complexity and in the pattern of restenosis. Focal restenosis was associated with lower incidence of target lesion failure compared with nonfocal restenosis in the case of treatment with bare-metal

stent¹³ and SES.^{8,9} Previous reports demonstrated that focal restenosis remained the most common pattern (71.3% to 79.0%) with SES in real-world clinical practice.^{14,15} Although we could not fully address the pattern of restenosis in the current analysis, it is possible that the prevalence of nonfocal restenosis might increase with increasing complexity of the original target lesions. Also, it is likely that the routine follow-up angiography often performed in Japanese clinical practice might increase the rate of angiographically driven TLR.

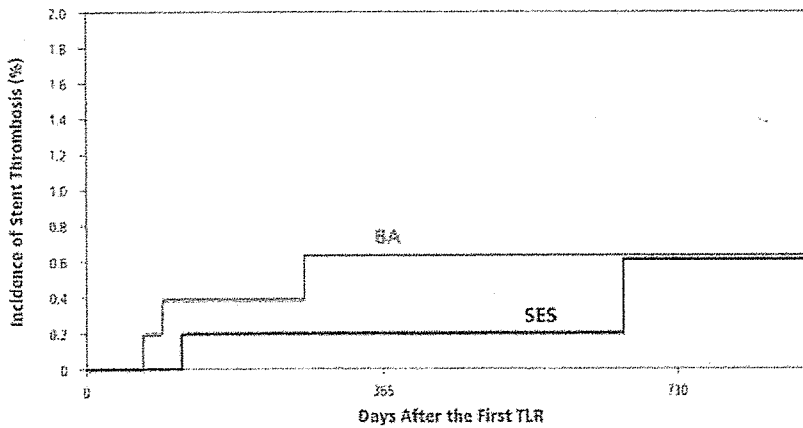


Figure 7. Cumulative incidences of stent thrombosis after the first TLR in lesions treated with SES as compared with those treated with BA for SES-associated restenosis.

Days after the First TLR	0	180	365	730
BA				
Cumulative incidence		0.4%	0.6%	0.6%
Number of events		2	3	3
Number of lesions at risk	557	462	393	191
SES				
Cumulative incidence		0.2%	0.2%	0.6%
Number of events		1	1	2
Number of lesions at risk	537	464	393	209

Predicting which patients would be likely to have refractory restenosis after SES implantation is clinically important when choosing between percutaneous coronary intervention and coronary artery bypass grafting surgery in patients with complex coronary lesions. Hemodialysis was identified as the only independent risk factor for recurrent TLR other than use of BA. Other risk factors identified by univariate analysis, such as severe calcification and in-stent restenosis, did not emerge as independent risk factors by multivariate analysis, probably due to the strong influence of the treatment modality (SES or BA) on the outcome. Future investigation on the risk factors for refractory restenosis should focus on those patients undergoing repeated SES implantation for SES-associated restenosis.

Although SES implantation was demonstrated to be associated with better outcome rates as compared with BA in the treatment of SES-associated restenosis, the incidence of recurrent TLR after repeated SES implantation (17.0% at 1 year) was far from satisfactory. Outcome of treatment of drug-eluting stent restenosis might be improved with different types of drug-eluting stent. However, a recent report from a relatively large randomized trial comparing paclitaxel-eluting versus sirolimus-eluting stents for the treatment of SES-associated restenosis demonstrated similar rates of recurrent TLR.¹⁶ Considering the unacceptably high recurrence rate of SES-associated restenosis, development of some innovative treatment strategies is obviously needed. Some randomized, double-blind, multicenter trials demonstrated that drug-eluting balloon reduced the need for TLR compared with uncoated-balloon¹⁷ and paclitaxel-eluting stent.¹⁸ Although there is little information about drug-eluting balloon versus SES for SES-associated restenosis, drug-eluting balloon might be a promising alternative.

As for safety concerns, repeated SES implantation inside the previously placed SES might lead to alterations in drug release, hypersensitivity to "double-dose" polymers, and an inadequate stent expansion at the area of stent overlap. One or more of these factors might cause unexpected adverse events such as ST or death. Because of the growing concerns for potentially higher risk of ST and/or death after SES implantation, we evaluated the incidences of these 2 events after SES implantation or BA treatment for SES-associated restenosis; however, we did not find any significant differences in the incidences of death or ST between the 2 groups. Although the statistical power is obviously insufficient, we did not find any safety signal with use of SES treatment for SES-associated restenosis.

Study Limitations

There are several important limitations in this study. First, selection of treatment strategies for SES-associated restenosis were not randomized but were left to the discretion of the individual operators. Baseline characteristics were significantly different between SES- and BA-treated lesions. Although adjusted comparison using a multivariable regression model was conducted, there still might be some unmeasured confounders. However, treatment effect of repeated SES implantation in preventing recurrent TLR was very strong, suggesting the robustness of our observation. Second, TLR

procedures constituting the study population were follow-up events in the j-Cypher registry. Although we had extensive data on clinical, lesion, and procedural characteristics at the time of the index procedures, information other than treatment modalities for TLR and angiographic findings were not collected at the time of the TLR procedures. Therefore, analysis of the risk factors for recurrent TLR was conducted based on baseline characteristics at the time of index procedures. Third, we did not systematically evaluate the reason why TLR was undertaken. We could not discriminate between clinically and angiographically driven TLR. Decisions on whether or not to perform TLR were largely dependent on the preferences of the patients and the attending physicians. It is likely that the routine follow-up angiography performed in many Japanese centers might increase the rate of angiographically driven TLR. Finally, we evaluated many baseline characteristics as potential risk factors. The issue of multiple comparison is unavoidable. However, our primary target is SES versus BA for SES-associated restenosis, and other factors were used only for adjustment. Therefore, this issue does not have strong impact on our result.

Conclusions

Despite these study limitations, we would conclude that repeated implantation of SES for treatment of SES-associated restenosis is more effective in preventing recurrent TLR than treatment with BA, without evidence of safety concerns.

Acknowledgments

The authors are indebted to Hiromi Maeda, Hiromi Yoshida, and Natsuko Nakajo for their secretarial assistance and to Naoko Okamoto, Etsuo Ota, and Yuriko Uchida for their devotion to data collection.

Sources of Funding

This study was supported by Cordis Cardiology Japan, a Johnson & Johnson company.

Disclosures

Dr Kimura serves on the advisory board and is a member of the speakers' bureau for Cordis Cardiology, and he has received honoraria from Cordis Cardiology. Dr Miyazaki serves on the advisory board for Cordis Cardiology. The remaining authors report no conflicts.

References

1. Moses JW, Leon MB, Popma JJ, Fitzgerald PJ, Holmes DR, O'Shaughnessy C, Caputo RP, Kereiakes DJ, Williams DO, Teirstein PS, Jaeger JL, Kuntz RE. Sirolimus-eluting stents versus standard stents in patients with stenosis in a native coronary artery. *N Engl J Med*. 2003; 349:1315-1323.
2. Win HK, Caldera AE, Maresh K, Lopez J, Rihal CS, Parikh MA, Granada JF, Marulkar S, Nassif D, Cohen DJ, Kleiman NS. Clinical outcomes and stent thrombosis following off-label use of drug-eluting stents. *JAMA*. 2007;297:2001-2009.
3. Kimura T, Morimoto T, Nakagawa Y, Tamura T, Kadota K, Yasumoto H, Nishikawa H, Hiasa Y, Muramatsu T, Meguro T, Inoue N, Honda H, Hayashi Y, Miyazaki S, Oshima S, Honda T, Shiode N, Namura M, Sone T, Nobuyoshi M, Kita T, Mitsudo K. Antiplatelet therapy and stent thrombosis after sirolimus-eluting stent implantation. *Circulation*. 2009; 119:987-995.
4. Kastrati A, Mehilli J, von Beckerath N, Dibra A, Hausleiter J, Pache J, Schühlen H, Schmitt C, Dirschinger J, Schomig A. Sirolimus-eluting stent or paclitaxel-eluting stent vs balloon angioplasty for prevention of

- recurrences in patients with coronary in-stent restenosis: a randomized controlled trial. *JAMA*. 2005;293:165-171.
5. Alfonso F, Perez-Vizcaino MJ, Hernandez R, Bethencourt A, Marti V, Lopez-Minguez JR, Angel J, Mantilla R, Moris C, Cequier A, Sabate M, Escaned J, Moreno R, Banuelos C, Suarez A, Macaya C. A randomized comparison of sirolimus-eluting stent with balloon angioplasty in patients with in-stent restenosis: results of the Restenosis Intrastent: Balloon Angioplasty Versus Elective Sirolimus-Eluting Stenting (RIBS-II) trial. *J Am Coll Cardiol*. 2006;47:2152-2160.
 6. Alfonso F, Perez-Vizcaino MJ, Hernandez R, Fernandez C, Escaned J, Banuelos C, Bethencourt A, Lopez-Minguez JR, Angel J, Cequier A, Sabate M, Moris C, Zueco J, Seabra-Gomes R. Sirolimus-eluting stents versus bare-metal stents in patients with in-stent restenosis: results of a pooled analysis of two randomized studies. *Catheter Cardiovasc Interv*. 2008;72:459-467.
 7. Holmes DR Jr, Teirstein P, Satler L, Sketch M, O'Malley J, Popma JJ, Kuntz RE, Fitzgerald PJ, Wang H, Caramanica E, Cohen SA. Sirolimus-eluting stents vs vascular brachytherapy for in-stent restenosis within bare-metal stents: the SISR randomized trial. *JAMA*. 2006;295:1264-1273.
 8. Cosgrave J, Melzi G, Biondi-Zoccai GG, Airolidi F, Chieffo A, Sangiorgi GM, Montorfano M, Michev I, Carlino M, Bonizzoni E, Colombo A. Drug-eluting stent restenosis the pattern predicts the outcome. *J Am Coll Cardiol*. 2006;47:2399-2404.
 9. Kitahara H, Kobayashi Y, Takebayashi H, Fujimoto Y, Nakamura Y, Kuroda N, Himi T, Miyazaki A, Haruta S, Komuro I. Re-restenosis and target lesion revascularization after treatment of sirolimus-eluting stent restenosis: retrospective analysis of 4 Japanese hospitals. *Circ J*. 2009;73:867-871.
 10. Kim YH, Lee BK, Park DW, Park KH, Choi BR, Lee CW, Hong MK, Kim JJ, Park SW, Park SJ. Comparison with conventional therapies of repeated sirolimus-eluting stent implantation for the treatment of drug-eluting coronary stent restenosis. *Am J Cardiol*. 2006;98:1451-1454.
 11. Cutlip DE, Windecker S, Mehran R, Boam A, Cohen DJ, van Es GA, Steg PG, Morel MA, Mauri L, Vranckx P, McFadden E, Lansky A, Hamon M, Krucoff MW, Serruys PW. Clinical end points in coronary stent trials: a case for standardized definitions. *Circulation*. 2007;115:2344-2351.
 12. Ellis SG, Vandormael MG, Cowley MJ, DiSciascio G, Deligonul U, Topol EJ, Bulle TM. Coronary morphologic and clinical determinants of procedural outcome with angioplasty for multivessel coronary disease: implications for patient selection Multivessel Angioplasty Prognosis Study Group. *Circulation*. 1990;82:1193-1202.
 13. Mehran R, Dangas G, Abizaid AS, Mintz GS, Lansky AJ, Satler LF, Pichard AD, Kent KM, Stone GW, Leon MB. Angiographic patterns of in-stent restenosis: classification and implications for long-term outcome. *Circulation*. 1999;100:1872-1878.
 14. Corbett SJ, Cosgrave J, Melzi G, Babic R, Biondi-Zoccai GG, Godino C, Morici N, Airolidi F, Michev I, Montorfano M, Sangiorgi GM, Bonizzoni E, Colombo A. Patterns of restenosis after drug-eluting stent implantation: insights from a contemporary and comparative analysis of sirolimus- and paclitaxel-eluting stents. *Eur Heart J*. 2006;27:2330-2337.
 15. Park CB, Hong MK, Kim YH, Park DW, Han KH, Lee CW, Kang DH, Song JK, Kim JJ, Park SW, Park SJ. Comparison of angiographic patterns of in-stent restenosis between sirolimus- and paclitaxel-eluting stent. *Int J Cardiol*. 2007;120:387-390.
 16. Byrne RA. ISAR-DESIRE 2: A prospective randomized trial of paclitaxel-eluting vs sirolimus-eluting stents for treatment of sirolimus-eluting stent restenosis. Oral presentation, Transcatheter Cardiovascular Therapeutics 2009; September 23, 2009; San Francisco, CA.
 17. Scheller B, Hehrlein C, Bocksch W, Rutsch W, Haghi D, Dietz U, Bohm M, Speck U. Treatment of coronary in-stent restenosis with a paclitaxel-coated balloon catheter. *N Engl J Med*. 2006;355:2113-2124.
 18. Unverdorben M, Vallbracht C, Cremers B, Heuer H, Hengstenberg C, Maikowski C, Werner GS, Antoni D, Kleber FX, Bocksch W, Leschke M, Ackermann H, Boxberger M, Speck U, Degehard R, Scheller B. Paclitaxel-coated balloon catheter versus paclitaxel-coated stent for the treatment of coronary in-stent restenosis. *Circulation*. 2009;119:2986-2994.

CLINICAL PERSPECTIVE

Optimal treatment strategies for restenosis of sirolimus-eluting stents (SES) have not been adequately addressed yet. A few previous small observational studies compared the use of SES for restenosis of SES with the use of balloon angioplasty (BA) in preventing recurrent target-lesion revascularization (TLR). However, there is no report from either randomized trials or large-scale observational studies investigating the efficacy of SES for restenosis associated with SES use. Our current analysis revealed that cumulative incidence of recurrent TLR in the SES-treated restenosis lesions was significantly lower than that in the BA-treated restenosis lesions (23.8% versus 37.7% at 2 years after the first TLR; $P < 0.0001$). Among 33 baseline variables evaluated, only hemodialysis was identified to be the independent risk factor for recurrent TLR by a multivariable logistic regression analysis. After adjusting for confounders, repeated SES implantation was associated with a strong treatment effect in preventing recurrent TLR over BA (odds ratio, 0.44; 95% confidence interval, 0.32 to 0.61; $P < 0.0001$). The 2-year mortality and stent thrombosis rates between the SES- and the BA-treated groups were 10.4% versus 10.8% ($P = 0.4$) and 0.6% versus 0.6%, respectively. Although other modalities like drug-eluting balloon catheters might be promising alternatives, our results indicate that repeated implantation of SES for SES-associated restenosis is more effective in preventing recurrent TLR than treatment with BA, without signals suggesting safety concerns. Until otherwise proven by adequately sized randomized trials, our current observation supports the choice of repeated SES implantation for SES-associated restenosis.

Supplemental Material

Supplemental Appendix: List of participating centers and investigators for the j-Cypher registry.

Chikamori-kai Medical Corporation: Kazuya Kawai, Shuichi Seki

Ehime Prefectural Central Hospital: Yukio Kazatani, Shinichi Hiramatsu, Tsuyoshi
Matsunaka, Aya Okino, Ai Nomoto

Fujita Health University Banbuntane Houtokukai Hospital: Masanori Nomura,
Hiroatsu Yokoi, Masato Mikawa

Fukuoka University Hospital: Keijiro Saku, Kazuyuki Shirai

Fukuyama Cardiovascular Hospital: Seiichi Haruta, Hiroshi Akanuma

Gunma Prefectural Cardiovascular Center: Shigeru Oshima, Hiroshi Hoshizaki, Ren
Kawaguchi, Hideki Tsurugaya

Hokko Memorial Hospital: Katsuhiko Sato, Yoichi Nozaki, Mitsuru Tamazawa

Japanese Red Cross Society Wakayama Medical Center: Akira Miura, Hiroki
Sakamoto, Hiroshi Ueda

Kanazawa Cardiovascular hospital: Masanobu Namura, Taketsugu Tsuchiya

Kawasaki Social Insurance Hospital: Tadashi Kikuchi, Toshiya Muramatsu,

Yoshiaki Ito

Kishiwada Tokushukai Hospital: Yoshiaki Yokoi, Nobuyuki Morioka, Ryuji Ishikawa

Kokura Memorial Hospital: Masakiyo Nubuyoshi, Hitoshi Yasumoto, Itsuo Yuda,

Shinichi Shirai

Kurashiki Central Hospital: Kazuaki Mitsudo, Kazushige Kadota, Hayato Shimizu,

Noriko Makita, Hideko Nakagawa, Nagisa Watanabe, Yoshimi Sano

Kyoto Second Red Cross Hospital: Hiroshi Fujita, Akiko Matsuo

Kyoto University Hospital: Takeshi Kimura, Toshihiro Tamura, Etsuo Ohta, Taisuke

Nakanoue, Yoshihisa Nakagawa, Yuriko Uchida, Masahiko Sakamoto

Maizuru Kyosai Hospital: Ryozo Tatami, Kinya Ashida, Takaaki Kitai

Matsue Red Cross Hospital: Nobuo Shiode

Mie Heart Center: Hideo Nishikawa, Fumiya Uchida

Miyazaki Ishikai Hospital: Yoshisato Shibata, Katsumasa Nomura

Nanpuh Hospital: Shinichiro Toyoshima

National Cardiovascular Center: Shunichi Miyazaki, Hiroshi Nonogi, Atsushi

Kawamura, Mitsuru Abe, Takuya Taniguchi, Hironori Yokoyama

National Hospital Organization Kagoshima Medical Center: Hitoshi Nakashima,

Manabu Setoguchi

- Noto General Hospital:** Yoshiharu Murata, Kinuyo Morita
- Ogaki Municipal Hospital:** Takahito Sone, Shuji Morikawa, Ejiro Hayashi
- Osaka City General Hospital:** Kazuo Haze, Akira Ito, Kei Yunoki
- Osaka Red Cross Hospital:** Masaru Tanaka, Tsukasa Inada
- Saiseikai Kumamoto Hospital:** Takashi Honda, Kenji Horiuchi, Naoko Takahashi,
Kana Tsukushima
- Saiseikai Noe Hospital:** Shunsuke Take, Tomoko Yano
- Sendai Kousei Hospital:** Taiichiroh Meguro, Hidehiko Honda, Naoto Inoue
- Shinbeppu Hospital:** Natsuki Nakamura, Kouichi Kikuta, Hidenori Tanaka
- Shin-Koga Hospital:** Tomohiro Kawasaki
- Shizuoka General Hospital:** Osamu Doi, Hiromichi Tamekiyo, Satoshi Kaburagi
- Shonan Kamakura General Hospital:** Shigeru Saito, Saeko Takahashi, Yoshio
Taketani
- Teikyo University Hospital:** Takaaki Isshiki, Ken Kozuma
- Tokushima Red Cross Hospital:** Yoshikazu Hiasa, Koichi Kishi
- Tsuchiya General Hospital:** Yasuhiko Hayashi, Mamoru Toyofuku, Toru Ishibashi,
Miyo Hatanari
- Yamaguchi University Hospital:** Masunori Matsuzaki, Jutaro Yamada, Takayuki

Okamura

Effects of Ghrelin Administration After Total Gastrectomy: A Prospective, Randomized, Placebo-Controlled Phase II Study

SHINICHI ADACHI,* SHUJI TAKIGUCHI,* KAZUYUKI OKADA,† KAZUYOSHI YAMAMOTO,* MAKOTO YAMASAKI,* HIROSHI MIYATA,* KIYOKAZU NAKAJIMA,* YOSHIYUKI FUJIWARA,* HIROSHI HOSODA,[§] KENJI KANGAWA,[§] MASAKI MORI,* and YUICHIRO DOKI*

*Department of Gastroenterological Surgery, Osaka University Graduate School of Medicine, Osaka; †Department of Surgery, Suita Municipal Hospital, Osaka; and §Department of Biochemistry, National Cardiovascular Center Research Institute, Osaka, Japan

BACKGROUND & AIMS: Body weight (BW) loss and reduction of blood ghrelin level are commonly observed after total gastrectomy (TG). A prospective study was designed to elucidate whether exogenous ghrelin administration prevents postoperative BW loss by improving appetite and oral food intake in patients with gastric cancer after undergoing TG. **METHODS:** In this randomized phase II study, 21 patients undergoing TG were assigned to a ghrelin (11 patients) or placebo group (10 patients). They received intravenous infusion of synthetic human ghrelin (3 µg/kg) or saline twice daily for 10 days after starting oral food intake following surgery. Changes in BW, appetite visual analog scale score, food intake calories, body composition, basal metabolic rate, and various blood test results were evaluated. **RESULTS:** Excluding one patient who developed profound diaphoresis during ghrelin infusion, 20 patients completed the study. Food intake and appetite were significantly higher with ghrelin compared with placebo (average, 13.8 vs 10.4 kcal/kg/day [$P = .030$] and 5.7 vs 3.9 cm [$P = .032$], respectively). BW loss was significantly lower in the ghrelin than in the placebo group (-1.4% vs -3.7%; $P = .044$). Fat mass, lean body mass, and basal metabolic rate decreased significantly in the placebo group; however, the reductions in lean body mass and basal metabolic rate were not significant in the ghrelin group, although that of fat mass was significant. **CONCLUSIONS:** Short-term administration of synthetic ghrelin was safe and successfully lessened postoperative BW loss and improved appetite and food intake after TG.

Keywords: Ghrelin; Total Gastrectomy; Gastric Cancer; Body Weight Loss.

Body weight loss is common and a serious outcome in patients with gastric cancer who have undergone total gastrectomy. It correlates well with decline in postoperative quality of life and is the most reliable indicator of malnutrition, which impairs immune function, infection susceptibility, and survival.¹⁻³ Although various mechanisms have been considered, such as perturbation of absorption due to reduced pancreatic excretion,^{4,5} de-

crease of gastric acid level,⁶ reflux esophagitis,⁷ intestinal floral alteration,⁸ and increased peristalsis and diarrhea,⁹ reduced food intake^{10,11} is the most conceivable explanation for body weight loss after total gastrectomy. Therefore, surgeons dealing with gastric cancers have tried to increase food intake by producing a gastric substitute, such as a jejunal pouch, but such procedures have not always been successful.¹² Another study indicated that the majority of patients with total gastrectomy could eat food as much as healthy subjects under a regulated program.¹³ Our own experience indicates that some patients do not show significant body weight loss after total gastrectomy by resorting to small but frequent meals. These changes suggest that reduced food intake after total gastrectomy could not be simply explained by loss of storage volume due to gastrectomy, but rather reflect a disturbance of eating activity through an unknown mechanism.

The 28-amino acid peptide ghrelin is the endogenous ligand for the growth hormone (GH) secretagogue receptor 1a, which stimulates GH release from the pituitary gland.¹⁴ The majority of ghrelin is produced by X/A-like cells of the oxyntic glands in the stomach, and a smaller amount is secreted from other organs, such as the intestine, pancreas, kidney, and hypothalamus.^{15,16} Ghrelin has various physiologic functions in addition to secretion of GH, such as promoting the appetite signal in the hypothalamus (in contrast to leptin),¹⁷ stimulating gastrointestinal activity (such as peristalsis, gastric acid secretion, and pancreatic excretion through the vagal nerves),¹⁸ and regulation of fat metabolism.¹⁹ In addition, ghrelin mitigates proinflammatory cytokine production and attenuates the stress signal.²⁰ Among the pleiotropic functions of ghrelin, this peptide is the only gastrointestinal hormone known to stimulate appetite. A randomized double-blind study of healthy volunteers

Abbreviations used in this paper: ANOVA, analysis of variance; BMR, body metabolic rate; GH, growth hormone; IGF, insulin-like growth factor.

© 2010 by the AGA Institute
0016-5085/10/\$36.00
doi:10.1053/j.gastro.2009.12.058

showed that ghrelin enhances appetite and increases food intake.^{21,22} Thereafter, several clinical trials of patients with heart failure,²³ pulmonary disease,²⁴ and cancer cachexia²⁵ concluded that ghrelin successfully improved the diseases along with increased oral food intake and body weight. In the field of surgical treatment for obesity, reduction in ghrelin levels after sleeve gastrectomy is associated with successful body weight loss and appetite suppression.²⁶ Taken together, the discovery of ghrelin allows the proposal of a new concept, body weight regulation by the stomach, which could be applied to various diseases with malnutrition.

We reported previously that serum ghrelin levels decreased to 10% to 20% of the preoperative level immediately after total gastrectomy^{27,28} and did not recover thereafter, accompanied by approximately 20% body weight loss.^{10,12,27} These findings suggest that loss of ghrelin could be involved in body weight loss observed after total gastrectomy. The present prospective, randomized, placebo-controlled phase II study investigated the effects of exogenous ghrelin administration on postoperative body weight loss by improving appetite and oral food intake in patients with gastric cancer who had undergone total gastrectomy. We report here the successful results of the study, and further use of ghrelin for these patients is discussed.

Patients and Methods

Patients

Twenty-one patients who underwent total gastrectomy at Osaka University Hospital between June 2006 and June 2008 were enrolled in the study. The inclusion criteria were as follows: (1) adenocarcinoma of the stomach confirmed by histopathologic examination, (2) preoperative clinical staging with less than stage II (International Union Against Cancer TNM stage classification), (3) curative surgical treatment (R0) (ie, total gastrectomy with D1 or D2 lymph node dissection), and (4) age between 20 and 80 years. The exclusion criteria were the presence of any of the following: (1) cardiopulmonary, liver, or renal dysfunction; (2) active dual malignancy; (3) pregnancy; (4) past history of gastrointestinal surgery; and (5) postoperative complications after total gastrectomy that could affect oral food intake, such as anastomotic leakage, pancreatitis, and mechanical ileus. Twenty-one patients were randomized by sealed envelope and divided into 2 study groups. The center office generated the allocation sequence and enrolled and assigned the patients to the 2 groups, and the random allocation sequence was concealed until interventions were assigned. Eleven patients received repeated administrations of ghrelin (ghrelin group), and 10 patients received repeated administrations of pure saline (placebo group). The study was approved by the Osaka University Ethics Committee, and all patients gave written informed consent

before study entry in accordance with the Declaration of Helsinki. The study was registered at UMIN (<http://www.umin.ac.jp>; clinical trial no. UMIN000001925).

Preparation of Synthetic Human Ghrelin

Synthetic human ghrelin, which consists of 99.4% acyl ghrelin and 0.6% des-acyl ghrelin, based on analysis by high-performance liquid chromatography, was obtained from Peptide Institute Inc (Osaka, Japan). Endotoxin examinations and the pyrogen test for ghrelin solutions were conducted as described previously.²⁹ Synthetic human ghrelin was dissolved in distilled water with 3.75% D-mannitol and sterilized by passage through a filter. Ghrelin solution was stored in 2-mL volumes, each containing 210 μ g. These solutions were stored at -20°C in sterile vials until preparation of ghrelin for administration.

End Points and Study Protocol

The primary end point of this study was an increase in orally ingested calories following ghrelin administration. The secondary end points included changes in body weight, appetite, body composition, basal metabolism, and blood tests. The study design is summarized in Figure 1A. The patient usually started oral food intake of rice porridge between postoperative day 5 and postoperative day 7. All patients were served standard postoperative meals, but they were always allowed to receive extra food when they desired. In the following 10 days after starting oral food intake, intravenous drip infusion of synthetic human ghrelin (3 μ g/kg) or placebo was administered twice a day (before breakfast and before dinner). Ghrelin solution and placebo (pure saline) were added to a 50-mL saline bottle, which was intravenously infused over a 30-minute period. The same amount of ghrelin was administered through intravenous infusion during the 10-day treatment; the dose was calculated based on the body weight on the day before oral food intake. During the study period, the same protocol of intravenous infusion and the same menu of meals were provided for the 2 groups. The composition of the intravenous infusion fluid was 43.0 g glucose, 35 mEq Na, 20 mEq K, 35 mEq Cl, and 20 mEq lactate in 1000 mL. The protocol of intravenous infusion was 2000 mL/day from postoperative day 1 to postoperative day 7 and 1000 mL/day from postoperative day 8 to postoperative day 14. The study was performed in a single-blind manner; patients without knowledge of their treatment assessed the amount of food intake, appetite, and body weight every day during the treatment by themselves without any intervention by the hospital staff. Food intake calories based on the food weight measured by the patient, including standard meal and extra foods, were calculated by dietitians using a calorimeter. Preprandial appetite at every meal was scored by the visual analog scale (possible scales, 0–10 cm) recorded in the account sheet by each

CLINICAL-
ALIMENTARY TRACT

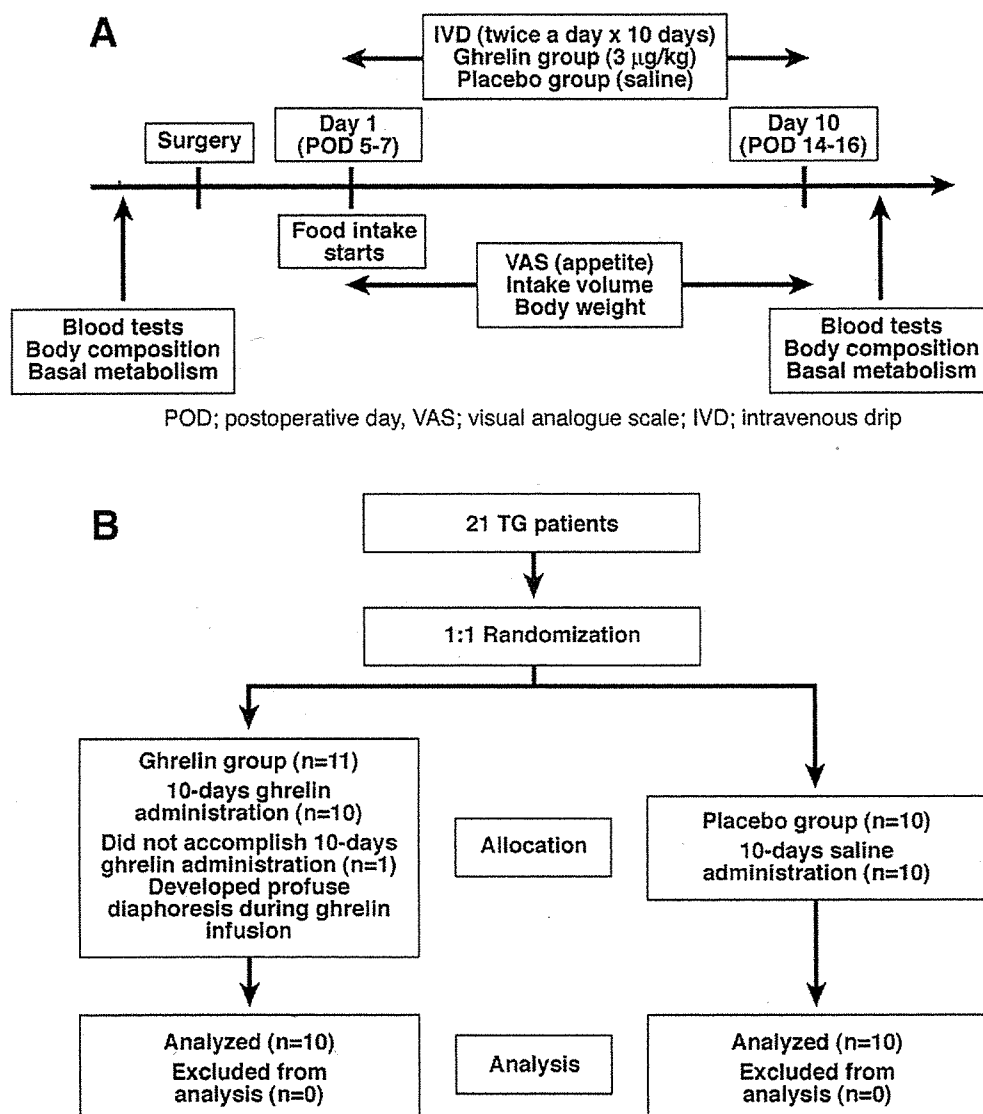


Figure 1. Study protocol and flow diagram.

patient. Body weight was measured with a beam scale to the nearest 0.1 kg, with patients standing barefoot and in light clothing.

Body composition was measured by using dual-energy x-ray absorptiometry (Hologic QDR-2000 instrument; Hologic Inc, Waltham, MA) to assess changes in lean body mass, fat mass, and bone mineral content before and after protocol treatment. The whole body was scanned in the single-beam mode, and the results were analyzed with body composition software. Basal metabolism was measured by using a metabolic analyzer (MedGem metabolic analyzer; HealthTech, Golden, CO) to assess changes in basal metabolism before and after treatment. All subjects breathed through the MedGem using a disposable, scuba-type mouthpiece. During the measurement, oxygen consumption (VO₂) and body meta-

bolic rate (BMR) were continuously and electronically recorded on a personal computer.

Blood Sampling and Assay

Blood samples were collected from patients before breakfast after an overnight fast, transferred into chilled tubes, stored on ice during collection, centrifuged, serum separated, and stored at -50°C until assay. Insulin-like growth factor (IGF)-I levels were measured by IGF-I IRMA "Daiichi" (TFB, Inc, Tokyo, Japan). Norepinephrine was measured using high-performance liquid chromatography (Tosoh Co, Tokyo, Japan). Cortisol and insulin were measured using the Cortisol Kit "TFB" (TFB, Inc, Tokyo, Japan) and chemiluminescent enzyme immunoassay (Fujirebio, Inc, Tokyo, Japan), respectively. Serum GH and leptin were

measured using GH Kit "Daiichi" (TFB, Inc, Tokyo, Japan) and Human Leptin RIA Kit (Linco Research Inc, St Charles, MO), respectively.

Sample Size Calculation and Statistical Analysis

We estimated that the difference in the effect of ghrelin or placebo on oral food intake calories should be at least 25% assuming 1200 and 1500 kcal/day in the placebo and ghrelin groups, respectively, with ±200 kcal for each SD. To analyze the difference in the effects in the ghrelin and placebo groups using Student *t* test, the study group should comprise at least 16 subjects, with a 5% α value and statistical power of 80%. Assuming that 20% of subjects in each group would not complete the study, the total number of subjects required in this study was estimated at 20.

Numerical values are expressed as mean ± SD unless otherwise indicated. Differences in parameters between the placebo and ghrelin groups were tested by Student *t* test or Mann-Whitney *U* test. Changes in parameters before and after total gastrectomy were tested statistically by the paired *t* test or Wilcoxon signed rank test. Changes in parameters between the 2 groups during the 10 days of follow-up were tested for significance by repeated-measures analysis of variance (ANOVA). A *P* value of <.05 was considered statistically significant. SAS for Windows software version 9 (SAS Institute, Inc, Cary, NC) was used to conduct repeated-measures ANOVA, whereas StatView version 5.0 (SAS Institute, Inc) was used for other tests.

Results

Patient Characteristics

The study flow diagram is summarized in Figure 1B. One of the 11 patients (9.1%) in the ghrelin group developed profuse diaphoresis during ghrelin infusion, equivalent to grade 1 by National Cancer Institute Common Terminology Criteria for Adverse Events version 3.0. Accordingly, we decided to stop ghrelin administration and the patient was excluded from further analysis. The 10-day course of ghrelin administration was well tolerated by the remaining 10 patients without any adverse events, although some reported transient periods of feeling warm and/or peristalsis during ghrelin infusion. Table 1 summarizes the clinical background of the 20 patients who completed the study. There was no significant difference in age, sex, body weight, body mass index, and clinical stage of gastric cancer between the 2 groups.

Effects of Ghrelin on Appetite, Food Intake, and Body Weight Loss

Appetite, oral food intake, and body weight were recorded by the patients throughout 10 days of ghrelin/saline administration. During this period, the patients in the 2 groups received the same amount (ie, volume and

Table 1. Patient Characteristics

Parameter	Ghrelin group	Placebo group	<i>P</i> value
n	10	10	
Age (y)	64.8 ± 10.4	61.6 ± 8.4	.46
Sex (male/female)	7/3	4/6	.19
Body weight (kg)	62.2 ± 13.6	62.9 ± 11.5	.89
Body mass index (kg/m ²)	23.1 ± 3.1	24.5 ± 3.8	.36
Procedure (LATG/COTG)	8/2	9/1	.54
Clinical TMN stage			
T (T1/T2/T3/T4)	7/1/2/0	8/2/0/0	.49
N (N0/N1/N2)	9/1/0	9/1/0	1.00
Stage (I/II/III/IV)	8/2/0/0	10/0/0/0	.15

LATG, laparoscopic assisted total gastrectomy; COTG, conventional open total gastrectomy.

calories) of intravenous infusion. The mean appetite visual analog scale score was significantly higher in the ghrelin group than the placebo group during the 10-day period (Figure 2A; repeated-measures ANOVA, *P* = .032).

Food intake calories (kcal/kg/day) during the 10-day period were significantly higher in the ghrelin group than in the placebo group (Figure 2B; repeated-measures ANOVA, *P* = .030). Food intake gradually increased at an earlier period of food intake and was then unchanged thereafter; both groups showed a similar difference throughout the 10-day period. The mean intake calorie over the 10-day period was 13.8 and 10.4 kcal/kg/day for the ghrelin and placebo groups, and ghrelin administration accounted for about 32.7% of the increase.

Body weight loss was calculated in reference to the first day of oral food intake. During this period, body weight gradually decreased in both groups, although the loss was more evident in the placebo group. At the end of the intravenous drip protocol (Day 10), body weight loss was -3.7% for the placebo group but only -1.4% for the ghrelin group. For the 10-day period, body weight loss of the ghrelin group was less than that of the placebo group (Figure 2C; repeated-measures ANOVA, *P* = .044).

Effects of Ghrelin on Body Composition and Basal Metabolism

Consistent with the body weight changes, both lean body mass and fat mass decreased gradually during the study period. The mean change in fat mass was -8.8% (14,100 ± 5400 to 12,900 ± 5200 g) and -7.6% (19,000 ± 8400 to 17,700 ± 8300 g) for the ghrelin and placebo groups, respectively. The reduction was statistically significant for each group (Figure 3A; *P* < .001). The mean change in lean body mass in the placebo group was -7.8% (41,800 ± 6500 to 38,500 ± 5700 g), which was also significant (Figure 3B; *P* < .001); however, the change in the ghrelin group was only -2.9% (44,600 ± 10,500 to 43,200 ± 9600 g, Figure 3B; *P* = .076). Figure 3C shows the BMR values before and after total gastrectomy. BMR decreased significantly after total gastrectomy in the placebo group (21.8 ± 4.0 to 19.4 ± 3.4

CLINICAL-ALIMENTARY TRACT

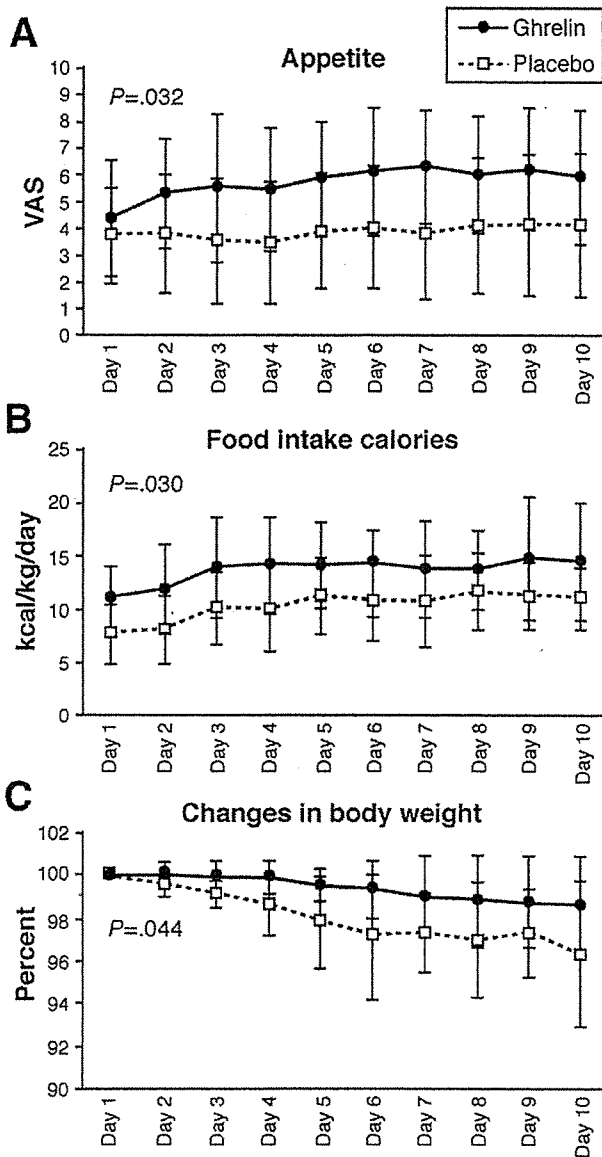


Figure 2. Serial changes in appetite, food intake, and body weight during the 10-day study in the ghrelin and placebo groups. Data are expressed as the mean \pm SD of visual analog scale scores of (A) preprandial appetite at every meal, (B) daily total food intake calories per body weight (kcal/kg/day), and (C) percent body weight relative to the first day of oral intake in the ghrelin and placebo groups. The visual analog scale score throughout the study period, which was evaluated by repeated-measures ANOVA, was significantly higher in the ghrelin group than in the placebo group (5.7 vs 3.9 cm; $P = .032$). Likewise, food intake calories were significantly higher in the ghrelin group than in the placebo group (average, 13.8 vs 10.4 kcal/kg/day; repeated-measures ANOVA, $P = .030$). Body weight loss in the ghrelin group was significantly lower than in the placebo group (-1.4% vs -3.7% ; repeated-measures ANOVA, $P = .044$).

kcal/kg; $P = .023$). In contrast, the reduction in BMR in the ghrelin group was smaller, and the difference between before and after treatment was not significant (22.6 ± 6.1 to 21.4 ± 6.0 kcal/kg; $P = .20$).

Blood Tests and Hormone Assays

Finally, we compared the results of certain blood tests that reflect the nutritional status and hormones (hemoglobin, total protein, albumin, total cholesterol, triglyceride, leptin, GH, cortisol, norepinephrine, insulin, and IGF-I) both before and after the 10-day period (Table 2). In the early recovery phase, the parameters associated with nutrition did not change in the placebo group but significantly improved in the ghrelin group. Leptin levels decreased significantly in both groups after total gastrectomy, consistent with the reduction in fat mass. On the other hand, there was no significant change in GH, cortisol, norepinephrine, insulin, and IGF-I levels after treatment in both groups.

Discussion

Body weight loss is a common finding in patients who undergo gastrectomy for gastric cancer, which not

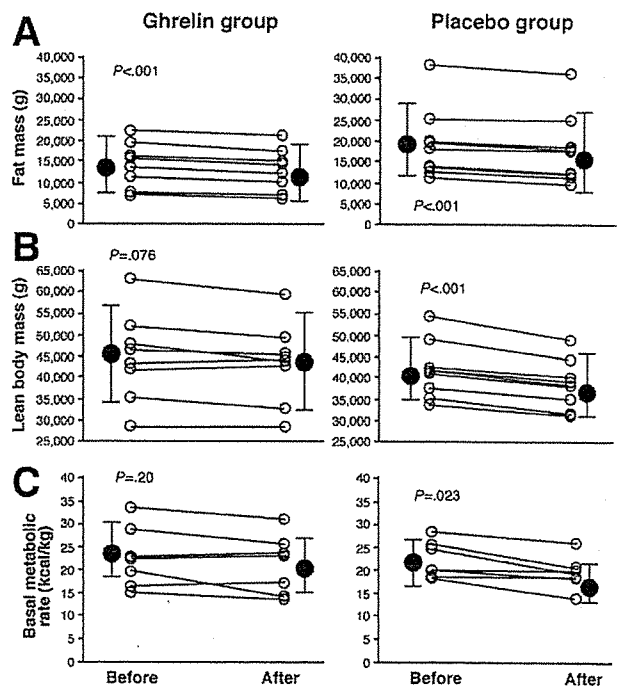


Figure 3. Body composition and basal metabolic rate before and after the study in the ghrelin and placebo groups. (A) Fat mass and (B) lean body mass measured by dual-energy x-ray absorptiometry and (C) basal metabolic rate were determined before and after the 10-day study. Changes for each patient (open circles) and the whole group (closed circles, \pm SD) are shown for the ghrelin and placebo groups. The reductions in all 3 parameters were statistically significant in the placebo group by Student *t* test (fat mass, $19,000 \pm 8400$ to $17,700 \pm 8300$ g [$P < .001$]; lean body mass, $41,800 \pm 6500$ to $38,500 \pm 5700$ g [$P < .001$]; BMR, 21.4 ± 6.0 to 19.4 ± 3.4 kcal/kg [$P = .023$]). In the ghrelin group, the reduction of fat mass was significant while that of lean body mass and BMR was less than in the placebo group and not statistically significant (fat mass, $14,100 \pm 5400$ to $12,900 \pm 5200$ g [$P < .001$]; lean body mass, $44,600 \pm 10,500$ to $43,200 \pm 9600$ g [$P = .076$]; BMR, 22.6 ± 6.1 to 21.4 ± 6.0 kcal/kg [$P = .20$]).

74

Table 2. Results of Laboratory Tests

	Ghrelin group	Placebo group
Hemoglobin (g/dL)		
Before	12.2 ± 0.8	12.7 ± 2.4
After	11.8 ± 1.1	11.7 ± 1.4
Total protein (g/dL)		
Before	5.7 ± 0.3	6.0 ± 0.7
After	6.6 ± 0.4 ^a	6.4 ± 0.3
Albumin (g/dL)		
Before	3.1 ± 0.2	3.4 ± 0.6
After	3.5 ± 0.4 ^a	3.5 ± 0.2
Total cholesterol (mg/dL)		
Before	148 ± 43	176 ± 26
After	174 ± 37 ^a	164 ± 32
Triglyceride (mg/dL)		
Before	82 ± 47	77 ± 29
After	113 ± 32 ^a	99 ± 44
Leptin (ng/mL)		
Before	3.1 ± 1.4	7.9 ± 6.7
After	1.2 ± 0.4 ^b	4.1 ± 4.0 ^b
GH (ng/mL)		
Before	0.87 ± 1.5	0.62 ± 0.8
After	0.55 ± 0.7	1.65 ± 2.7
Cortisol (μg/dL)		
Before	18.6 ± 4.8	16.9 ± 4.6
After	17.0 ± 4.0	17.9 ± 6.7
Norepinephrine (pg/mL)		
Before	314 ± 132	294 ± 171
After	366 ± 122	269 ± 158
Insulin (μIU/mL)		
Before	6.1 ± 3.5	10.3 ± 5.5
After	5.1 ± 2.5	6.5 ± 6.0
IGF-I (ng/mL)		
Before	108 ± 33	92 ± 36
After	85 ± 53	76 ± 37

^aP < .05, ^bP < .01 (paired t test; before vs after).

only associates with various pathologic conditions but also affects patients' social activity. Therefore, postoperative body weight loss needs to be investigated thoroughly, especially in Japan, where early gastric cancer accounts for more than 50% of the total incidence of gastric cancer,³⁰ and the 5-year survival rate of early gastric cancer is more than 90%.³¹ Previous studies reported that body weight loss after total gastrectomy was approximately 15% to 20% of the preoperative weight.^{10,12,27} Because the incidence of gastric cancer is associated with low body weight in not only Japan and Asian countries but also in the Western world, the estimated average body mass index after total gastrectomy is expected to be 18 to 20 kg/m², which is lower than the ideal body mass index. The correlation between low body weight and long-term survival rate has not been analyzed thoroughly even in healthy individuals. A large cohort study of healthy Japanese subjects surveyed over 10 years concluded that a body mass index less than 19 kg/m² was associated with high mortality risk at an odds ratio of 2.26 due to various diseases, including infectious, cardiovascular, and malignant diseases.³ Although there are no concrete data for patients who undergo gastrectomy,

these patients could be at risk for a higher mortality rate due to low body weight. Based on this background, the major purpose of this study was to minimize postoperative body weight loss by ghrelin administration through up-regulation of GH secretion and appetite.

At the end of the 10-day study period, ghrelin reduced more than half of postoperative body weight loss from -3.7% in the placebo group to -1.4% in the ghrelin group. Although this is a limited result in the early postoperative period, which is associated with the most profound body weight loss, to the best of our knowledge, ghrelin administration is the most effective procedure among various studies that were designed for the same purpose.^{12,32}

After numerous experimental studies, clinical application of ghrelin commenced in healthy volunteers and then extended to patients with heart failure,²³ pulmonary disease,²⁴ and cancer cachexia.²⁵ The results of these studies confirmed the safety of ghrelin administration. In our study, the patients in the 2 groups showed no differences in postoperative complications (eg, infections, delayed wound healing, thromboembolism) and length of hospital stay. However, 1 of the 11 patients developed diaphoresis, corresponding to National Cancer Institute Common Terminology Criteria for Adverse Events grade 1. Although we stopped ghrelin administration following the study protocol, this symptom was consistently reported in previous trials although it was tolerated by patients.^{23-25,29} The overall positive effects of ghrelin such as body weight gain and increase in food intake calories were observed consistently in all clinical trials, including the present study.²¹⁻²⁵ In addition, improvement of disease-specific status has been reported, including patients with chronic heart failure²³ and those with chronic obstructive pulmonary disease.²⁴

To our knowledge, the present study is the first clinical trial in the field of gastroenterological surgery. Moreover, the present study differs in 2 aspects from previous studies.²³⁻²⁵ The first difference related to the study subjects; the subjects enrolled in previous clinical studies were cachexic emaciated patients in whom the level of circulating ghrelin was predicted to rise. It has been considered that the efficacy of exogenous ghrelin is limited because of down-regulation by high endogenous ghrelin. In contrast, in the present study, in which circulating ghrelin levels were extremely low due to total gastrectomy, we replaced the low levels of endogenous ghrelin with an exogenous one; therefore, it seems more physiologically related to study the effect of ghrelin administration. Another point is that complete vagotomy at the esophagogastric junction was performed during total gastrectomy in our patients. Because the vagus nerve mediates both efferent and afferent ghrelin signals,³³⁻³⁵ it was suspected that exogenous ghrelin would not adequately interact in the hypothalamus. In animal experiments, vagotomy or chemical blockade of the vagal

signal abolished the effects of intravenously administered ghrelin.³⁶ In vagotomized patients, ghrelin administration did not increase food intake.³⁷ However, other studies reported that ghrelin administered intraperitoneally successfully stimulated food intake after vagotomy in rats³⁸ and that ghrelin administration in vagotomized patients enhanced GH secretion.³⁹ These animal experiments and clinical studies indicate that the effects of ghrelin administration are still controversial, at least in vagotomized patients. In the present study, intravenous administration of exogenous ghrelin successfully stimulated food intake and appetite immediately after total gastrectomy. Our results suggest that the administered ghrelin crossed the blood-brain barrier to the central nervous system, probably increasing the appetite signal through not only the vagal pathway but also the circulation. The relationship between ghrelin and vagotomy remains poorly defined, and further studies should be performed in the future.

BMR accounts for between 60% and 70% of the total energy expenditure in adults.⁴⁰ Furthermore, the fat-free mass is considered the best single predictor of energy expenditure, and 53% to 88% of the variation in BMR is accounted for by fat-free mass.⁴¹ In the placebo group, the BMR decreased significantly after total gastrectomy, whereas it did not change in the ghrelin group. This result was consistent with the significant decrease in lean body mass, which was limited to the placebo group. In animal experiments, ghrelin enhances abdominal fat storage in white adipose tissue in rats,¹⁹ whereas clinical studies, including the present study, have shown that ghrelin increases lean body mass relative to fat mass.^{23,24} Differences in species and patient status may influence the effect of ghrelin administration on fat metabolism. Preservation of lean body mass against the postoperative catabolic metabolism might be caused by ghrelin-stimulated GH secretion from the pituitary gland. However, serum GH levels were stable in the 2 groups, probably due to the rapid turnover of GH. This phenomenon was already reported in a previous phase I study.²⁹ Baseline leptin levels tended to be lower in the ghrelin group, probably because this group included more men, who generally have lower leptin levels than women.^{42,43} Leptin levels significantly decreased in parallel with the decrease in fat mass in both the ghrelin and placebo groups.

The influence of cancer proliferation is another issue of safety in ghrelin studies. Several *in vitro* studies reported the expression of ghrelin receptor in cancer cells and that ghrelin weakly enhanced their proliferation, for example, in prostate⁴⁴ and pancreatic⁴⁵ cancer cells. However, another study reported that ghrelin inhibited proliferation and increased apoptosis in a lung cancer cell line.⁴⁶ In a preliminary experiment in our laboratory using various gastric cancer cell lines, all cells examined were negative for ghrelin receptor

and showed no growth response to exogenous ghrelin (unpublished observation, March 2005). In clinical studies of cancer cachexic patients, no adverse events concerning tumor growth stimulation have been reported.²⁵ With respect to the present clinical trial, this argument was partly evaded because patients who met the inclusion criteria accounted for more than 90% curability by surgery alone³¹ and ghrelin was administered for only 10 days. However, care should be taken when administering ghrelin over longer periods.

Although we successfully demonstrated a short-term effect of ghrelin administration on food intake, appetite, body weight, and other parameters, its long-term effect and benefit still need to be evaluated before clinical application. Because ghrelin secretion does not recover even several years after total gastrectomy, long-term administration of ghrelin is probably required to maintain the short-term effects. For this purpose, ghrelin poses a practical problem in that it is an unstable short-acting peptide and needs to be administered intravenously. An easier administration route, such as subcutaneous injection and inhalation, should be investigated to allow outpatient and home use. GH secretagogues, which were discovered before ghrelin, are orally available and perhaps could be used as ghrelin substitutes. For example, RC-1291 is orally available, well tolerated, and effective in promoting body weight gain, as demonstrated in a phase I study in healthy volunteers.⁴⁷ Another issue worth further investigation is the clinical benefits of ghrelin therapy, because it is argued that increases in appetite and body weight are not sufficient reasons for medication. Thus, further studies are needed to evaluate other aspects of ghrelin administration, such as reduction of total medical cost and hospital admission, improvement of social activity and quality of life, and postoperative survival. For example, postoperative body weight loss is most progressive and rehabilitation is most important in the first 3 months after surgery. It is possible that ghrelin administration for at least 3 months would improve postoperative recovery.

In conclusion, this prospective randomized study in a limited number of patients provides convincing data for the beneficial effects of ghrelin on body weight and dietary activity after total gastrectomy. Although there are some issues to be resolved before clinical application, including drug delivery system, duration of administration, and adequate assessment of clinical benefits, surgeons dealing with gastric cancers and other gastroesophageal diseases should be encouraged by the availability of ghrelin. Because surgery is essentially not physiologic and highly invasive for the body but the most reliable therapeutic option to cure cancer, it is our obligation to invent novel procedures to minimize its side effects.

References

1. Demas GE, Drazen DL, Nelson RJ, et al. Reductions in total body fat decrease humoral immunity. *Proc Roy Soc B-Biol Sci* 2003; 270:905-911.
2. Marinho LA, Rettori O, Vieira-Matos AN, et al. Body weight loss as an indicator of breast cancer recurrence. *Acta Oncol* 2001;40: 832-837.
3. Tsugane S, Sasaki S, Tsubono Y. Under- and overweight impact on mortality among middle-aged Japanese men and women: a 10-y follow-up of JPHC Study cohort I. *Int J Obes Relat Metab Disord* 2002;529-537.
4. Bae JM, Park JW, Yang HK, et al. Nutritional status of gastric cancer patients after total gastrectomy. *World J Surg* 1998;22: 254-260.
5. Friess H, Bohm J, Muller MW, et al. Maldigestion after total gastrectomy is associated with pancreatic insufficiency. *Am J Gastroenterol* 1996;91:341-347.
6. Melissas J, Kampitakis E, Schoretsanitis G, et al. Does reduction in gastric acid secretion in bariatric surgery increase diet-induced thermogenesis? *Obes Surg* 2002;12:399-403.
7. Adachi S, Takeda T, Fukao K. Evaluation of esophageal bile reflux after total gastrectomy by gastrointestinal and hepatobiliary dual scintigraphy. *Surg Today* 1999;29:301-306.
8. Armbrecht U, Lundell L, Stockbruegger RW. Nutrient malassimilation after total gastrectomy and possible intervention. *Digestion* 1987;37:56-60.
9. Iesato H, Ohya T, Ohwada S, et al. Jejunal pouch interposition with an antiperistaltic conduit as a pyloric ring substitute after standard distal gastrectomy: a comparison with the use of an isoperistaltic conduit. *Hepatogastroenterology* 2000;47:756-760.
10. Braga M, Zuliani W, Foppa L, et al. Food intake and nutritional status after total gastrectomy: results of a nutritional follow-up. *Br J Surg* 1998;75:477-480.
11. Bergh C, Sjostedt S, Hellers G, et al. Meal size, satiety and cholecystokinin in gastrectomized humans. *Physiol Behav* 2003; 78:143-147.
12. Fein M, Fuchs KH, Thalheimer A, et al. Long-term benefits of Roux-en-Y pouch reconstruction after total gastrectomy: a randomized trial. *Ann Surg* 2008;247:759-765.
13. Liedman B. Symptoms after total gastrectomy on food intake, body composition, bone metabolism, and quality of life in gastric cancer patients: is reconstruction with a reservoir worthwhile? *Nutrition* 1999;15:677-682.
14. Kojima M, Hosoda H, Date Y, et al. Ghrelin is a growth-hormone-releasing acylated peptide from stomach. *Nature* 1999;402: 656-660.
15. Date Y, Kojima M, Nakazato M, et al. Ghrelin, a novel growth hormone-releasing acylated peptide, is synthesized in a distinct endocrine cell type in the gastrointestinal tracts of rats and humans. *Endocrinology* 2000;141:4255-4260.
16. Leite-Moreira AF, Soares JB. Physiological, pathological and potential therapeutic roles of ghrelin. *Drug Discov Today* 2007;12: 276-288.
17. Shintani M, Ogawa Y, Ebihara K, et al. Ghrelin, an endogenous growth hormone secretagogue, is a novel orexigenic peptide that antagonizes leptin action through the activation of hypothalamic neuropeptide Y/Y1 receptor pathway. *Diabetes* 2001;50:227-232.
18. Masuda Y, Tanaka T, Inomata N, et al. Ghrelin stimulates gastric acid secretion and motility in rats. *Biochem Biophys Res Commun* 2000;276:905-908.
19. Davies JS, Kotokorpi P, Eccles SR, et al. Ghrelin induces abdominal obesity via GHS-R-dependent lipid retention. *Mol Endocrinol* 2009;23:914-924.
20. Wu R, Dong W, Zhou M, et al. Ghrelin attenuates sepsis-induced acute lung injury and mortality in rats. *Am J Respir Crit Care Med* 2007;176:805-813.
21. Wren AM, Seal LJ, Cohen MA, et al. Ghrelin enhances appetite and increases food intake in human. *J Clin Endocrinol Metab* 2001;86:5992-5995.
22. Neary NM, Small CJ, Wren AM, et al. Ghrelin increases energy intake in cancer patients with impaired appetite: acute, randomized, placebo-controlled trial. *J Clin Endocrinol Metab* 2004;89: 2832-2836.
23. Nagaya N, Moriya J, Kangawa K, et al. Effects of ghrelin administration on left ventricular function, exercise capacity, and muscle wasting in patients with chronic heart failure. *Circulation* 2004;110:3674-3679.
24. Nagaya N, Itoh T, Kangawa K, et al. Treatment of cachexia with ghrelin in patients with COPD. *Chest* 2005;128:1187-1193.
25. Strasser F, Lutz TA, Maeder MT, et al. Safety, tolerability and pharmacokinetics of intravenous ghrelin for cancer-related anorexia/cachexia: a randomised, placebo-controlled, double-blind, double-crossover study. *Br J Cancer* 2008;98:300-308.
26. Karamanakos SN, Vagenas K, Kalfarentzos F, et al. Weight loss, appetite suppression, and changes in fasting and postprandial ghrelin and peptide-YY levels after Roux-en-Y gastric bypass and sleeve gastrectomy: a prospective, double blind study. *Ann Surg* 2008;247:401-407.
27. Takachi K, Doki Y, Ishikawa O, et al. Postoperative ghrelin levels and delayed recovery from body weight loss after distal or total gastrectomy. *J Surg Res* 2006;130:1-7.
28. Doki Y, Takachi K, Ishikawa O, et al. Ghrelin reduction after esophageal substitution and its correlation to postoperative body weight loss in esophageal cancer patients. *Surgery* 2006;139: 797-805.
29. Akamizu T, Takaya K, Kangawa K, et al. Pharmacokinetics, safety, and endocrine and appetite effects of ghrelin administration in young healthy subjects. *Eur J Endocrinol* 2004;150:447-455.
30. Shiraiishi N, Yasuda K, Kitano S. Laparoscopic gastrectomy with lymph node dissection for gastric cancer. *Gastric Cancer* 2006; 9:167-176.
31. Nomura S, Kaminishi M. Surgical treatment of early gastric cancer. *Dig Surg* 2007;24:96-100.
32. Lehnert T, Buhl K. Techniques of reconstruction after total gastrectomy for cancer. *Br J Surg* 2004;91:528-539.
33. Asakawa A, Inui A, Kaga T, et al. Ghrelin is an appetite-stimulatory signal from stomach with structural resemblance to motilin. *Gastroenterology* 2001;120:337-345.
34. Sato N, Kanai S, Takano S, et al. Central administration of ghrelin stimulates pancreatic exocrine secretion via the vagus in conscious rats. *Jpn J Physiol* 2003;53:443-449.
35. Simonian HP, Kresge KM, Boden GH, et al. Differential effects of sham feeding and meal ingestion on ghrelin and pancreatic polypeptide levels: evidence for vagal efferent stimulation mediating ghrelin release. *Neurogastroenterol Motil* 2005;17:348-354.
36. Date Y, Murakami N, Nakazato M, et al. The role of the gastric afferent vagal nerve in ghrelin-induced feeding and growth hormone secretion in rats. *Gastroenterology* 2002;123:1120-1128.
37. le Roux CW, Neary NM, Halsey TJ, et al. Ghrelin does not stimulate food intake in patients with surgical procedures involving vagotomy. *J Clin Endocrinol Metab* 2005;90:4521-4524.
38. Arnold M, Mura A, Langhans W, et al. Gut vagal afferents are not necessary for the eating-stimulatory effect of intraperitoneally injected ghrelin in the rat. *J Neurosci* 2006;26:11052-11060.
39. Takeno R, Okimura Y, Iguchi G, et al. Intravenous administration of ghrelin stimulates growth hormone secretion in vagotomized

CLINICAL-
ALIMENTARY TRACT

patients as well as normal subjects. *Eur J Endocrinol* 2004;151:447-450.

40. Shetty P. Energy requirements of adults. *Public Health Nutr* 2005;8:994-1009.

41. Nelson KM, Weinsier RL, Long CL, et al. Prediction of resting energy expenditure from fat-free mass and fat mass. *Am J Clin Nutr* 1992;56:848-856.

42. Kennedy A, Gettys TW, Watson P, et al. The metabolic significance of leptin in humans: gender-based differences in relationship to adiposity, insulin sensitivity, and energy expenditure. *J Clin Endocrinol Metab* 1997;82:1293-1300.

43. Ostlund RE Jr, Yang JW, Klein S, et al. Relation between plasma leptin concentration and body fat, gender, diet, age, and metabolic covariates. *J Clin Endocrinol Metab* 1996;81:3909-3913.

44. Yeh AH, Jeffery PL, Duncan RP, et al. Ghrelin and a novel proghrelin isoform are highly expressed in prostate cancer and ghrelin activates mitogen-activated protein kinase in prostate cancer. *Clin Cancer Res* 2005;11:8295-8303.

45. Duxbury MS, Waseem T, Ito H, et al. Ghrelin promotes pancreatic adenocarcinoma cellular proliferation and invasiveness. *Biochem Biophys Res Commun* 2003;309:464-468.

46. Cassoni P, Allia E, Marrocco T, et al. Ghrelin and cortistatin in lung cancer: expression of peptides and related receptors in human primary tumors and in vitro effect on the H345 small cell carcinoma cell line. *J Endocrinol Invest* 2006;29:781-790.

47. Garcia JM, Polvino WJ. Effect on body weight and safety of RC-1291, a novel, orally available ghrelin mimetic and growth hormone secretagogue: results of a phase I, randomized, placebo-controlled, multiple-dose study in healthy volunteers. *Oncologist* 2007;12:594-600.

Received July 20, 2009. Accepted December 17, 2009.

Reprint requests

Address requests for reprints to: Shuji Takiguchi, MD, PhD, Department of Gastroenterological Surgery, Osaka University Graduate School of Medicine, 2-2 Suita City Yamadaoka, Osaka, Japan. e-mail: stakiguchi@gesurg.med.osaka-u.ac.jp; fax: (81) 6-6879-3259.

Acknowledgments

Online registry: <http://www.umin.ac.jp>; clinical trial no. UMIN000001925.

The authors thank Tomoyuki Sugimoto from the Department of Biomedical Statistics, Osaka University, for the advice on statistical analysis as well as the nutritional management room staff of Osaka University Hospital for calculating food intake calories per day in this study.

Conflicts of interest

The authors disclose no conflicts.